Synthesis, Structure, and Lone Pair Activity of Bismuth Coordination Compounds Supported by Chelating Nitrogen Donor Ligands

by

Shubhra Srivastava

B.Tech., Dr.M.G.R. Educational and Research Institute, 2010

Thesis Submitted in Partial Fulfillment of the
Requirements for the Degree of
Master of Science

in the
Department of Chemistry
Faculty of Science

SIMON FRASER UNIVERSITY
Summer 2024

Declaration of Committee

Name:	**Shubhra Srivastava**
Degree:	**Master of Science**
Title:	**Synthesis, Structure, and Lone Pair Activity of Bismuth Coordination Compounds Supported by Chelating Nitrogen Donor Ligands**
Committee:	**Chair:** **Paul C. H. Li** Professor, Chemistry
	Daniel B. Leznoff Co-Supervisor Professor, Chemistry
	Jeffrey J. Warren Co-Supervisor Associate Professor, Chemistry
	Corina Andreoiu Committee Member Professor, Chemistry
	Robert Britton Committee Member Professor, Chemistry
	Loren G. Kaake Examiner Associate Professor, Chemistry

Abstract

The primary objective of this research is to evaluate whether bismuth (Bi) can be used as a substitute for lead (Pb) in cyanoaurate-containing coordination polymers. Lead is toxic to health and a general environmental concern, so finding a safer alternative is crucial. Bismuth, which is in the same period of the periodic table as lead, can have the same electronic configuration, i.e., Bi^{3+} and Pb^{2+} ions. This research concentrates on examining the structural patterns and comparing the stereochemical behavior of the lone pairs in Bi^{3+} and Pb^{2+}. A wide range of compounds were prepared using a systematically varied set of ligands and reaction conditions. Structural data were collected and analysed. In general, a range of coordination compounds were made, with fewer coordination polymers. It is hypothesized that different reaction conditions are needed to make the target materials. Ultimately, a series of new Bi coordination compounds are described. By conducting these analyses, the research aims to ascertain if Bi can be a suitable alternative to Pb in these materials. The findings could significantly contribute to the development of synthetic methods that are safer and more efficient routes to making coordination polymers, while reducing the reliance on Pb and enhancing material performance. This exploration into the substitution of Pb with Bi not only aims to improve the safety of these polymers but also to optimize their functional properties, leading to broader applications and advancements in the field of materials science.

Keywords: Bismuth; dicyanoaurate; coordination polymers; stereochemical lone pair; X-ray crystal structures; chelating ligands

Dedication

I dedicate my research work to the most wonderful person I've ever encountered, who, fortunately, is also my research supervisor, Dr. Daniel Leznoff.

Acknowledgements

With profound gratitude and respect, I acknowledge Dr. Daniel Leznoff (**Danny**) for being my greatest source of support and blessing. There are no words that can adequately convey the depth of my appreciation for Danny's contributions to my journey. His impact on my life is immeasurable, and I am forever indebted to him for his kindness, wisdom, and support. Danny has been the most significant blessing in my life. Throughout my journey, his unwavering support and guidance have been invaluable, and I am profoundly thankful for his influence and encouragement.

From the beginning, Danny believed in my potential and provided the mentorship necessary for my growth. His insights, patience, and dedication have been pivotal in shaping my academic and professional path. Danny's ability to inspire and motivate has pushed me to strive for excellence, and his faith in my abilities has given me the confidence to overcome numerous challenges. Danny has been a constant source of encouragement, not only in providing intellectual guidance but also emotional support. His compassion and understanding have made a profound impact on my life, helping me navigate through difficult times and celebrating my successes with genuine joy. He explained all the research concepts in an easy-to-understand manner and stood by me throughout my research journey. Danny's motivation and encouragement for all my results and ideas were invaluable.

He inspired me to think outside the box and helped me developing a research aptitude. He was always available whenever needed it and stood by me in my tough times. With deep gratitude and respect, I recall how Danny stood by me during a family emergency in India, offering emotional support during that difficult time. His unwavering support extended to my job, where he assisted me in every possible way. His extraordinary kindness and assistance, especially during my thesis writing when I was physically unwell, for his invaluable help, not only I but my entire family, including my children, will always remain deeply grateful. It has left a lasting impression on my heart that I will carry for my entire life.

I vividly recall the way he explained my research project, transforming it into an engaging and comprehensible endeavor. I recall how Danny explained my research project, making it both fascinating and comprehensible. His ability to make complex

concepts interesting and accessible was instrumental in igniting my passion for the subject. Throughout my research journey, Danny's enthusiasm and motivation for my results were truly inspiring. He celebrated every milestone with genuine excitement, which fueled my determination to push forward. He had a unique talent for making intricate topics crystal clear, which not only deepened my understanding but also provided a strong foundation for my research. His clarity and insight were pivotal in enabling me to conduct successful experiments and draw meaningful conclusions.

One of the most memorable experiences was taking his course in coordination chemistry. I vividly remember, Danny's teaching methods and explanations were nothing short of incredible. His teaching methods and explanations were exceptional, clarifying all my concepts and enabling me to conduct successful research. Danny's ability to understand his students' perspectives is unparalleled. He possesses a remarkable empathy and awareness of the challenges we face, and he consistently provides the support and guidance needed to overcome them. His approach fosters an environment of trust and respect, where students feel valued and motivated to excel. Those fortunate enough to be part of Danny's research group are truly blessed. His mentorship goes beyond academic instruction; it encompasses personal growth and professional development. Danny's unwavering dedication to his students' success is a testament to his exceptional character and commitment. In sum, Danny's influence has been transformative. His exceptional teaching, profound understanding, and unwavering support have left an indelible mark on my academic journey. I am deeply grateful for the privilege of having him as my mentor, and his impact will continue to resonate throughout my career. His ability to understand his students' perspectives is truly remarkable and unparalleled. I am fortunate enough to be in his research group are indeed blessed.

I am profoundly, incredibly, deeply, and immensely grateful to Danny for the enduring impact that will remain with me forever and beyond.

Another expression of gratitude goes to my co-supervisor, **Dr. Jeffery Warren**, for his steadfast support throughout my research journey. I am deeply grateful to, Dr. Jeff Warren, for his unwavering support throughout my research journey. His encouragement and insightful ideas have been instrumental in shaping my work and bolstering my confidence. Dr. Warren has a remarkable ability to create a supportive and empowering

environment for his students, making every interaction with him a source of comfort and reassurance.

I vividly recall the summer of 2021 when I took Dr. Warren's course. His teaching style was not only engaging but also transformative, making the subject matter fascinating and easy to grasp. Under his guidance, I gained invaluable knowledge and skills that proved invaluable in my academic pursuits. His encouragement during exams and presentations was particularly uplifting, instilling in me a sense of capability and determination. His feedback on my coursework was constructive and motivating, highlighting areas for improvement while acknowledging my strengths, which significantly boosted my confidence. His mentorship extended beyond the classroom, as he provided invaluable advice on assignments and exams, ensuring that I was well-prepared and confident in my abilities. Without his unwavering support and guidance, achieving a good grade and ultimately earning my degree would have been unattainable. His influence and assistance have played a crucial role in my academic journey at SFU, providing the foundation and encouragement necessary for my success.

During a challenging period when I was unwell, Dr. Warren provided invaluable assistance with my thesis writing. His timely support was crucial in enabling me to meet my submission deadline. I am profoundly grateful to him, knowing that without his assistance, achieving this milestone would have been considerably more difficult. His dedication not only benefited me but also alleviated stress for my entire family, underscoring the profound impact of his mentorship and support.

Dr. Warren's role in my academic journey has been indispensable, and I attribute a significant part of my success and degree attainment to his guidance. I am filled with gratitude beyond words for his unwavering support, encouragement, and belief in my abilities. His mentorship has not only shaped my academic achievements but has also inspired me to strive for excellence in all aspects of my life.

I would further like to thank my supervisory committee **Dr. Corina Andreoiu** and **Dr. Robert Britton**, for their exceptional support and guidance. Their priceless guidance significantly impacted my research's progress. Their invaluable insights during committee meetings significantly helped me in advancing my research.

One of the most important aspects of life is having the support of both family and friends. I am deeply grateful to my family—my father, mother, brother, and sister—for their incredible motivation. I am grateful to my mother for being my greatest source of inspiration, and to my sister for being my strongest pillar of support. She will undoubtedly be the happiest person to witness me receiving my degree.

My degree would not have been possible without my husband's support in managing all the responsibilities while I was at SFU. My husband's support was indispensable in enabling me to complete my degree at SFU. He effectively managed our son, household responsibilities, and external commitments while I focused on my research. His dedication and encouragement were irreplaceable throughout this journey.

I am also thankful to my son, daughter, and friends. Special thanks to Priyadarshini Balaraman for her unwavering and unconditional support throughout my journey. I am also grateful to my research group members, especially Jefferson Pells, Thomas Karpiuk, and Leanna Karn, for their guidance and availability whenever I needed them.

Finally, I am grateful to SFU. Without their financial support, this research would not have been feasible. Therefore, I would like to extend my personal thanks to SFU for their belief in both me and my project.

Table of Contents

Declaration of Committee ii
Abstract iii
Dedication iv
Acknowledgements v
Table of Contents ix
List of Tables xii
List of Figures xiii
List of Acronyms xvi

Chapter 1. Introduction 1
1.1. Coordination polymers 1
1.2. Components of Coordination polymers 2
1.2.1. Metal cations 2
1.2.2. Bridging ligands 3
1.2.3. Capping ligands 4
1.3. Synthesis of coordination polymers 4
1.3.1. Methods for synthesizing coordination polymers 6
1.4. Gold(I) in coordination complexes and polymers 6
1.4.1. Aurophilicity and its impact on the properties and structure of coordination complexes 7
1.5. Cyanometallate-based coordination polymers and $[Au(CN)_2]^-$ containing materials 9
1.5.1. $[Au(CN)_2]^-$ as a building block and its role and importance 11
1.6. Characterization of coordination polymers 11
1.6.1. Single crystal X-ray crystallography 11
Bragg's Law 12
A Simple derivation of Bragg's law 12
Symmetry and unit cell and space group 13
Symmetry in Crystals 13
Unit Cell 14
Space Group 14
Structure solution 15
Calculated versus Experimental Data: 15
1.6.2. Thermogravimetric Analysis (TGA) 17
1.6.3. FT-IR spectroscopy 17
1.6.4. Elemental analysis 18
1.6.5. Solid state emission spectroscopy 18

Chapter 2. Research Objectives 19
2.1. Pb(II) and the $d^{10}s^2$ stereochemical lone pair 19
2.2. Lead(II) Dicyanoaurate coordination polymers 20
2.3. Similarity between lead(II) and bismuth(III) with respect to lone pair 22
2.4. Building Blocks targeted in this research 23

Chapter 3. Synthesis and structures of bismuth-based complexes and cyanoaurate-containing materials 26
3.1. Introduction 26
3.2. Terpyridine-containing bismuth cyanoaurate complexes and coordination polymers 26
3.2.1. $[Bi(Terpy)(\mu\text{-}OH)]_2[Au(CN)_2]_4$ (1) 26
3.2.2. $Bi(Terpy)(NO_3)_2[Au(CN)_2](H_2O)$ (2) 29
3.2.3. $[Bi(terpy)(H_2O)(\mu\text{-}OH)]_2[Au(CN)_2]_4$ (3) 32
3.2.4. $Bi(Terpy)[Au(CN)_2]_2(NO_3)(DMSO)_2$ (4) 38
3.2.5. $[Bi(Terpy)(\mu\text{-}OH)(DMSO)_2]_2[Au(CN)_2]_4$ (5) 41
3.2.6. $Bi(Chloro\text{-}Terpy)(NO_3)_2[Au(CN)_2]$ (6) 44
3.2.7. $[Chloro\text{-}terpy\text{-}H_2](NO_3)[Au(CN)_2]\bullet H_2O$ (7) 46
3.3. Phenanthroline-containing bismuth cyanoaurate coordination polymers 48
3.3.1. $[Bi(Phen)_2(\mu\text{-}OH)]_2[Au(CN)_2]_4 \bullet 2MeOH$ (8) 48
3.3.2. $[Bi(Phen)_2(\mu{-}OH)(H_2O)]_2[Au(CN)_2]_2(CF_3SO_3)_2$ (9) 51
3.4. Bismuth(III) coordination complexes of terpy- and phen- based ligands 55
3.4.1. $Bi(Terpy)(H_2O)_2(\mu\text{-}OH)(Triflate)_2$ (10) 55
3.4.2. $Bi(4'\text{-}Amino\text{-}Terpy)(NO_3)_3$ (11) 57
3.4.3. $Bi(4'\text{-}para\text{-}bromoPhenyl\text{-}Terpy)(NO_3)_3$ (12) 59
3.4.4. $\{Bi(Phen)(NO_3)_2(\mu\text{-}OH)\}_2$ (13) 61
3.4.5. $[H\text{-}Phen][Bi(Phen)(NO_3)_4]$ (14) 62
3.4.6. $[H\text{-}Phen][Bi(Phen)Cl_3NO_3]$ (15) 64
3.4.7. $\{Bi(Phen)(H_2O)_2(\mu\text{-}OH)(Triflate)_2\}_2\bullet H_2O$ (16) 66
3.4.8. $[H\text{-}Phen][Bi(Phen)(NO_3)_4]$ polymorph (17) 68
3.5. Structural comparison of Bi(III) complexes and coordination polymers in this thesis 70
3.6. Global Conclusions and Future Work 74
3.7. Experimental Section 76
3.7.1. General procedures and physical measurements 76
3.7.2. Synthesis of $[Bi(Terpy)(\mu\text{-}OH)]_2[Au(CN)_2]_4$ (1) 77
3.7.3. Synthesis of $Bi(Terpy)(NO_3)_2[Au(CN)_2](H_2O)$ (2) 78
3.7.4. Synthesis of $[Bi(terpy)(H_2O)(OH)]_2[Au(CN)_2]_4$ (3) 78
3.7.5. Synthesis of $Bi(Terpy)[Au(CN)_2]_2(NO_3)(DMSO)_2$ (4) 78
3.7.6. Synthesis of $Bi(Terpy)(OH)(DMSO)_2[Au(CN)_2]_2$ (5) 78
3.7.7. Synthesis of $Bi(Chloro\text{-}Terpy)(NO_3)_2[Au(CN)_2]$ (6) 79
3.7.8. Synthesis of $[Chloro\text{-}terpy\text{-}H_2](NO_3)[Au(CN)_2]\bullet H_2O$ (7) 79
3.7.9. Synthesis of $[Bi(Phen)_2(\mu\text{-}OH)]_2[Au(CN)_2]_4 \bullet 2MeOH$ (8) 79
3.7.10. Synthesis of $[Bi(Phen)_2(\mu{-}OH)(H_2O)]_2[Au(CN)_2]_2(CF_3SO_3)_2$ (9) 80
3.7.11. Synthesis of $Bi(Terpy)(H_2O)_2(m\text{-}OH)(Triflate)_2$ (10) 80
3.7.12. Synthesis of $Bi(4'\text{-}Amino\text{-}Terpy)(NO_3)_3$ (11) 80
3.7.13. Synthesis of $Bi(4'\text{-}para\text{-}bromophenyl\text{-}Terpy)(NO_3)_3$ (12) 80
3.7.14. Synthesis of $\{Bi(Phen)(NO_3)_2(\mu\text{-}OH)\}_2$ (13) 81
3.7.15. Synthesis of $[H\text{-}Phen][Bi(Phen)(NO_3)_4]$ (14) 81
3.7.16. Synthesis of $[H\text{-}Phen][Bi(Phen)Cl_3NO_3]$ (15) 81

3.7.17. Synthesis of {Bi(Phen)(H_2O)$_2$(μ-OH)(Triflate)$_2$}$_2$•H_2O (16).....82
3.7.18. Synthesis of [H-Phen][Bi(Phen)(NO_3)$_4$]-Polymorph of (14-17) 82

References.....83

List of Tables

Table 3.1. Selected bond lengths and angles for 1. 28
Table 3.2. Selected bond lengths and angles in 2. 31
Table 3.3. Selected bond lengths and angles in 3. 38
Table 3.4. Selected bond lengths and angles in 4. 41
Table 3.5. Selected bond lengths and angles in 5. 44
Table 3.6. Selected bond lengths and angles in 6. 46
Table 3.7. Selected bond lengths and angles in 7. 47
Table 3.8. Selected bond lengths and angles in 8. 51
Table 3.9. Selected bond lengths and angles in 9. 54
Table 3.10. Selected bond lengths and angles for 10. 57
Table 3.11. Selected bond lengths and angles for 11. 59
Table 3.12. Selected bond lengths and angles for 12. 60
Table 3.13. Selected bond lengths and angles for 13. 62
Table 3.14. Selected bond lengths and angles for 14. 64
Table 3.15. Selected bond lengths and angles for 15. 66
Table 3.16. Selected bond lengths and angles for 16. 68
Table 3.17. Selected bond lengths and angles for 17. 70
Table 3.18. Structural comparisons of the coordination polymers and complexes in this thesis. 71

List of Figures

Figure 1.1 Using nodes (metals) and bridging ligands to make 1-D, 2-D and 3-D coordination polymer frameworks. 3

Figure 1.2. Graphical Derivation of Bragg's Law (Picture source: https://testbook.com/physics/braggs-law) 12

Figure 1.3. Cartoon of asymmetric unit and unit cell (Image source: https://pdb101.rcsb.org/) 13

Figure 2.1. Holodirectional and Hemidirectional coordination sphere 19

Figure 2.2. Selected prior Leznoff group lead (II) cyanoaurate coordination polymers 21

Figure 2.3. Capping ligands used in this thesis 23

Figure 3.1. Crystal structure of $[Bi(Terpy)(\mu\text{-}OH)]_2[Au(CN)_2]_4$ (1), focusing on the asymmetric unit. Colour Scheme: Carbon, gray; Nitrogen, blue; Oxygen, red; Gold, yellow; Bismuth, purple. 27

Figure 3.2 Coordination sphere of the bismuth centre in $[Bi(Terpy)(\mu\text{-}OH)]_2[Au(CN)_2]_4$ (1) 27

Figure 3.3. Polymeric supramolecular structure of $[Bi(Terpy)(\mu\text{-}OH)]_2[Au(CN)_2]_4$ (1). Colour Scheme: Carbon, gray; Nitrogen, blue; Oxygen, red; Gold, yellow; Bismuth, purple. 28

Figure 3.4. Solid state emission spectrum of $[Bi(Terpy)(\mu\text{-}OH)]_2[Au(CN)_2]_4$ (1). 29

Figure 3.5. Dimeric form of $Bi(Terpy)(NO_3)_2[Au(CN)_2](H_2O)$ (2). Colour Scheme: Carbon, gray; Nitrogen, blue; Oxygen, red; Gold, yellow; Bismuth, purple. 30

Figure 3.6. Coordination sphere of the bismuth centre in $Bi(Terpy)(NO_3)_2[Au(CN)_2](H_2O)$ (2) 31

Figure 3.7. Supramolecular 1-D chain structure of $[Bi(terpy)(H_2O)(\mu\text{-}OH)]_2[Au(CN)_2]_4$ (3). Colour Scheme: Carbon, gray; Nitrogen, blue; Oxygen, red; Gold, yellow; Bismuth, purple. 33

Figure 3.8. Coordination sphere of Bi1 and Bi2 in $[Bi(Terpy)(H_2O)(\mu\text{-}OH)]_2[Au(CN)_2]_4$ (3). 34

Figure 3.9. Au-Au 1-D chain motifs in $[Bi(Terpy)(H_2O)(\mu\text{-}OH)]_2[Au(CN)_2]_4$ (3). Colour Scheme: Carbon, gray; Nitrogen, blue; Oxygen, red; Gold, yellow; Bismuth, purple. 34

Figure 3.10. Solid state emission spectra of $[Bi(terpy)(H_2O)(\mu\text{-}OH)]_2[Au(CN)_2]_4$ (3) at 77K (top) and room temperature (below) 35

Figure 3.11. Thermo-gravimetric analysis (TGA) traces of $[Bi(terpy)(H_2O)(\mu\text{-}OH)]_2[Au(CN)_2]_4$ 36

Figure 3.12. First derivative of the TGA data for $[Bi(terpy)(H_2O)(\mu\text{-}OH)]_2[Au(CN)_2]_4$ 37

Figure 3.13. Crystal structure of $Bi(Terpy)[Au(CN)_2]_2(NO_3)(DMSO)_2$ (4). Colour Scheme: Carbon, gray; Nitrogen, blue; Oxygen, Sulphur Dark yellow; red; Gold, yellow; Bismuth, purple 39

Figure 3.14. 1-D zig-zag chain structure of Bi(Terpy)[Au(CN)$_2$]$_2$(NO$_3$)(DMSO)$_2$ (4) Colour Scheme: Carbon, gray; Sulphur, pale yellow ; Nitrogen, blue; Oxygen, red; Gold, yellow; Bismuth, purple. 40

Figure 3.15. Coordination sphere of Bi in Bi(Terpy)[Au(CN)$_2$]$_2$(NO$_3$)(DMSO)$_2$ (4). Colour Scheme: Carbon, gray; Nitrogen, blue; Oxygen, red; Bismuth, purple. 40

Figure 3.16. Crystal structure of [Bi(Terpy)(μ-OH)(DMSO)$_2$]$_2$[Au(CN)$_2$]$_4$ (5). Colour Scheme: Carbon, gray; Nitrogen, blue; Oxygen, red; Gold, yellow; Bismuth, purple. 42

Figure 3.17. 1-D chain structure of [Bi(Terpy)(μ-OH)(DMSO)$_2$]$_2$[Au(CN)$_2$]$_4$ (5). Colour Scheme: Carbon, gray; Nitrogen, blue; Oxygen, red; Gold, yellow; Bismuth, purple. 43

Figure 3.18. Coordination sphere of Bi in [Bi(Terpy)(μ-OH)(DMSO)$_2$]$_2$[Au(CN)$_2$]$_4$ (5) .. 43

Figure 3.19. Solid state emission spectrum of [Bi(Terpy)(μ-OH)(DMSO)$_2$]$_2$[Au(CN)$_2$]$_4$ (5) 44

Figure 3.20. Dimer of Bi(Chloro-Terpy)(NO$_3$)$_2$[Au(CN)$_2$] (6). Colour Scheme: Carbon, gray; Nitrogen, Blue; Oxygen, red; Gold, yellow; Bismuth, purple, Chlorine, green. 45

Figure 3.21. Coordination sphere of Bi in Bi(Chloro-Terpy)(NO$_3$)$_2$[Au(CN)$_2$] (6) 46

Figure 3.22. Solid-state structure of [Chloro-terpy-H$_2$](NO$_3$)[Au(CN)$_2$]•H$_2$O (7). Colour Scheme: Carbon, gray; Nitrogen, blue; Oxygen, red; Gold, yellow; Chlorine, green. 47

Figure 3.23. Asymmetric unit of the solid-state structure of [Bi(Phen)$_2$(μ-OH)]$_2$[Au(CN)$_2$]$_4$ • 2MeOH (8). Colour Scheme: Carbon, gray; Nitrogen, blue; Oxygen, red; Gold, yellow; Bismuth purple. 49

Figure 3.24. Coordination sphere of [Bi(Phen)$_2$(μ-OH)]$_2$[Au(CN)$_2$]$_4$ • 2MeOH (8). Colour Scheme: Nitrogen, blue; Oxygen, red; Bismuth purple. 49

Figure 3.25. 1-D chain structure of [Bi(Phen)$_2$(μ-OH)]$_2$[Au(CN)$_2$]$_4$ • 2MeOH (8). Colour Scheme: Carbon, gray; Nitrogen, blue; Oxygen, red; Gold, yellow; Bismuth, purple. Solvent molecules are omitted for clarity. 50

Figure 3.26. Gold-Gold interaction in [Bi(Phen)$_2$(μ-OH)]$_2$[Au(CN)$_2$]$_4$ • 2MeOH (8). Colour Scheme: Carbon, gray; Nitrogen, blue; Oxygen, red; Gold, yellow; Bismuth, purple. Solvent molecules are omitted for clarity. 50

Figure 3.27. Solid-state structure of Bi(Phen)$_2$(μ−OH)(H$_2$O)]$_2$[Au(CN)$_2$]$_2$(CF$_3$SO$_3$)$_2$ (9). Colour Scheme: Carbon, gray; Nitrogen, blue; Oxygen, red; Gold, yellow; Sulfur, yellow; Fluorine, green; Bismuth, purple. 52

Figure 3.28. Coordination sphere of bismuth in Bi(Phen)$_2$(μ−OH)(H$_2$O)]$_2$[Au(CN)$_2$]$_2$(CF$_3$SO$_3$)$_2$ (9). 53

Figure 3.29. Aurophilic interaction in Bi(Phen)$_2$(μ−OH)(H$_2$O)]$_2$[Au(CN)$_2$]$_2$(CF$_3$SO$_3$)$_2$ (9). Colour Scheme: Carbon, gray; Nitrogen, blue; Oxygen, red; Gold, yellow; Sulfur, yellow; Fluorine, green; Bismuth, purple. 53

Figure 3.30. Structure of Bi(Terpy)(H$_2$O)$_2$(μ-OH)(Triflate)$_2$ (10). Colour Scheme: Carbon, gray; Nitrogen, blue; Oxygen, red; Sulfur, yellow; Fluorine, green; Bismuth, purple. 56

Figure 3.31 Coordination sphere of Bi(III) in Bi(Terpy)(H$_2$O)$_2$(μ-OH)(Triflate)$_2$ (10) 56

Figure 3.32 Structure of Bi(4'-Amino-Terpy)$(NO_3)_3$ (11). Colour Scheme: Carbon, gray; Nitrogen, blue; Oxygen, red; Bismuth, purple. 58
Figure 3.33. Coordination sphere of Bi(4'-Amino-Terpy)$(NO_3)_3$ (11) 58
Figure 3.34. Bi(Bromo-Phenyl-Terpy)$(NO_3)_3$ (12). Colour Scheme: Carbon, gray; Nitrogen, blue; Oxygen, red; Bismuth, purple; Bromine, pale yellow.....60
Figure 3.35. Coordination sphere of Bi(Bromo-Phenyl-Terpy)$(NO_3)_3$ (12).....60
Figure 3.36. Structure of {Bi(Phen)$(NO_3)_2$(μ-OH)}$_2$ (13). Colour Scheme: Carbon, gray; Nitrogen, blue; Oxygen, red; Bismuth, purple. 61
Figure 3.37. Coordination Sphere of {Bi(Phen)$(NO_3)_2$(μ-OH)}$_2$ (13). Two Bi-O2 bonds are present, but only one is shown. 62
Figure 3.38. Structure of [H-Phen][Bi(Phen)$(NO_3)_4$] (14). Colour Scheme: Carbon, gray; Nitrogen, Blue; Oxygen, red; Bismuth, purple. 63
Figure 3.39. Coordination sphere of [[H-Phen][Bi(Phen)$(NO_3)_4$] (14) 63
Figure 3.40. Structure of [H-Phen][Bi(Phen)Cl_3NO_3] (15). Colour Scheme: Carbon, gray; Nitrogen, Blue; Oxygen, red; Chlorine, green; Bismuth, purple. 65
Figure 3.41. Coordination sphere of [H-Phen][Bi(Phen)Cl_3NO_3] (15) 65
Figure 3.42. Structure of {Bi(Phen)$(H_2O)_2$(μ-OH)(Triflate)$_2$}$_2$•H_2O (16), Colour Scheme: Carbon, gray; Nitrogen, Blue; Oxygen, Red; Fluorine, green; Sulfur, yellow; Bismuth, purple. 67
Figure 3.43. Coordination sphere of Structure of {Bi(Phen)$(H_2O)_2$(μ-OH)(Triflate)$_2$}$_2$•H_2O....67
Figure 3.44. Structure of [H-Phen][Bi(Phen)$(NO_3)_4$] (17). Colour Scheme: Carbon gray; Nitrogen Blue; Oxygen, Red; Bismuth purple. 69
Figure 3.45. Coordination sphere of [H-Phen][Bi(Phen)$(NO_3)_4$] polymorph 17. 69

List of Acronyms

Å	Ångstrom
Bipy	4,4-bipyridine
°C	degree Celsius
1-D, 2-D, 3-D	1-dimensional, 2-dimensionla, 3-dimensional
DMF	*N*,*N*-Dimethylformamide
DMSO	Dimethylsulfoxide
DNA	Deoxyribonucleic acid
en	Ethylenediamine
FTIR	Fourier-Transform Infrared
MLCT	Metal-to-Ligand Charge Transfer
mmol	Millimole
MOF	Metal Organic Framework
Mol	Mole
MW	Molecular Weight
NMR	Nuclear Magnetic Resonance
Ph	Phenyl
Phen	1,10-Phenanthroline
Terpy	2,2':6',2"-Terpyridine
THF	Tetrahydrofuran
TGA	Thermogravimetric Analysis
Triflate	Trifluoromethanesulfonate

Chapter 1.

Introduction

1.1. Coordination polymers

Coordination polymers are a particular class of polymeric material consisting of repeating units created by the coordination of metal ions with bridging (often organic) ligands.[1] These materials contain a repeating 1D, 2D, or 3D network structure[2] and offer a variety of intriguing properties, including porosity, catalytic activity, magnetism, luminescence, and conductivity.[1] A subset of coordination polymers are metal-organic frameworks (MOFs),[3] which are classified in particular as porous materials using organic bridging ligands; they have a variety of uses, such as medication delivery, gas storage, and catalysis.[4] In coordination polymers, the ligands function as links or connectors, and the metal ions as nodes or vertices in a multi-dimensional framework structure. A three-dimensional network is generated by the coordination bonds between the cationic metal ions/nodes and ligands. By adjusting the kind and size of the metal ions and bridging ligands employed in the synthesis of coordination polymers, their properties can be customized.

Coordination polymers are a particular class of polymeric material consisting of repeating units created by the coordination of metal ions with bridging (often organic) ligands.[1] These materials contain a repeating 1D, 2D, or 3D network structure[2] and offer a variety of intriguing properties, including porosity, catalytic activity, magnetism, luminescence, and conductivity.[1] A subset of coordination polymers are metal-organic frameworks (MOFs),[3] which are classified in particular as porous materials using organic bridging ligands; they have a variety of uses, such as medication delivery, gas storage, and catalysis.[4] In coordination polymers, the ligands function as links or connectors, and the metal ions as nodes or vertices in a multi-dimensional framework structure. A three-dimensional network is generated by the coordination bonds between the cationic metal ions/nodes and ligands. By adjusting the kind and size of the metal ions and bridging ligands employed in the synthesis of coordination polymers, their properties can be customized.

Coordination polymers are promising materials for numerous applications, including:

Gas storage and separation: Coordination polymers' surface areas and potentially porous structures (especially for MOFs) make them potentially useful for gas storage and separation.[4] Their flexibility in the solid-state also allows tuning of their ability to uptake and release gases as a function of pressure.[5]

Catalysis: Due to their large surface area and distinctive structural characteristics, coordination polymers and especially, MOFs can be used as heterogeneous catalysts. Examples include the use of specific coordination polymers as catalysts for organic processes like oxidation and hydrogenation.[6]

Sensing: The optical and magnetic features of coordination polymers (depending on the choice of metal and ligand) make them suitable as materials for sensing applications. For instance, coordination polymers have been utilised as magnetic sensors for organic analytes (especially using the high/low-spin transition in Fe(II)) and others as fluorescence sensors for metal ions or toxic gases such as ammonia.[7]

Thus, coordination polymers are a rich area of research for materials science, chemistry, and engineering since they have a variety of features and uses and researchers worldwide have made substantial advancements in their design, synthesis, characterization, and applications.

1.2. Components of Coordination polymers

As mentioned above, coordination polymers are made up of two main components: metal ions and ligands, which can be either bridging or capping ligands, although at least one bridging unit is required to propagate the dimensionality.[1]

1.2.1. Metal cations

Metal ions act as the nodes and connect with bridging ligands via metal-ligand coordination bonds. Metal ions utilized span the entire periodic table, from main-group metals to transition-metals (the most common case) and f-block ions as well. Metal cations such as iron, cobalt, copper, zinc, and nickel are particularly common. The coordination polymer's structure and properties can be considerably impacted by the metal ion used.

The characteristics of the coordination polymer can also be influenced by the metal ion's oxidation state. For instance, copper(II) ions tend to form octahedral geometries while copper(I) ions are usually tetrahedral, which leads to very different network structures. In addition, the synthesis and characteristics of coordination polymers may be influenced by the size of the metal ion. Larger ligands with more binding sites may be necessary for larger metal ions to establish stable coordination bonds; with proper control, this can lead to a more porous structure with greater pore diameter. Thus, the structure, stability, porosity, and reactivity of coordination polymers can all be considerably influenced by the metal ion that is used. This thesis will focus on bismuth(III)-based coordination polymers, i.e., a $d^{10}s^2$ main-group metal centre with a potentially stereochemically active lone- pair.

1.2.2. Bridging ligands

Bridging ligands link the cationic metal nodes together into a multidimensional network. Thus, these ligands can coordinate to two or more metal ions at once, thus "bridging" them. These ligands typically have two or more coordination sites, which can bind to metal ions. Cyano, oxo, hydroxo, carboxylato, and thiocyanoato ligands are typical examples of anionic bridging ligands, which will be the focus of this thesis, although there are also limitless organic-based bridging ligands as well, such as 4,4'-bipyridine, 1,4-benzenedicarboxylate.[8] The geometry of the bridging ligand, which may be linear, square planar, or even octahedral, has a substantial impact on the overall geometry of the polymer. For instance, an octahedral bridging ligand may result in a 3- dimensional array while a linear bridging ligand may give a 1-dimensional chain.

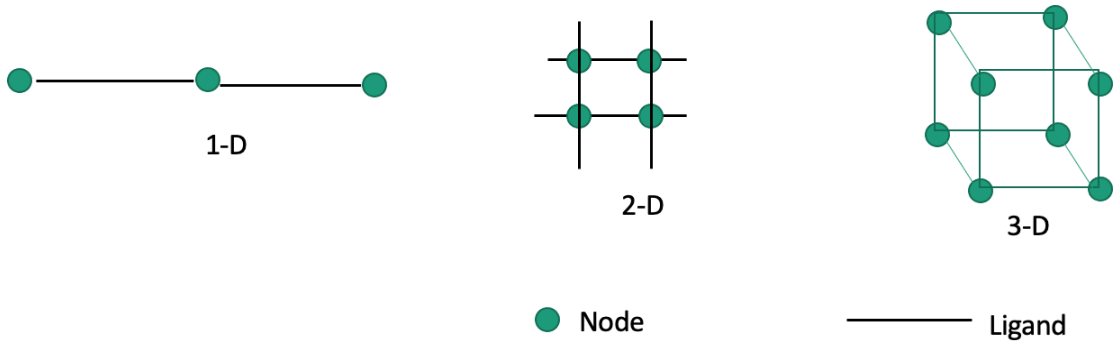

Figure 1.1 Using nodes (metals) and bridging ligands to make 1-D, 2-D and 3-D coordination polymer frameworks.

1.2.3. Capping ligands

Capping ligands are ligands that bind to one metal ion but don't bridge to another metal ion on the other side. These ligands can be described as "capping" the metal ion, blocking coordination sites, and can be mono- or multidentate. Monodentate ligands including halides, ammonia, and water are typical examples of capping ligands. However, typically, the capping ligands are multi-dentate ligands featuring donor atoms such as oxygen, sulphur, and nitrogen. By adjusting the coordination sphere of the cationic metal centre, they aid in maintaining a regular repeating structure and control the dimensionality. They can also bring additional physical and chemical properties to the system, e.g., if the ligand is emissive. Thus, depending on the selection of the metal centres as well as the bridging and capping ligands, a wide range of physical and chemical properties of interest can be designed and incorporated into the material, including optical, magnetic, or conductive properties. Due to the flexible structure of these polymers, one or more of these fascinating characteristics can be incorporated into the polymeric framework.

To further increase the dimensionality of the structure, coordination polymers can also harness several additional weak interactions in addition to direct coordination around the cationic metal centres. These weak interactions include hydrogen bonding, pi-pi stacking, van der Waals forces, ionic/dipole interactions, and metal-metal interactions. The strength of these forces typically ranges from 5 to 120 kJ/mol.[9]

1.3. Synthesis of coordination polymers

The general procedures for the synthesis of coordination polymers are as follows:[1]

1. Selection of metal ions and organic ligands: As noted above, the formation of coordination polymers depends on the selection of metal ions and bridging and capping ligands. The ligands should be chosen to propagate a particular dimensionality and cap a given number of coordination sites, whereas the metal ions should be chosen to favour a particular coordination geometry and incorporate properties of interest.

2. Solvent. The solvent utilized in the synthesis also can impact the structure and properties, particularly on whether it can act as a donor/capping ligand or not. For example, water is often used as a solvent for the synthesis of coordination polymers, particularly hydrophilic ones, and it also can remain bound to the metal cation, thereby

restricting the ability of bridging ligands to bind and limiting the dimensionality growth. A wide range of organic solvents can also be used in coordination polymer synthesis, including methanol, ethanol, isopropanol, acetonitrile, DMF, DMSO, and THF. Since organic solvents can more easily dissolve non-polar ligands, they are frequently chosen for the synthesis of hydrophobic coordination polymers; most of the examples above can still act as donors, or at least be incorporated into the final crystalline products, and thus impact the structure. Blends of solvents can also be used, particularly to ensure solubility of both metal and ligand units simultaneously.

3. Mixing of metal ions and bridging/capping ligands: The metal ions and organic ligands are dissolved in an appropriate solvent (as noted above) and combined. The desired reaction conditions, the solubility of the metal ions and organic ligands, and the solvent of choice are all considerations. Upon mixing, coordination bonds that connect the metal ions and organic ligands into a multi-dimensional network develop; this can either generate a rapid precipitate (especially if the resulting material is high dimensionality) or the components can remain in solution.

4. Crystallization: If the precipitation of the product is not too rapid (or forms a powder), then ideally the coordination polymer product would slowly form crystals from the solution. The form and size of the crystals is strongly affected by the crystallization conditions, and a great deal of effort is made in controlling and modifying the conditions (concentration, solvent type/blend, speed of diffusion, evaporation etc.) to favour slow formation of high-quality single crystals for further analysis.[10]

5. Purification: If crystals can be obtained, the crystals are washed and purified with solvents in which they do not dissolve, to remove any impurities, including any unreacted metal ions or ligands.

6. Characterization: To examine the structure, characteristics, and prospective applications of the coordination polymer, a variety of methods are used, including X-ray diffraction, spectroscopy, and thermal analysis; these are outlined in further detail below.

Overall, careful metal ion and capping/bridging ligand selection, control of stoichiometry and counterion choice, and reaction condition optimization are necessary for the synthesis of coordination polymers to produce a clean, isolable material.

1.3.1. Methods for synthesizing coordination polymers

Typically, the synthesis is carried out on the benchtop at room temperature using solvents that are benign to the environment, including water, methanol, or ethanol.[11] Additional solvents used in the production of coordination polymers in this thesis include methanol, acetonitrile, DMSO, nitromethane and DMF. The appropriate solvent is used to dissolve each component. As noted above, the amount of free coordination sites on the metal cation is often reduced by adding capping ligands first, but an extended network can only form if there are still at least two coordination sites on the metal cation. The bridging ligand is then added to the metal/capping ligand mixture. As noted above, if the synthesis proceeds, one of two things may occur: either the solvent slowly evaporates, resulting in crystals of a coordination polymer, or a coordination polymer immediately precipitates. There are several widely used methods that regulate the crystallisation of appropriate material, but the details of crystal growth techniques are beyond the scope of this introduction. That said, generally there are two types of synthesis/crystallization processes for coordination polymers: conventional and non-conventional; in conventional synthesis, any additional energy is provided by conventional electric heating. On the other hand, in unconventional synthesis, alternative energy inputs such as microwave heating, electrochemistry, mechanochemistry, or sonochemistry can add energy to the mixture. Note that in this thesis, only very standard room-temperature bench-top mixing procedures were utilized and other methods, such as solvothermal or hydrothermal synthesis, which involves heating the ligands and metal ions or clusters under high pressure in a sealed vessel above the boiling point of the solvent (or water, in the case of hydrothermal) followed by slow cooling to form crystals, was not used. Other methodologies, including microwave-assisted synthesis (where the reaction mixture is microwave-irradiated, causing a quick heating and cooling process to form coordination polymers) or gas-phase synthesis (utilizing gas-phase deposition of each component, often to form thin-films), exist but were not used herein.[1]

1.4. Gold(I) in coordination complexes and polymers

Gold has always drawn attention because of its distinctive appearance, as well as its physical and chemical properties. Although gold in its metallic form is famously chemically inert, the most prevalent oxidation state in the field of molecular gold chemistry

is gold(I), followed by gold(III).[12] The gold(I) ion has gained considerable attention because of the discovery of an unusual tendency for gold(I) atoms to behave as though they are attracted in the solid state, termed "aurophilicity" (see below), which is one of the central points of interest in this thesis. More generally, due to its distinctive chemical characteristics, which make it suited for a variety of applications in industries including medicine, electronics, and catalysis, gold(I) is a significant metal ion utilized in coordination compounds.[12] For example, d^{10} gold(I) forms stable complexes with biomolecules like proteins and DNA because it has a high affinity for ligands that include sulphur, such as thiolates.[13] Due to their ability to engage preferentially with cancer cells that have a high concentration of thiol-containing biomolecules, gold(I) complexes have been developed as possible anticancer treatments. More generally, gold(I) compounds can be used as catalysts in several different chemical processes.[14] They can be utilised, for instance, as homogeneous catalysts to convert alcohols into aldehydes and ketones, and as heterogeneous catalysts for the oxidation of carbon monoxide. Given the historical inertness of gold, this recognition that both gold(I) and gold(III) can be highly active catalysts has been very surprising.

In addition, many gold(I) complexes are luminescent, especially when incorporating aurophilic interactions; this makes them ideal as sensors for detecting metal ions, gases, and volatile organic compounds. Examples include the employment of specific gold(I) complexes as fluorescence probes for the detection of poisonous gases like carbon monoxide and nitrogen dioxide. The emissive properties of gold(I)-containing coordination polymers will be explored in this thesis. Hence, the unique properties of gold(I) make it an important metal ion in coordination chemistry, with many potential applications in various fields.

1.4.1. Aurophilicity and its impact on the properties and structure of coordination complexes

Aurophilicity is a term used in chemistry to describe the tendency of gold atoms or complexes to interact through attractive gold-gold interactions in a coordination complex or a molecule containing gold atoms.[15] In this thesis, this interaction is also employed to increase structural dimensionality. The properties of coordination complexes with gold(I) can be significantly impacted by aurophilicity. Aurophilic interactions can affect the

complex's solubility, stability, and emissive properties, among other physical and chemical characteristics.

Aurophilic interactions usually occur at distances greater than typical covalent bonding distances. Given this point, crystallographic data is frequently used to evaluate whether there are gold-gold interactions present, where an interaction between two or more gold(I) atoms is stated to exist when their distances from one another are less than the sum of their van der Waals radii, which is thought to be 3.6 Å.[16] Aurophilic Au-Au distances that range from as short as 2.8 Å up to 3.6 Å have been observed. In supramolecular chemistry, where aurophilic interactions can promote the self-assembly of molecules containing gold, aurophilicity is of special importance.

Aurophilic interactions are similar in strength to other fairly strong non-covalent interactions, with energies of approximately 20-50 kJ/mol, similar to some hydrogen bonds.[9] There are two key factors that influence how strong the aurophilic contact is overall: First, it is recognized that the van der Waals forces between the large, polarizable, closed-shell gold(I) atoms are the most important aspect. Also, gold(I) is subject to unusually powerful relativistic effects.[16] As a result, overall aurophilicity is sometimes referred to as a "super van der Waals" force. Aurophilicity can be used as a tool to modify supramolecular structures.

Simple gold(I) complexes that contain gold-gold interactions that increase their structural dimensionality can be seen in molecular AuR2 systems (R = ionic or neutral donors). Discrete molecules containing two or more gold(I) atoms can also join to form dimers through aurophilic interactions. This results in the formation of multidimensional systems.[17] Thus, overall, aurophilicity is an important phenomenon that has a significant impact on the characteristics and applications of coordination complexes containing gold(I) atoms. Its exploration and study have produced innovative materials with outstanding attributes and applications.

Critically, materials with aurophilicity are often luminescent.[18] Photoluminescence occurs when a material absorbs light and then re-emits it at a different wavelength, often in the visible range. The presence of gold-gold interactions, which lead to the creation of excited states with extended lifetimes, is generally mentioned as the cause of the photoluminescence that may be seen in several aurophilic compounds. These excited

states can emit light when they decay through radiative mechanisms like fluorescence or phosphorescence.

The structure and electronic characteristics of an aurophilic material may affect the process and energy of photoluminescence. In particular, the emission wavelength is known to be sensitive to the Au-Au distance in the material, with shorter distances leading to lower emission energies;[18] the Au-Au-Au angles in an aurophilic chain can also impact the observed energy.[19] Both fluorescent and phosphorescent emission can be observed, depending on the system. Also, in addition to, or instead of the aurophilicity-based emission, under some circumstances, the emission may be attributed to gold atom-based metal-to-ligand charge transfer (MLCT) transitions, although this is often more prominent at lower temperatures. Here are some examples of aurophilic compounds that exhibit photoluminescence:

• Gold(I) cyano/nitro complexes: These are small clusters of gold atoms that are stabilized by ligands. They often exhibit bright yellow or orange photoluminescence. Examples include $Pb(terpy)[Au(CN)_2]_2$ [20] and $[^nBu_4N]_2[Ln(NO_3)_4Au(CN)_2]$ (Ln = Nd, Eu, Tb, Ce).[21]

• Gold(I) alkynyl complexes: These are organometallic compounds that contain a gold atom bound to a carbon-carbon triple bond. They often exhibit red or near-infrared photoluminescence. Examples include $[Au(C{\equiv}CR)(PPh_3)]$ (R = Ph, Butyl).[22]

Overall, the study of photoluminescence in aurophilic compounds could provide insight into the electronic properties of these materials and their potential applications in areas such as optoelectronics, sensing, and imaging.[23]

1.5. Cyanometallate-based coordination polymers and $[Au(CN)_2]^-$ containing materials

Cyanometallate-containing coordination polymers refer to a class of coordination polymers that contain cyanometallate anions, termed $[M(CN)x]^{n-}$, as bridging ligands, where M can include a wide range of metals, such as Cr, Mn, Fe, Co, Ni, Pt and others, with geometries including linear (Ag, Au; see below), square-planar (Ni, Pd, Pt), octahedral (Cr-Co) and higher coordination numbers (e.g., Nb, W, Re etc.).[24] Cyanometallate-containing coordination polymers exhibit a variety of interesting properties, including magnetic, electrical, optical, and catalytic properties. These materials have received

significant attention in recent years due to their potential applications in fields such as sensors, electronics, and catalysis.

The most famous cyanometallate-containing coordination polymer - indeed, the first coordination polymer ever reported, in 1710 - is Prussian Blue ($Fe_4[Fe(CN)_6]_3 \bullet 14\ H_2O$), which is a well-known blue pigment originally used in paintings, but now used for a wide range of applications. Prussian Blue consists of an alternating array of Fe(II) and Fe(III) ions bridged by cyanide ligands, forming a three-dimensional cubic lattice structure; more specifically, the Fe(III) centres are N-bound to $Fe(II)(CN)_6$-units.[25]

Another well-studied series of cyanometallate coordination polymers are based on the tetra-cyanonickelate/platinate building blocks - these are termed Hofmann clathrates, $Ni(NH_3)_2[M(CN)_4]$ (M=Ni, Pd, Pt),which form a 2-D, square-planar network that is responsive the inclusion of guests between the sheets.[25]

Other examples of cyanometallate-containing coordination polymers include metal- organic frameworks (MOFs) such as Cu(I)-CN-based MOFs, Fe(II)-CN-based MOFs, and Zn(II)- CN-based MOFs. These materials have been studied for their gas storage and separation properties, as well as their potential applications in electrocatalysis and photocatalysis.[26]

In all cases, the cyanide anion functions as an ambidentate linearly bridging ligand. Both the nitrogen and the carbon atoms have a single pair of electrons that function as donors and can connect two metal centres. Additionally, the metal cation can provide electron density to the cyanide anion's antibonding orbitals, increasing the MC and MN bond strength (and decreasing the CN bond strength simultaneously); this can be monitored by IR and Raman spectroscopy.[24]

For this thesis, another particularly relevant example of a cyanometallate coordination polymer is $Zn[Au(CN)_2]_2$, which forms several polymorphs and is an excellent emission-based ammonia sensor.[27] In another related example, a series of Pb(II) dicyanoaurate-containing coordination polymers were prepared and show different structures depending on the coordination geometry of the Pb(II) centre: in $[Pb(1,10\text{-phenanthroline})_2][Au(CN)_2]_2$, the $Au(CN)_2^-$ units propagate a 2-D brick-wall structure, while in the case of $[Pb(2,2'\text{bipyridine})_2][Au(CN)_2]_2$, the 8-coordinate Pb(II) centre has more

asymmetric Pb-N bond lengths and the supramolecular structure forms a 1-D chain/ribbon motif.[20]

1.5.1. $[Au(CN)_2]^-$ as a building block and its role and importance

$[Au(CN)_2]^-$ is a linear, two-coordinate cyanometallate with a d^{10} Au(I) metal and can act as a bridging ligand, as with other cyanometallates. It is used in electroplating to deposit a thin layer of gold onto other metals, and it is also used in the extraction of gold from ores. Compared to other cyanometallates, the linear geometry of $[Au(CN)_2]^-$ can lead to more consistent coordination polymer superstructures. For instance, the only way to create a 1-D chain using $[Au(CN)_2]^-$ is by using the two trans-cyanides to create an M−NC−Au−CN−M chain. In addition, although the majority of cyanometallates can only create M-CN-M' linkages to increase structural dimensionality, $[Au(CN)_2]^-$ offers an extra way to boost structural dimensionality: via aurophilic interactions.[17] This is discussed further in Chapter 2.

1.6. Characterization of coordination polymers

Characterization refers to the process of determining the chemical and physical properties of the coordination polymers that were prepared, which is essential for understanding their behavior and potential applications. Some common methods utilized in this thesis to characterize coordination polymers are outlined below.

1.6.1. Single crystal X-ray crystallography

This is a technique used to determine the three-dimensional atomic structure of a crystalline material. To discover more about the arrangement of atoms within a crystal lattice, X- rays are used in this process. The method is widely used in biology, materials science, and chemistry to identify the structures of molecules, proteins, and other materials. In this method, an X-ray beam is directed towards a crystal, and the scattered/diffracted X-rays are detected, and their intensity measured. To determine the positions of the atoms within the crystal lattice, the X- ray diffraction pattern produced by the crystal is examined. Details of the theory behind X-ray diffraction are found in a wide range of textbooks,[28] but a brief summary is provided here:

Bragg's Law

Bragg's Law relates the angle at which X-rays are diffracted by the atomic planes in a crystal to the wavelength of the X-rays and the distance between the planes. The law is expressed as:

$$2d\sin\theta = n\lambda$$

where:

- d is the distance between the crystal planes,
- θ is the angle of incidence (and reflection) of the X-ray,
- λ is the wavelength of the X-rays,
- n is an integer (the order of the diffraction peak)

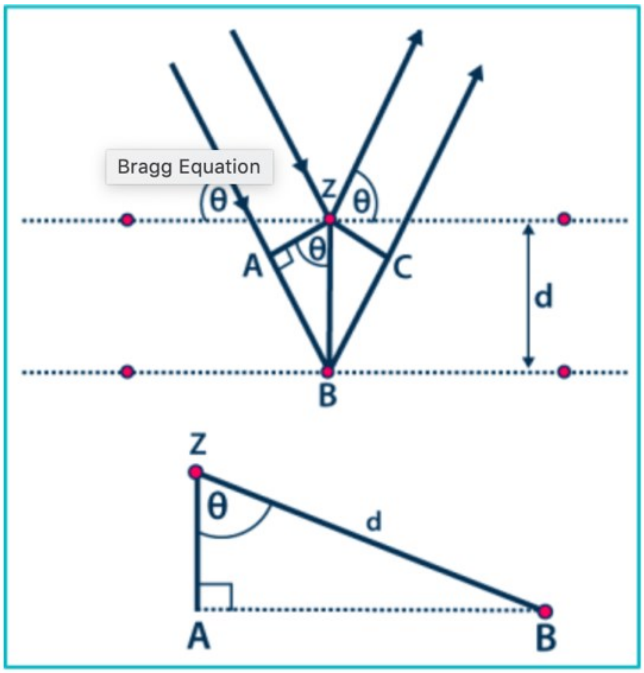

Figure 1.2. Graphical Derivation of Bragg's Law (Picture source: https://testbook.com/physics/braggs-law)

A Simple derivation of Bragg's law

Consider the figure of beams in Fig 1.2. The phases of the beams align when the incident angle match the reflecting angle. The incident beams stay parallel to each other until they reach point Z. At this point, they strike the surface and travel upwards. At point B, the

second beam is scattered. The distance traveled by the second beam is AB + BC. This additional distance is an integral multiple of the wavelength.

- $n\lambda = AB + BC$
- We also know that AB = BC
- $n\lambda = 2AB$ (equation 1)
- d is the hypotenuse of the right triangle ABZ. AB is the opposite of the angle θ.
- $AB = d \sin\theta$ (equation 2)
- Substituting equation 2 in equation 1, we get:

  $n\lambda = 2d \sin\theta$, which is the final expression for Bragg's law.

Symmetry and unit cell and space group

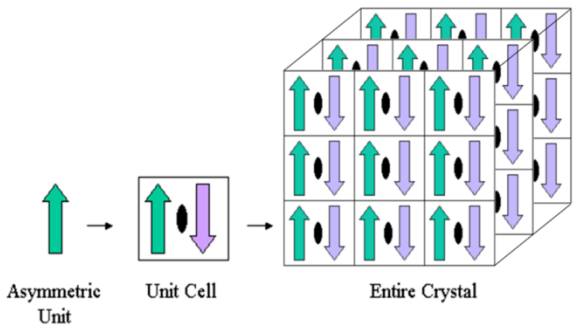

Figure 1.3. Cartoon of asymmetric unit and unit cell (Image source: https://pdb101.rcsb.org/)

Symmetry in Crystals

Symmetry in crystals refers to the orderly and repetitive arrangement of atoms, ions, or molecules in a crystalline material. This arrangement gives the crystal its overall shape and properties. The symmetry of a crystal can be described using the symmetry elements, specifically rotation axes, mirror planes, inversion centers, glide planes and screw axes.[28]

Unit Cell

The unit cell is the smallest repeating unit in the crystal lattice that, when repeated in all directions, generates the entire crystal structure (Figure 1.3). It is characterized by:

• **Lattice Parameters**: These include the lengths of the unit cell edges (a, b, c) and the angles between them (α, β, γ).

• **Lattice Points**: Points at which atoms, ions, or molecules are positioned. These points define the geometric arrangement within the unit cell.

The unit cell is classified into different types based on its geometry:

1. Primitive (P): Lattice points only at the corners.
2. Body-Centered (I): Lattice points at the corners and a single point in the center.
3. Face-Centered (F): Lattice points at the corners and at the centers of each face.
4. Base-Centered (C): Lattice points at the corners and in the centers of two opposite faces.

Space Group

Space groups describe the symmetry of the crystal in three dimensions, combining the translational symmetry of the lattice with the point symmetry of the unit cell. Each space group represents a unique combination of symmetry operations, including rotations, reflections, translations, and glide reflections.[28] There are 230 unique space groups, which are classified into seven crystal systems:

1. Cubic: High symmetry, with three equal axes at right angles (e.g., NaCl).
2. Tetragonal: One axis different in length, all axes at right angles (e.g., rutile TiO_2).
3. Orthorhombic: Three unequal axes at right angles (e.g., olivine).
4. Hexagonal: Two equal axes at 120° to each other, third axis perpendicular and different in length (e.g., graphite).

5. Trigonal (Rhombohedral): Axes are equally inclined and of equal length (e.g., calcite).

6. Monoclinic: Three unequal axes, with one axis (usually β) not at 90° (e.g., gypsum).

7. Triclinic: Three unequal axes, none at 90° (e.g., kyanite).

Space groups are essential for understanding and predicting the properties of crystals, as they provide a comprehensive description of the symmetry and arrangement of atoms within the crystal lattice.

Structure solution

Crystal structure solution involves determining the arrangement of atoms within a crystal. This process typically includes collecting diffraction data, calculating and comparing theoretical patterns to experimental data, and refining the structure to minimize discrepancies.

• Collection of Data: X-ray diffraction (XRD) or neutron diffraction is used to collect data. When a crystal is exposed to X-rays or neutrons, the waves are scattered by the atoms in the crystal, producing a diffraction pattern according to Bragg's Law.

• Diffraction Pattern Analysis: The diffraction pattern consists of spots (peaks) whose positions and intensities provide information about the crystal lattice and the atomic arrangement.

Calculated versus Experimental Data:

Using an initial model of the crystal structure, theoretical diffraction patterns are calculated. These patterns are based on the proposed positions and identities of atoms within the crystal. The actual diffraction pattern is obtained from the crystal experiment. The calculated diffraction pattern is compared to the experimental pattern. Discrepancies between the two highlight areas where the model may need refinement, which is an iterative process where the model is adjusted to improve the fit between the calculated and experimental diffraction patterns.

The R value (reliability factor) measures the agreement between the observed diffraction data and the data calculated from a proposed model of the crystal structure. A

lower R value indicates better agreement between the experimental data and the model, suggesting a more accurate crystal structure solution. Thus, the solution of a crystal structure involves collecting diffraction data, developing an initial model, comparing calculated and experimental diffraction patterns, and refining the model to achieve a good fit. The R value is a crucial parameter in evaluating the quality of the fit, and the refinement process aims to minimize this value, leading to a precise and accurate crystal structure.

From a practical perspective the process of determining a structure using single crystal X-ray crystallography typically involves the following steps:

1. **Obtaining a high-quality single crystal**: To generate a high-quality diffraction pattern, a single crystal of the molecule of interest must be grown that is of sufficient size and quality to produce a good diffraction pattern.

2. **Collecting X-ray diffraction data**: The crystal is mounted on a goniometer and exposed to a beam of X-rays. A diffraction pattern appears on a detector because of the X-rays diffracting off the crystal's atoms. The detector keeps track of each diffraction spot's intensity and location, which can be used to determine the molecule's structure.

3. **Solving the structure**: The diffraction pattern is used to determine the arrangement of atoms, specifically, their electron density, which would produce the observed diffraction pattern. This process is known as solving the structure, and is accomplished using computational techniques embedded in the X-ray crystallographic software.

4. **Refining the structure**: Once the initial structure has been solved, the atomic positions are refined to improve the accuracy of the model. This involves adjusting the positions of the atoms to better fit the observed diffraction data, using a statistical measure termed the "R-value" to represent the difference between the observed and calculated diffraction pattern. A lower R-value indicates a better agreement and a higher-quality structure.

5. **Validating the structure**: The final step involves validating the structure to ensure that it is accurate as well as reliable. To do this, it may be necessary to examine the model for flaws or consistency issues, compare the structure to the molecule's

known chemical and physical characteristics, and confirm that the model is consistent with other experimental results.

Overall, single crystal X-ray crystallography is a very potent method for figuring out the three-dimensional structure of molecules. It has had a significant impact on how we understand molecular structure and function and has aided in the development of several scientific fields, including chemistry, biochemistry, and materials science.

1.6.2. Thermogravimetric Analysis (TGA)

The TGA technique probes the thermal stability of materials by measuring changes in their mass as a function of temperature or time. A small quantity (several mg) of the substance is heated in a controlled setting while the weight is continuously tracked. The substance may experience physical or chemical changes when the temperature rises, such as evaporation, decomposition, ligand-loss, oxidation, or reduction, which can cause a loss or gain in mass. The TGA instrument records changes in mass that depend on temperature or time and produces a thermogram, which is a graphical depiction of the data. This data illustrates a combination of composition, purity and for this thesis, stability with respect to ligand loss and decomposition and the temperatures at which those occur. The mass losses can be matched sometimes to mass- fragments of the material.

1.6.3. FT-IR spectroscopy

This is a spectroscopic technique used to study the vibrational modes of molecules. In this thesis the cyanide CN bond vibration is of particular interest, and is typically in the region of 2000- 2250 cm^{-1} in cyanometallates. The CN stretching frequency is sensitive to both the metal to which it is C-bound, as well as whether the N-terminus is bound to an additional metal or not, and how strongly it is bound; hydrogen-bonding interactions with the N-terminus can also impact the ν(CN) stretch. Thus, valuable structural and electronic information can be gained by from analyzing the CN-stretching frequency region. The presence of other functional groups, especially anions such as nitrato or triflate, can also be confirmed using IR spectroscopy.

1.6.4. Elemental analysis

Identifying the presence and %-amount of the elements carbon (C), hydrogen (H), nitrogen (N), and sulphur (S) in a specific sample is known as elemental analysis (CHNS). In a combustion chamber, typically with oxygen present, a small portion of the sample is burned to completely oxidise all the carbon, hydrogen, nitrogen and sulphur, resulting in carbon dioxide, water, nitrogen-oxides and sulphur dioxide, respectively. The gases produced during the combustion process are then separated and detected, mainly using gas chromatography. The CHNS% values are then utilized to help determine the composition of the coordination polymer in question, especially the relative stoichiometry of metal:ancillary ligand:cyanometallate bridging ligand.

1.6.5. Solid state emission spectroscopy

This spectroscopic technique probes the excitation/absorption and emission of light from a solid material;[29] solution-analogues are more common, but in this thesis the emissive properties of solid-state cyanoaurate-based materials are examined. In this technique, the sample is scanned with an exciting energy at a particular wavelength (the excitation energy), and the emitted light is collected with a detector and its wavelength and intensity graphed.

Chapter 2. Research Objectives

2.1. Pb(II) and the $d^{10}s^2$ stereochemical lone pair

Lead(II) has a $5d^{10}6s^26p^0$ electronic configuration. Although the s^2 electrons, situated in the s-orbital, are formally spherical and therefore should not occupy any specific region of the coordination sphere, depending on the ligands on Pb(II), s-p mixing can occur to different extents and the lone-pair can become what is called "stereochemically active", and thereby occupy a specific region of the coordination sphere. When the lone-pair is evenly distributed (i.e., is mostly in the s-orbital), then the coordination sphere is not impacted significantly by this lone-pair and the coordination environment is termed "holo-directional" (Figure 2.1). Conversely, if the ligands induce a stereochemically active lone-pair then the coordination sphere will be very asymmetric, and the lone-pair position can be readily observed; in this case the coordination sphere is termed "hemi- directional. [20,30] The extent of this stereochemical activity can be determined primarily using X-ray crystallography, where a hemi-directional coordination sphere shows a broad range of short and very long M-L bond lengths (in which the position of the very long lengths indicates the lone-pair position; Figure 2.1). ^{207}Pb Solid-state NMR spectroscopy has also been used to spectroscopically measure the extent of stereochemical activity in Pb(II) complexes.[31] Generally, the more basic and "harder" the ligands used, the more stereochemically active the lone-pair on Pb(II) becomes.[32]

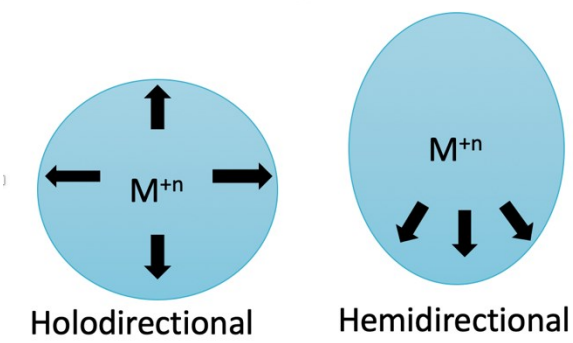

Figure 2.1. Holodirectional and Hemidirectional coordination sphere

Lead(II)-containing compounds are crucial in a variety of applications, particularly in materials science, due in part to the lone-pair characteristics; they are often featured in

materials with piezo-electric and ferroelectric behaviour, materials with high birefringence/refractive index, and in solar cells.[20] and refs. therein

Thus, lead(II), with its potentially stereochemically active lone pair, can form coordination bonds with ligands to produce intricate structures where both the coordination sphere and the supramolecular structure are impacted by the lone pair. Considering the properties of molecules containing lead(II) and the remarkable coordination chemistry of lead(II), it is surprising that the inclusion of lead(II) into coordination polymers has gotten so little attention historically. However, in recent years, research has focused on investigating the function of lead(II) and its lone pair in coordination polymers in efforts to exploit this lone pair of lead(II) as a design element and as a source of chemical properties of interest. There is now a substantial literature regarding lead(II)- based coordination polymers.[33]

2.2. Lead(II) Dicyanoaurate coordination polymers

The Leznoff group has previously prepared a range of Pb(II)-containing coordination polymers using $[Au(CN)_2]^-$ as the bridging unit, with the fundamental goals of exploring the impact of the lone-pair on the supramolecular structures of these cyanometallate coordination polymers, while also exploring their properties, particularly their emission (from aurophilic interactions) and their birefringence. In collaboration with the Kroeker group (Univ. Manitoba), solid-state ^{207}Pb- NMR spectroscopy was utilized to quantify the extent of stereochemical activity of the Pb(II) lone- pairs in the systems.[31] A few representative examples of this prior work are shown below:

- $Pb(H_2O)[Au(CN)_2]_2$: In this 2-D slab structure (Figure 2.2, left), the eight-coordinate lead(II) centre exhibits an asymmetry in the lengths of the bonds towards one of the lead(II)'s hemispheres, indicating that the lead(II) is stereochemically active and produces a hemidirectional structure. The dehydrated version, $Pb[Au(CN)_2]_2$, is a 3-D structure with a much more symmetric (and therefore less stereochemically active) lone-pair: the structure consists of a lead(II)centre surrounded by eight N-bound cyanides, with approximately equally Pb-N bond lengths. These materials also contain aurophilic interactions and show substantial birefringence.[34]

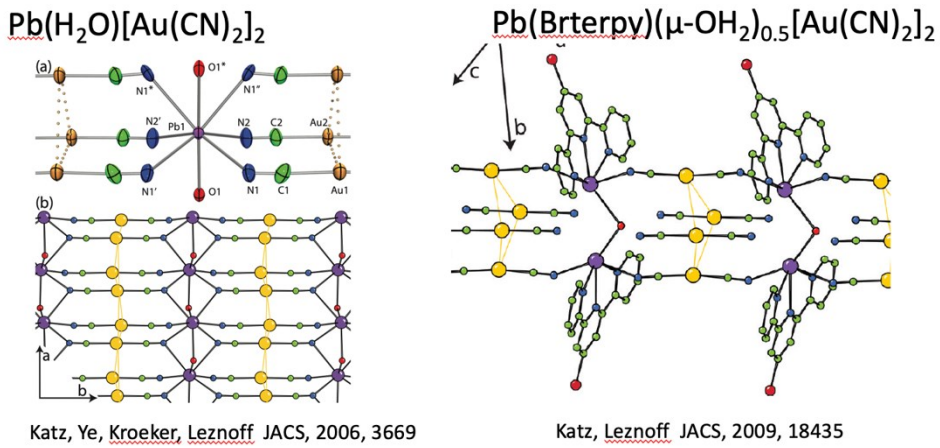

Figure 2.2. Selected prior Leznoff group lead (II) cyanoaurate coordination polymers

Pb(Brterpy)(μ-OH_2)$_{0.5}$[$Au(CN)_2$]: This compound has a stereochemically active lone pair, which contributes to its high birefringence. The Pb(II) center in Pb(Brterpy)(μ-OH_2)$_{0.5}$[$Au(CN)_2$] is six-coordinate, being bonded to a Br-terpy unit, two $Au(CN)_2^-$ units, and a bridging water molecule (Figure 2.2, right). Additionally, two cyanide units may also be associated with the Pb(II): one unit is approximately 3.3 Å away, which is longer than any other reported Pb−N bond lengths, while the second cyanide is closer but is crystallographically disordered. Depending on whether or not those long interactions were included the Pb(II) coordination could be octahedral or a distorted pentagonal bipyramid. The cyanourate anions form a tetranuclear cluster. The birefringence of the crystal is influenced by the orientation of its molecular components and was measured to be 0.26.

Pb(phen)$_2$[$Au(CN)_2$]$_2$: This compound is another example of a two-dimensional lead(II) coordination polymer, with an eight-coordinate distorted square-antiprismatic lead(II) core containing two trans-phen ligands in the lead(II) coordination sphere. The remaining four sites are occupied by two sets of N-bound cyanides that are also trans to one another. This Pb(II) centre is mostly holo-directional, consistent with the lower basicity of phen relative to another related example, Pb(bipy)$_2$[$Au(CN)_2$]$_2$, which is a 1-D chain with an eight-coordinate distorted square lead(II) centre with two bipy units that bind cis to the lead(II).[20]

Pb(en)[$Au(CN)_2$]$_2$: It has a complex topological structure, including a coordination-bonded 1-D zigzag chain with $Au(CN)_2^-$ units at the chain's termini, which form weak

aurophilic interactions of 3.3798 Å, which link the chains into a 2-D sheet. Given the greater basicity of the ethylenediamine ligand, this Pb(II) centre has an even more distinct stereochemically active lone-pair and the lowest coordination number (5), along with a rare Pb-Au interaction.[20]

2.3. Similarity between lead(II) and bismuth(III) with respect to lone pair

Both lead and bismuth are members of the same period; lead has an electronic configuration of [Xe]$4f^{14}$ $5d^{10}$ $6s^2$ $6p^2$, which readily loses the 6p-electrons to generate Pb(II), with an s^2 lone-pair, as described above. Similarly, bismuth has the electronic configuration [Xe] $4f^{14}$ $5d^{10}6s^26p^3$, where the 6p-electrons are again easily lost, forming Bi(III), which has the same electronic configuration of Pb(II), with the same (formally) s^2 lone-pair, i.e., the two are isoelectronic $d^{10}s^2$ systems.[33] Generally, like Pb(II), bismuth(III) has a huge coordination sphere, is polarizable, and has coordination numbers ranging from 3-10.

Thus, the properties and applications of materials that contain a Pb(II) stereochemically active lone-pair can theoretically be manifested in the electronically similar Bi(III) systems. This is of particular importance because, unlike highly toxic Pb, bismuth is a non-toxic element; indeed, it is the active ingredient in Pepto-Bismol, a common remedy for upset stomach. However, there is much less research conducted on bismuth(III) coordination polymers,[33] and the bismuth cyanoaurate-based coordination polymers analogous to the aforementioned Pb(II) cyanoaurate materials remain unexplored.

Ultimately, the goal of the research is to determine whether bismuth can take the place of lead in cyanoaurate-containing coordination polymers, investigate structural trends and the extent of the stereochemical activity of the lone-pair in Bi(III) vs. Pb(II) and explore the properties (especially emission) of the resulting bismuth-cyanoaurate coordination polymer materials.

2.4. Building Blocks targeted in this research

As discussed in Chapter 1, there are a wide variety of ligands that can be used in the synthesis of coordination polymers, ranging from simple monodentate ligands to more complex multidentate ligands. Since the primary goal of the research herein is to prepare coordination polymers with analogous building blocks to the Pb(II) research previously conducted in the Leznoff group,[20] this section describes the scope of the building blocks to be utilized herein.

(a) **Bridging Ligand.** Dicyanoaurate, $[Au(CN)_2]^-$, was used as a bridging ligand throughout the thesis, to facilitate a direct comparison with the analogous Pb(II) work. More generally,dicyanoaurate is linear, can form aurophilic interactions and has distinctive IR/Raman stretches associated with its cyanide groups; specifically, the ν(CN) stretch of $KAu(CN)_2$ is at 2141 cm^{-1}.

(b) **Capping/Ancillary Ligands.** Three heterocyclic multidentate nitrogen donors were chosen to use as ancillary capping ligands (Figure 2.3). The ligand 2,2';6',2"-terpyridine (Terpy) is tridentate; 2,2'-bipyridine (Bipy) is the bidentate version of this poly-pyridyl ligand system, and 1,10 phenanthroline (Phen) is another bidentate ligand, but of lower basicity and tighter bite-angle than bipy. All three of these chelating ligands were utilized herein.

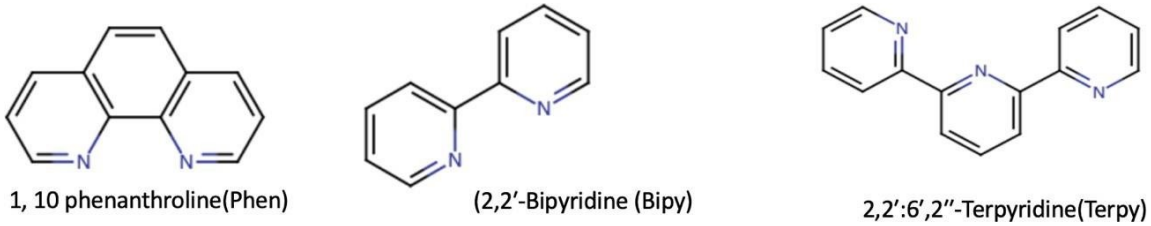

Figure 2.3. Capping ligands used in this thesis

(c) **Bismuth salts.** Bismuth(III) nitrate is a common source of bismuth(III) in the synthesis of coordination polymers. $Bi(NO3)_3$ (which is purchased as a pentahydrate) is soluble in water but at pH7 can form insoluble bismuth oxo/hydroxo clusters, along with highly acidic aqueous solutions. The solubility can be maintained by the addition of nitric acid, although this also provides large concentrations of nitrate anion, which can act as a competing ligand.

An alternative option that is less acidic is bismuth(III) trifluoromethanesulfonate (triflate), which is a generally non-coordinating counterion. This salt is soluble in methanol, water, ethanol and other organic solvents, providing a wider range of options for synthesis. A third option, bismuth(III) chloride ($BiCl_3$) proved to have too limited solubility and was not utilized herein.

(d) **Solvents.** Here are the specifics of the various types of solvents used in the project, based upon their solubility with the bismuth salts, the ancillary ligands and the dicyanoaurate:

- **Acidic Water**: As mentioned above, bismuth nitrate is a commonly used starting material for the synthesis of bismuth-containing coordination compounds. It is often dissolved in water, but the solubility of bismuth nitrate in water is limited. Acidic water (e.g., pH 1, adjusted using HNO_3) can increase the solubility of bismuth nitrate by ensuring that hydroxo/oxo clusters are not formed and do not precipitate.

- **Organic solvents**: Methanol, DMF, and DMSO organic solvents were used.

  Methanol- It can dissolve a wide variety of organic and inorganic compounds, including metal salts. Methanol is a polar solvent that has a reasonably high boiling point. Given that it readily dissolves gold and bismuth salts, methanol is an ideal solvent for the synthesis of bismuth cyanometallate coordination polymers.

  N,N-dimethylformamide (DMF) is a commonly used solvent for the synthesis of bismuth coordination polymers. Bismuth coordination polymers are often synthesized using a solvothermal method, in which the reactants are dissolved in a suitable solvent and heated under autogenous pressure to promote the formation of coordination bonds. DMF is a popular solvent for solvothermal synthesis of bismuth coordination polymers because of its high boiling point (154°C) and its ability to dissolve a wide range of organic and inorganic compounds. DMF is also a polar solvent, which facilitates the dissolution of metal salts and promotes the formation of coordination bonds between the metal ions and the organic ligands. However, although multiple attempts at solvothermal

crystallization with DMF was utilized in this thesis research, none gave usable crystals and thus no solvothermal syntheses are reported herein.

Dimethyl sulfoxide (**DMSO**) is another commonly used solvent for the synthesis of bismuth coordination polymers. Like DMF, DMSO is a polar solvent capable of dissolving a variety of organic and inorganic substances. Additionally, DMSO is a powerful solvating agent that can aid in the dissolving of organic ligands and metal salts which promotes the synthesis of coordination bonds. One of the major benefits of using DMSO as a solvent for bismuth coordination polymer synthesis is that it has a high boiling point (189°C) and a low toxicity compared to other polar solvents. However, there are also some drawbacks to using DMSO as a solvent for bismuth coordination polymer synthesis: due to its high boiling point, it can take up to several months for it to evaporate, which means that crystal growth will be exceedingly slow.

To summarize: Bismuth dicyanoaurate coordination polymers containing terpy, phen, and bipy will be targeted for synthesis and characterization, their structures determined and lone-pair stereochemical activity examined, and where appropriate, their emission properties explored. Coordination polymer products as a function of bismuth salt (i.e., triflate or nitrate), stoichiometry and solvent will be systematically examined, and structural trends uncovered.

Chapter 3. Synthesis and structures of bismuth-based complexes and cyanoaurate-containing materials

3.1. Introduction

In this section, the synthesis of bismuth cyanoaurate complexes with support from nitrogen donor ligands was conducted. Subsequently, an examination of the structure and potential material applications of bismuth coordination compounds ensued, employing techniques such as single crystal X-ray crystallography, thermogravimetric analysis (TGA), and solid-state emission spectroscopy.

3.2. Terpyridine-containing bismuth cyanoaurate complexes and coordination polymers

3.2.1. $[Bi(Terpy)(\mu\text{-}OH)]_2[Au(CN)_2]_4$ (1)

The addition of a methanol solution of one equivalent of terpyridine to an aqueous solution of one equivalent of bismuth(III) triflate, followed by addition of 3 equivalents of methanolic $KAu(CN)_2$ yielded a yellow solution, and then crystals of $[Bi(Terpy)(\mu\text{-}OH)]_2[Au(CN)_2]_4$ (**1**) were produced after a week of slow evaporation. Single crystal X-ray diffraction reveals that the polymeric structure of $[Bi(Terpy)(\mu\text{-}OH)]_2[Au(CN)_2]_4$ contains a hydroxide-bridged dimer of the [Bi(terpy)] unit (Figure 3.1). Each bismuth centre is 7-coordinate, consisting of a single terpy ligand, two bridging OH units and two $[Au(CN)_2]^-$ moieties; an additional $[Au(CN)_2]^-$ counterion is unligated. The Bi-N(terpy) bond lengths are 2.519(15), 2.556(15) and 2.46(15) Å respectively. The $[Bi(terpy)(\mu\text{-}OH)_2]_2$ units are linked via two parallel $[Au(CN)_2]^-$ units (Au(1)), having Bi-N(cyano) bond lengths of 2.665(16) and 2.798(18) Å. The Bi-O bond lengths are 2.183(13) and 2.339(12) Å. Hence, the local coordination geometry around the bismuth(III) centre is asymmetric (Figure 3.2.), consistent with the presence of a stereochemically active lone pair. Thus, overall, the structure can be described as a 1-D columnar chain of $[Bi(terpy)(\mu\text{-}OH)_2]_2$ units propagated by $[Au(CN)_2]^-$ bridges (Figure 3.3.). These cyanoaurate bridges, along with the unligated $[Au(CN)_2]^-$ units, form a diamondoid-shaped tetramer of Au(I) centres between the $[Bi(terpy)(\mu\text{-}OH)_2]_2$ units, with aurophilic interactions of 3.261(14) (Au1-Au1),

3.46 Å (Au1-Au2) and 3.439 Å (Au1'-Au2 (Figure 3.3), all of which are well within the sum of the van der Waals radii for two Au(I) centres of 3.6 Å (considered the limit of aurophilicity);[16] this gives the 1-D chain a more "columnar"-type thickness. The column is also reinforced by Bi-OH•••NC hydrogen bonding (N(4)-O(1) distance =3.040 Å). Note that **1** is structurally very similar to the Pb bromoterpy complex (Fig. 2.2) which is also a 1D gold chain with tetranuclear cyanoaurate clusters.

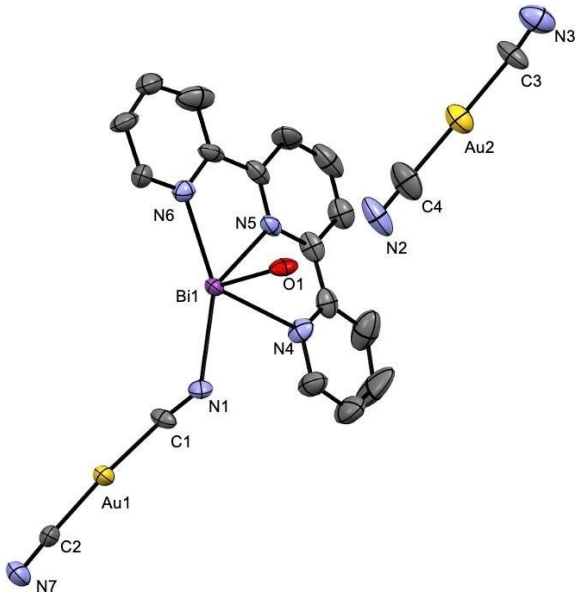

Figure 3.1. Crystal structure of [Bi(Terpy)(μ-OH)]$_2$[Au(CN)$_2$]$_4$ (1), focusing on the asymmetric unit. Colour Scheme: Carbon, gray; Nitrogen, blue; Oxygen, red; Gold, yellow; Bismuth, purple.

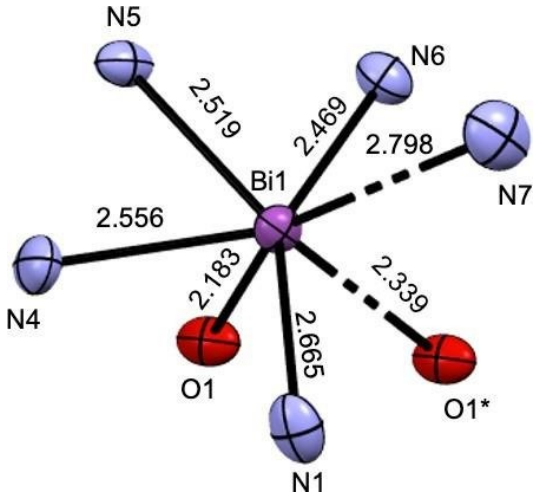

Figure 3.2 Coordination sphere of the bismuth centre in [Bi(Terpy)(μ-OH)]$_2$[Au(CN)$_2$]$_4$ (1)

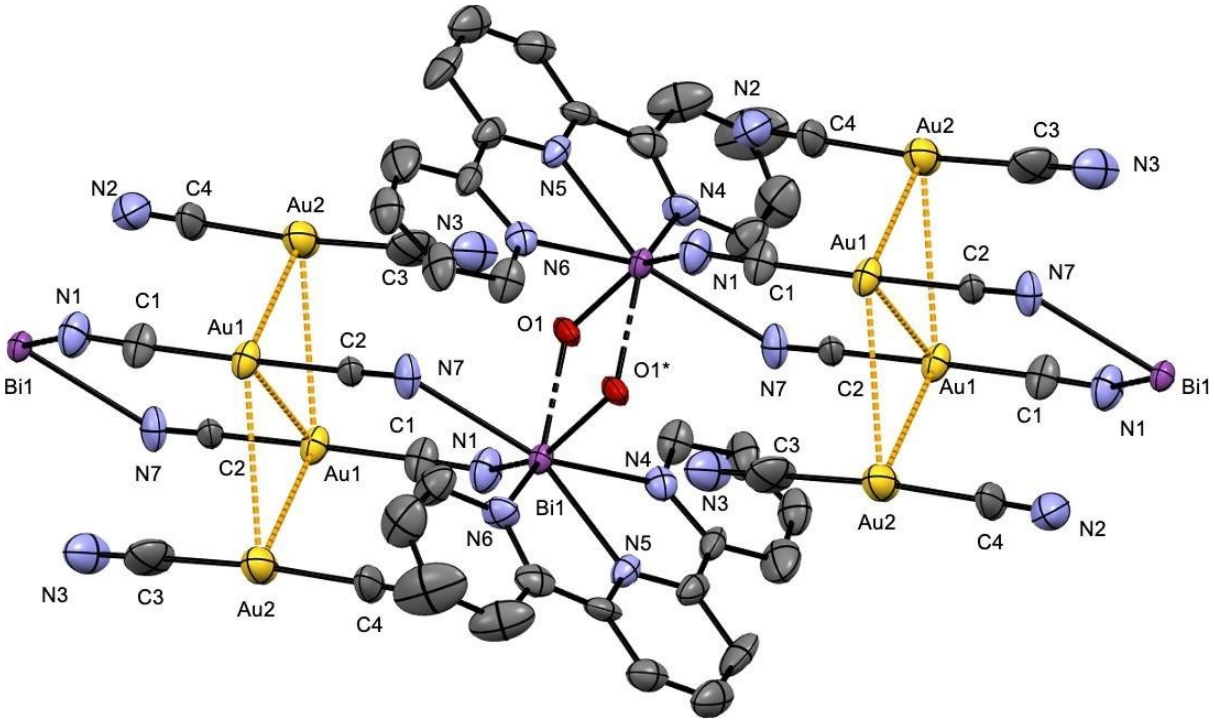

Figure 3.3. **Polymeric supramolecular structure of $[Bi(Terpy)(\mu\text{-}OH)]_2[Au(CN)_2]_4$ (1). Colour Scheme: Carbon, gray; Nitrogen, blue; Oxygen, red; Gold, yellow; Bismuth, purple.**

Table 3.1. **Selected bond lengths and angles for 1.**

Type	Bond length (Å)	Type	Bond angle (°)
Bi1 – N1	2.665 (16)	N5–Bi1– N6	64.5(5)
Bi1 – N5	2.519 (15)	N5–Bi1– N4	66.99
Bi1 – N7	2.798 (18)	N6–Bi1– N1	80.23(5)
Bi1 – N4	2.469 (15)	N7–Bi1– N4	74.48(5)
Bi1 – N6	2.556 (15)	N1–Bi1– N7	84.17(5)
Au1 – Au1	3.2611(14)	O4–Bi1– O4*	69.59
Au1 – Au2	3.461	N1–Bi1– O1	74.74(5)
Au1' – Au2	3.439	C1–N1– Bi1	131.28(15)
Bi1 – O1*	2.339 (12)	O1–Bi1– N5	81.20(5)
Bi1 – O1	2.183 (13)	N5–Bi1– N4	66.99(5)
Au1 – C1	2.000 (18)	O1–Bi1– N4	74.489(5)
Au2 – C4	2.000 (3)	O1*–Bi1– N7	77.25(5)
Au2 – C3	2.001 (2)	C1–Au1-C2	175.52(8)
Au1 – C2	1.970 (2)		

The IR spectrum shows ν(CN) peaks at 2144 and 2161 cm^{-1}. The peak at 2144 cm^{-1} can be assigned to the free Au-CN moiety as it is similar in energy to the 2145 cm^{-1} observed for [^{n}Bu4N][$Au(CN)_2$]. Other peaks such as 3112 cm^{-1}, and 3081 cm^{-1} likely correspond to hydroxide O-H stretches, while peaks such as 3042 cm^{-1} correspond to C-H bonds of terpy.[35] Consistent with the presence of aurophilic interactions, **1** also is emissive in the solid-state, with emission at 560 nm when excited at 370 nm. However, the quantum yield is quite low, at 0.29%.

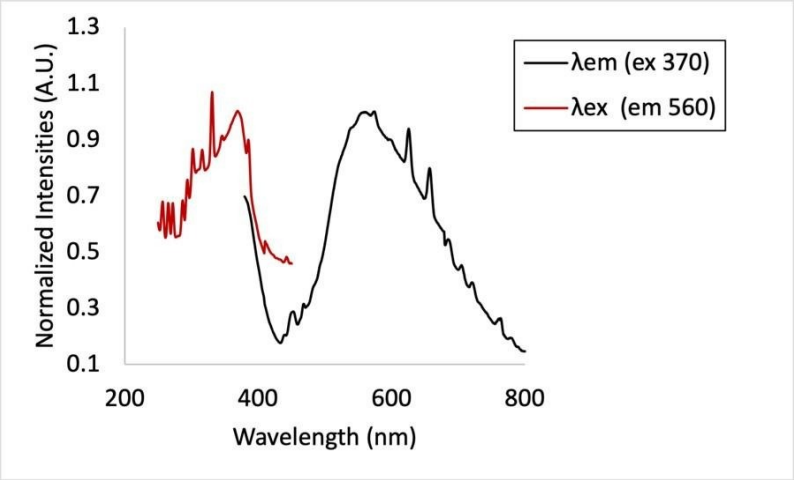

Figure 3.4. Solid state emission spectrum of [Bi(Terpy)(μ-OH)]$_2$[$Au(CN)_2$]$_4$ (1).

3.2.2. Bi(Terpy)(NO_3)$_2$[$Au(CN)_2$](H_2O) (2)

The addition of two equivalents of a methanol solution of terpyridine to two equivalents of a nitric acid solution of bismuth(III) nitrate (i.e., a stock solution of nitric acid with bismuth nitrate dissolved therein; see experimental section for details), followed by the addition of an aqueous solution of 3 equivalents of $KAu(CN)_2$ yielded a yellow solution, from which crystals of Bi(Terpy)(NO_3)$_2$[$Au(CN)_2$](H_2O) (**2**) were produced after a week. The use of dilute nitric acid ensures that the bismuth(III) nitrate salt remains soluble; in the absence of added nitric acid, insoluble bismuth hydroxides tend to form. Single crystal X-ray diffraction reveals that the polymeric structure of Bi(Terpy)(NO_3)$_2$[$Au(CN)_2$](H_2O) (**2**) contains a cyanoaurate-bridged dimer of a [Bi(terpy)(nitrate)$_2$(H_2O)] unit (Figure 3.5). Each bismuth centre in the dimer is 9-coordinate, consisting of two η^2-chelating nitrate units, a terpy ligand, an N(cyano) unit from a bound [$Au(CN)_2$] moiety and an aqua ligand. The Bi-N(terpy) bond lengths are 2.504(15), 2.475(15) and 2.475(8) Å (Table 3.2). The

$[Bi(terpy)(NO_3)_2]_2$ units are linked via two parallel $[Au(CN)_2]^-$ units, having Bi-N bond lengths of 2.664(4) Å, although note that the bismuth(III) centres are not linked by N-cyano bonding from the same $[Au(CN)_2]^-$ unit, but instead these cyanoaurate bridges form the dimer via Au(I) aurophilic interactions of 3.544 Å (Figure 3.5). The Bi-O bond lengths from the chelating nitrate anions are 2.733(3), 2.378(3), 2.599(3) and 2.519(3) Å and, for the aqua ligand, 2.546(12) Å. Hence, the local coordination geometry around the bismuth (III) centre is asymmetric (Figure 3.6), consistent with the presence of a stereochemically active lone pair. The Au-Au bond length of 3.544 Å is at the outer range of the sum of the van der Waals radii (3.6 Å), and so should be considered as being a very weak interaction.

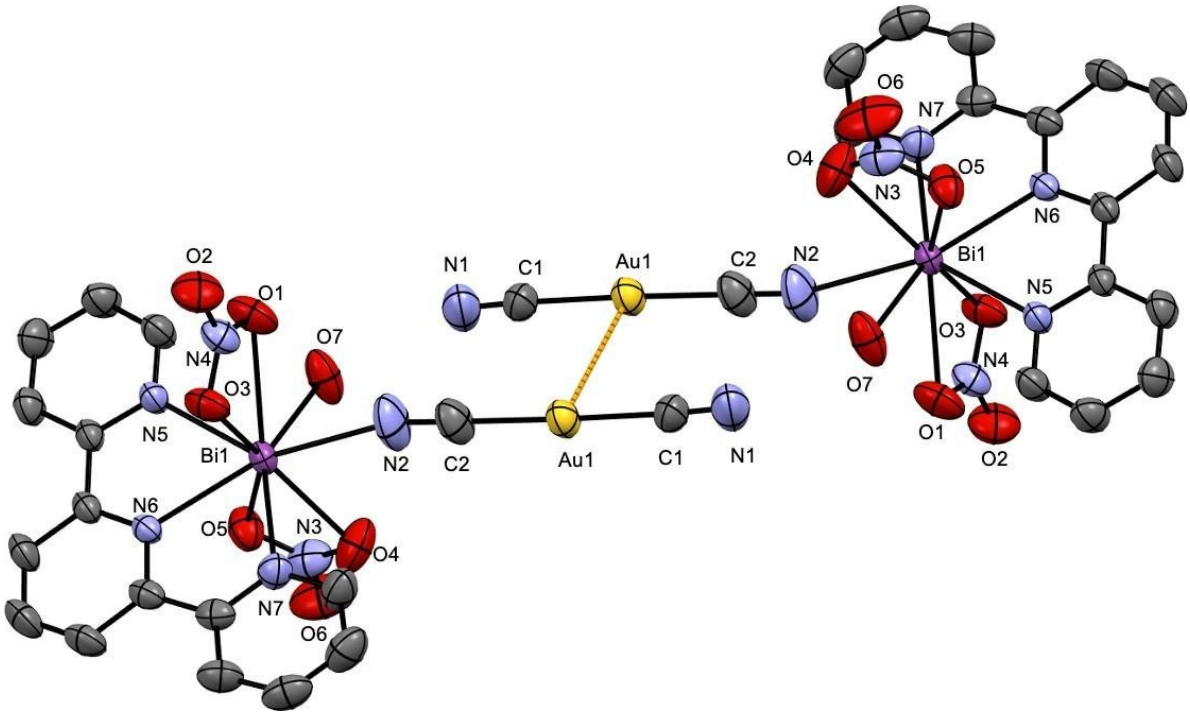

Figure 3.5. Dimeric form of $Bi(Terpy)(NO_3)_2[Au(CN)_2](H_2O)$ (2). Colour Scheme: Carbon, gray; Nitrogen, blue; Oxygen, red; Gold, yellow; Bismuth, purple.

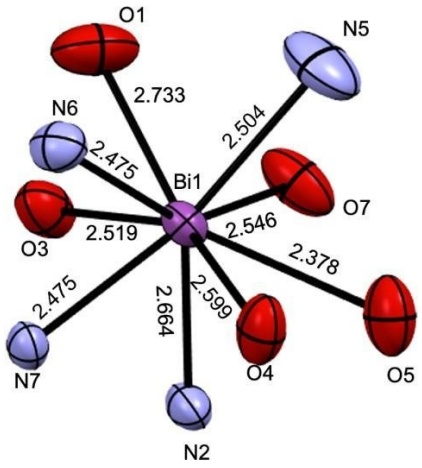

Figure 3.6. Coordination sphere of the bismuth centre in $Bi(Terpy)(NO_3)_2[Au(CN)_2](H_2O)$ (2)

Table 3.2. Selected bond lengths and angles in 2.

Type	Bond lengths (Å)	Type	Bond angles (°)
Bi1 – N5	2.504(3)	N7–Bi1– N6	66.02(10)
Bi1 – N6	2.475(3)	N6–Bi1– N5	65.91(9)
Bi1 – N7	2.475(3)	N5–Bi1– O3	83.52(10)
Bi1 – N2	2.664(4)	O3–Bi1– O1	48.00(8)
Bi1 – O7	2.546(3)	O1–Bi 1– N2	72.20
Bi1 – O3	2.519(3)	N2–Bi1– O4	76.85(16)
Bi1 – O1	2.733(3)	O4–Bi1– O5	51.09(3)
Bi1 – O4	2.599 (3)	O1–N1– O7	74.84(12)
Bi1 – O5	2.378(3)	O7–Bi1– N5	78.18(10)
Au1 – Au1	3.544	N7–Bi1– N2	83.44(13)
Au1 – C1	1.997(4)	Bi1–N2– C2	154.42
Au1 – C2	1.980(4)	Bi1–C2– N2	17.99
		C1–Au1-C2	176.10

The IR spectrum shows a ν(CN) peak at 2150 cm^{-1}, assignable as the unbound N(cyano) end of the $[Au(CN)_2]^-$ units; the bound ν(CN) value would be expected to be shifted to higher energy but was not observed. This compound was not visibly emissive on a 375 nm light.

3.2.3. $[Bi(terpy)(H_2O)(\mu\text{-}OH)]_2[Au(CN)_2]_4$ (3)

The addition of two equivalents of terpyridine in a methanol solution to a methanol solution of three equivalents of $KAu(CN)_2$, followed by the addition of this mixture to an acidic solution (10 mL water : 0.1 mL conc. HNO_3) of one equivalent of bismuth(III) nitrate, yielded a yellow solution, from which crystals of $[Bi(terpy)(H_2O)(\mu\text{-}OH)]_2[Au(CN)_2]_4$ (**3**) were produced after 5 days.

Single crystal X-ray diffraction reveals that the polymeric structure of $[Bi(terpy)(H_2O)(\mu\text{-}OH)]_2[Au(CN)_2]_4$ contains a hydroxide-bridged dimer of the [Bi(terpy)] unit (Figure 3.7). Compared to the preparation of **2**, the relative stoichiometries are different and the amounts of methanol are higher, resulting in a slightly less acidic solution; this can account for the incorporation of the hydroxo-unit in **3**, whereas in **2** a neutral aqua ligand completed the coordination sphere. The higher relative stoichiometry of added $KAu(CN)_2$ in **3** also presumably influences the final structure, which has a higher 1:2 ratio of Bi:Au (and no nitrates) compared to **2**. There are two unique bismuth centres: one (Bi2) is 8-coordinate, consisting of a single terpy ligand, two bridging OH units, two N(cyano) ligands from $Au(CN)_2$ moieties, and an aqua (H_2O) ligand with a Bi2-O3 distance of 2.718(16) Å. The second bismuth centre (Bi1) is very similar, but lacks the aqua ligand within the coordination sphere; an H_2O molecule is present in the lattice, with a Bi1-O distance of 3.134 Å (Figure 3.8). Examining the $[Au(CN)_2]^-$ anions in more detail, each bismuth centre has one unique $[Au(CN)_2]^-$ unit bound terminally (Au1 and Au3), *i.e.*, one N(cyano) unit binds to the Bi(III), while the other end dangles free. As well, a $[Au(CN)_2]^-$ unit (Au4) bridges between dimers by utilizing both N(cyano) ends as ligands, and an additional $[Au(CN)_2]^-$ counterion (Au2) is free, with no N(cyano) moieties bound to any metal centre (Figure 3.8).

Focusing on the bismuth coordination spheres, the N(cyano) Bi-N bond lengths for the dangling $[Au(CN)_2]^-$ units are 2.684(12) Å and 2.813(13) Å, while the long bridging N(cyano) bonds are 2.813(13) and 2.900(11) (Table 3.3). The Bi-μ-OH bond lengths for Bi1 are 2.384(5) and 2.147(5) Å and a very similar 2.151(5) and 2.374 Å for Bi2. The Bi-N(terpy) bond lengths range between 2.457(5) - 2.900 (11) Å. Hence, the local coordination geometry around each bismuth(III) centre is asymmetric (Figure 3.9), consistent with the presence of a stereochemically active lone pair. Overall, the structure can be described as a 1-D columnar chain of $[Bi(terpy)(\mu\text{-}OH)_2]_2$ units propagated by

$[Au(CN)_2]^-$ bridges (Figure 3.8). These cyanoaurate bridges, along with the unligated $[Au(CN)_2]^-$ units, form an asymmetric meandering 1-D chain of Au(I) centres between the $[Bi(terpy)(\mu\text{-}OH)_2]_2$ units, with aurophilic interactions of 3.201(5) (Au1-Au2), 3.129(5) (Au1-Au4) and 3.354(5) Å (Au3-Au4) (Figure 3.3.2), all of which are well within the sum of the van der Waals radii for two Au(I) centres of 3.6 Å. The column is also reinforced by Bi-OH•••NC hydrogen bonding (N(2)-O(1) distance = 2.875 Å and N(10)-O(4) = 2.893 Å. (Table 3.3).

The bound water is lost above 150 °C, as illustrated by the thermo-gravimetric analysis (TGA) data; more drastic decomposition occurs above 190 °C (Figure 3.10).

Consistent with the presence of aurophilic interactions, complex **3** is emissive in the solid- state; measurements were made at both room temperature at 77 K. At both temperatures, two emission peaks were observed, with λ_{max} of 360 and 540 nm at 77 K (with an intensity ratio of 2.5 between them) and λ_{max} of 390 and 510 nm at room temperature (intensity ratio = 1.73). These two peaks could be attributed to fluorescent and phosphorescent emission from the aurophilic interactions, consistent with many other similar observations.[27] The low-energy peak appears to vary more between temperatures. (Figure 3.9). A room temp. solid-state quantum yield of 1% was measured, consistent with a low intensity of emission.

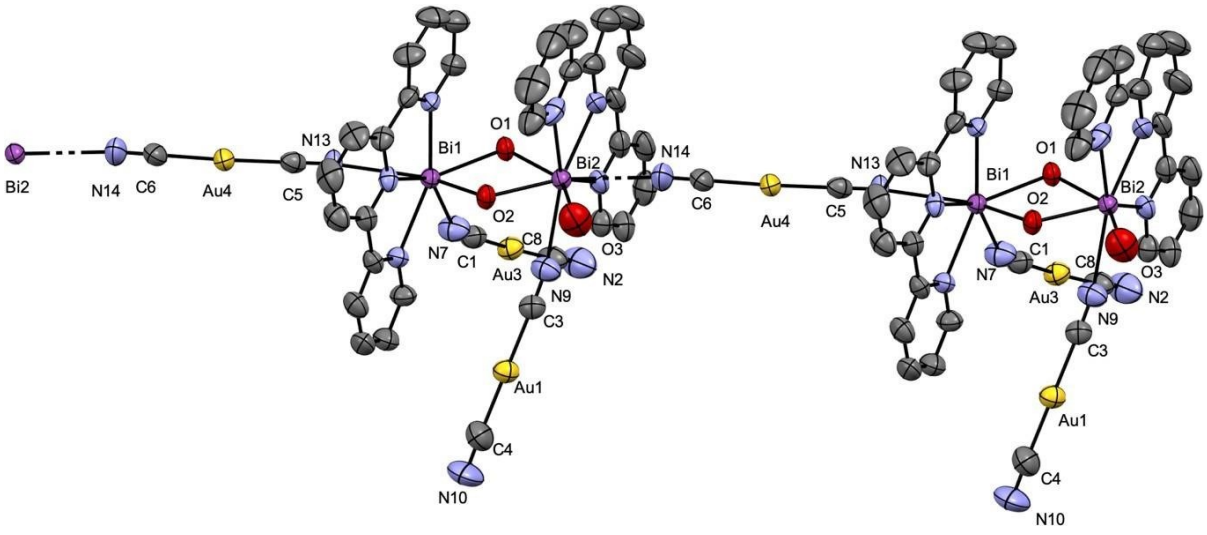

Figure 3.7. Supramolecular 1-D chain structure of $[Bi(terpy)(H_2O)(\mu\text{-}OH)]_2[Au(CN)_2]_4$ (3). Colour Scheme: Carbon, gray; Nitrogen, blue; Oxygen, red; Gold, yellow; Bismuth, purple.

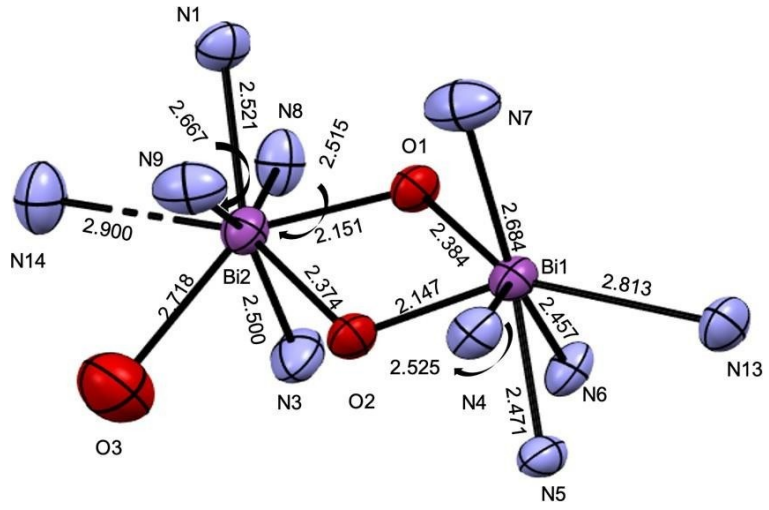

Figure 3.8. Coordination sphere of Bi1 and Bi2 in $[Bi(Terpy)(H_2O)(\mu\text{-}OH)]_2[Au(CN)_2]_4$ (3).

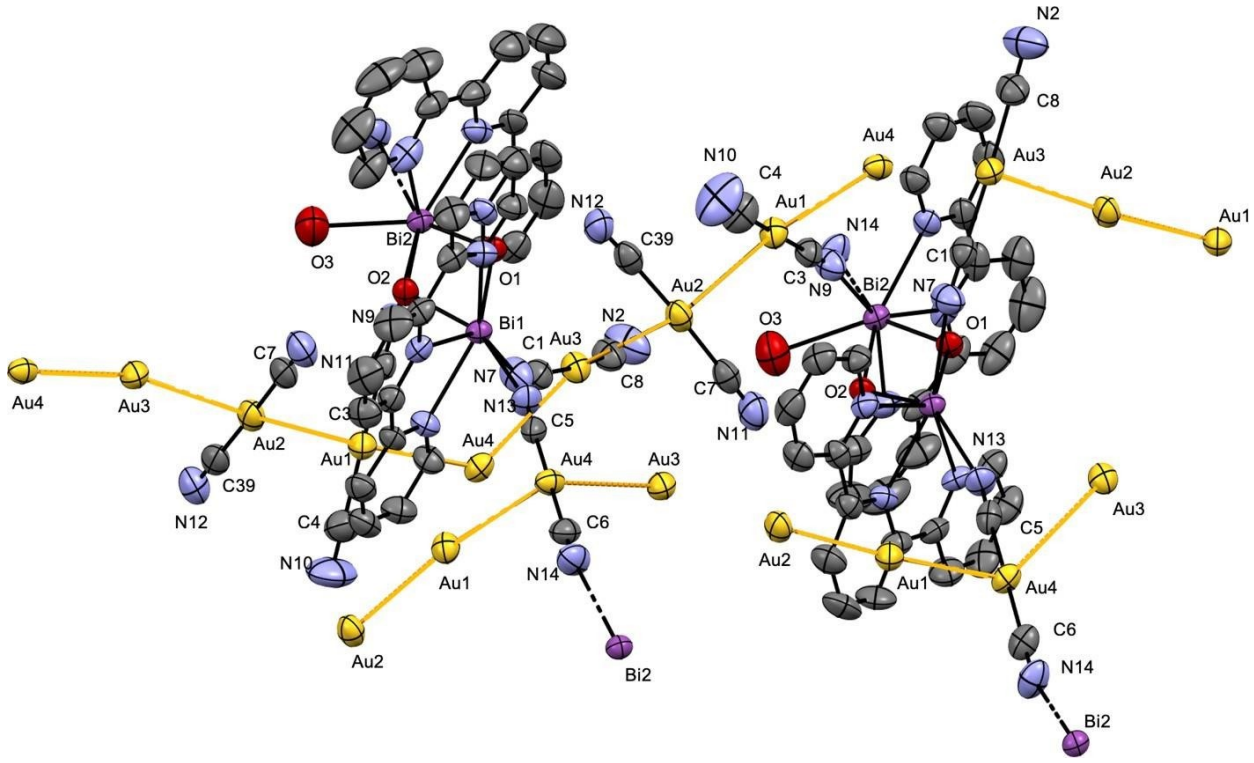

Figure 3.9. Au-Au 1-D chain motifs in $[Bi(Terpy)(H_2O)(\mu\text{-}OH)]_2[Au(CN)_2]_4$ (3). Colour Scheme: Carbon, gray; Nitrogen, blue; Oxygen, red; Gold, yellow; Bismuth, purple.

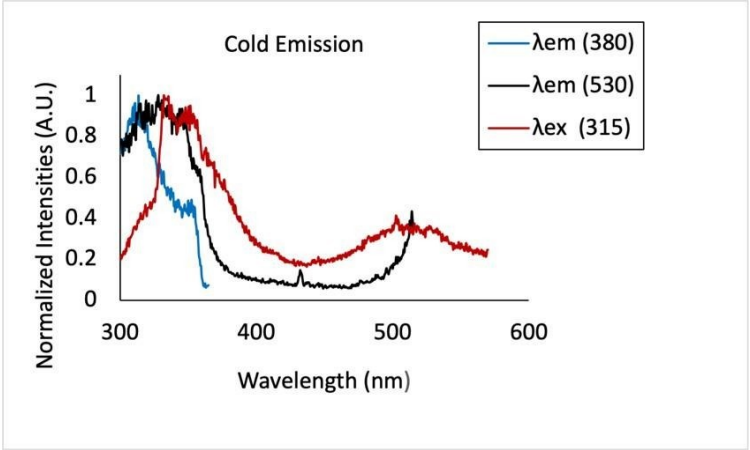

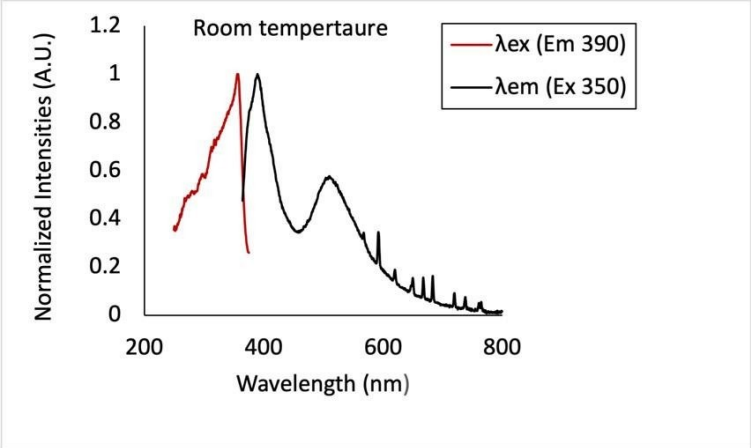

Figure 3.10. Solid state emission spectra of $[Bi(terpy)(H_2O)(\mu\text{-}OH)]_2[Au(CN)_2]_4$ (3) at 77K (top) and room temperature (below)

[This space is intentionally blank. Text continues below.]

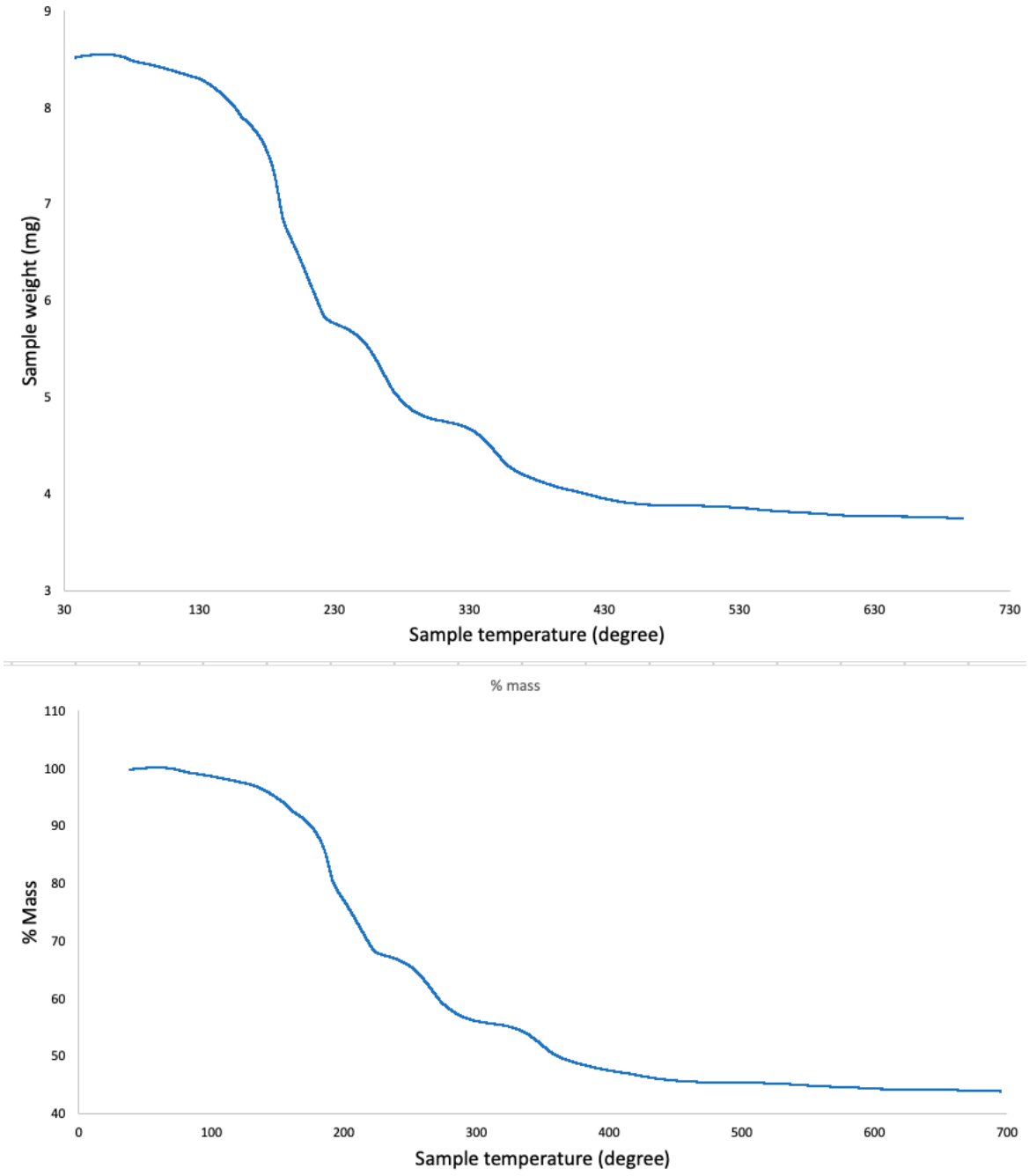

Figure 3.11. Thermo-gravimetric analysis (TGA) traces of $[Bi(terpy)(H_2O)(\mu\text{-}OH)]_2[Au(CN)_2]_4$

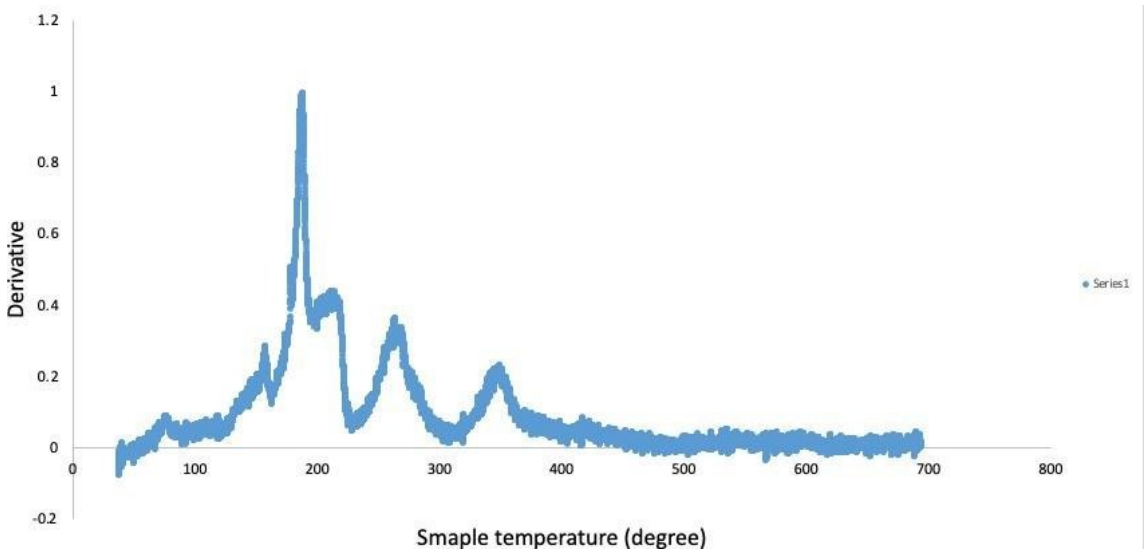

Figure 3.12. First derivative of the TGA data for $[Bi(terpy)(H_2O)(\mu\text{-}OH)]_2[Au(CN)_2]_4$

[This space is intentionally blank. Text continues below.]

Table 3.3. Selected bond lengths and angles in 3.

Type	Bond lengths (Å)	Type	Bond angles (°)
Bi1 – O1	2.384(5)	O1–Bi1– O2	66.69(19)
Bi1 – O2	2.147(5)	N6–Bi1– N5	66.64(2)
Bi2 – O1	2.151(5)	N5–Bi1– N4	65.84(2)
Bi2 – O2	2.374(5)	N4–Bi1– N13	77.70
Bi2 – O3	2.718(8)	N13–Bi 1– N7	104.90
Bi2 – N1	2.521(7)	N7–Bi1– O1	74.71(2)
Bi2 – N8	2.515	N13–Bi 1– N6	85.11
Bi2 – N9	2.667(8)	N4–Bi1– O2	83.79(2)
Bi2 – N3	2.500(7)	N6–Bi1– O1	79.68(19)
Bi2 – N14	2.900(11)	N1–Bi2– N8	64.84
Bi1 – N7	2.684(12)	N8–Bi2– N3	64.89
Bi1 – N13	2.813(13)	N3–Bi2– O2	81.18(2)
Bi1 – N6	2.457(6)	N1–Bi2– O1	81.12(2)
Bi1 – N5	2.471(6)	N6–Bi2-N13	84.74
Bi1 – N4	2.525(6)	N1–Bi2-N9	80.89(2)
Au1 – Au2	3.201(5)	N9–Bi2-O2	73.99(2)
Au1 – Au4	3.129(5)	N8–Bi2-N14	68.96
Au4 – Au3	3.354(5)	N1–Bi2-N4	73.36
		N1–Bi2-N4	73.36
		C3–Au1-Au2	84.50(2)
		C7–Au2-Au3	93.23(3)
		Au1–Au2-C7	96.12(3)
		Au4–Au1-C3	90.09 (3)
		Au4–Au1-C4	89.15(4)
		C4–Au1-Au2	96.29(4)
		Au1–Au2-C39	86.29
		C39–Au2-Au3 Au1–Au4-Au3 C1–Au3-Au4 C1–Au3-Au2 C8–Au3-Au2 C8–Au3-Au4	84.57 120.52 74.05 (2) 91.90 (3) 89.25 106.51

3.2.4. Bi(Terpy)[Au(CN)$_2$]$_2$(NO$_3$)(DMSO)$_2$ (4)

The addition of a mixture of 1 equivalent of each of terpyridine and bismuth(III) nitrate in DMSO solutions were mixed and added to 3 equivalents of KAu(CN)$_2$ in a

separate DMSO solution. This mixture yielded a few shiny yellow crystals of Bi(Terpy)[Au(CN)$_2$]$_2$(NO$_3$)(DMSO)$_2$ (**4**) after 10 months of very slow evaporation of DMSO. There was not enough crystals to obtain any analytical data beyond the single crystal structure.

The solid-state diffraction data reveals a 1-D polymeric structure for Bi(Terpy)[Au(CN)$_2$]$_2$(NO$_3$)(DMSO)$_2$ (**4**). The Bi(III) centre is 9-coordinate, binding to a single terpyridine unit, one bidentate nitrate, two O-bound DMSO molecules and two N-cyano donors from two separate [Au(CN)$_2$]$^-$ units, each of which bridges to an adjacent Bi(III) centre, thereby generating the zig-zag 1-D chain (Figure 3.14); an additional [Au(CN)$_2$]$^-$ counterion is unligated. The Bi-N(terpy) bond lengths are 2.520(8), 2.505(8) and 2.539(9) Å respectively .The [Bi(terpy)(DMSO)$_2$(NO$_3$) units are linked via two parallel [Au(CN)$_2$] units (Au(1), having Bi-N bond lengths of 2.516(10) Å and 2.715(12) Å .The Bi-O(nitrate) bond lengths are 2.476(8) and 2.731(9) Å, reflecting an asymmetric chelating bonding mode for the nitrate; Bi-O(DMSO) bond lengths are 2.449(7) and 2.512(7) Å. Hence, the local coordination geometry around the bismuth(III) centre is asymmetric (Figure 3.14), consistent with the presence of a stereochemically active lone pair. Each cyanoaurate bridge forms Au-Au interactions of 3.119(8) Å (Au1-Au2) with unligated [Au(CN)$_2$]$^-$ units on either side, to form linear trinuclear Au3 units in the structure (Figure 3.15).

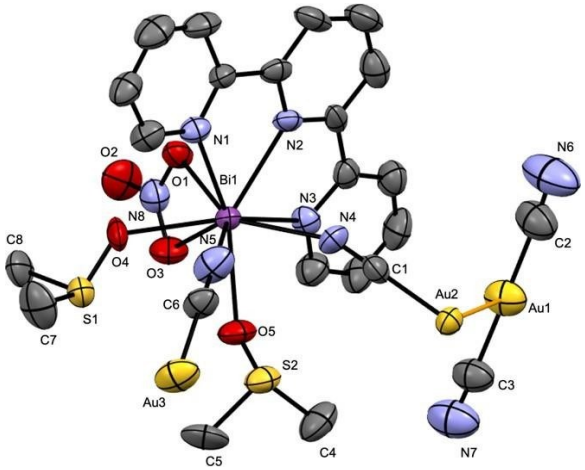

Figure 3.13. Crystal structure of Bi(Terpy)[Au(CN)$_2$]$_2$(NO$_3$)(DMSO)$_2$ (4). Colour Scheme: Carbon, gray; Nitrogen, blue; Oxygen, Sulphur Dark yellow; red; Gold, yellow; Bismuth, purple

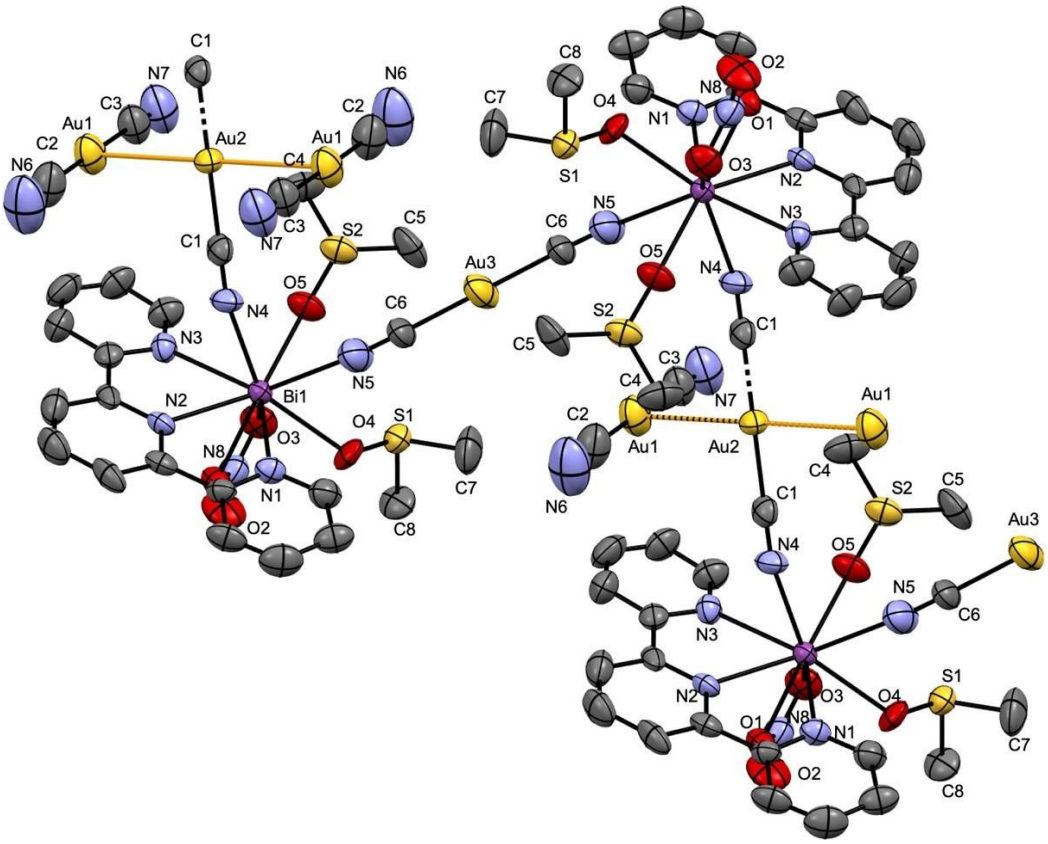

Figure 3.14. 1-D zig-zag chain structure of Bi(Terpy)[Au(CN)$_2$]$_2$(NO$_3$)(DMSO)$_2$ (4) Colour Scheme: Carbon, gray; Sulphur, pale yellow ; Nitrogen, blue; Oxygen, red; Gold, yellow; Bismuth, purple.

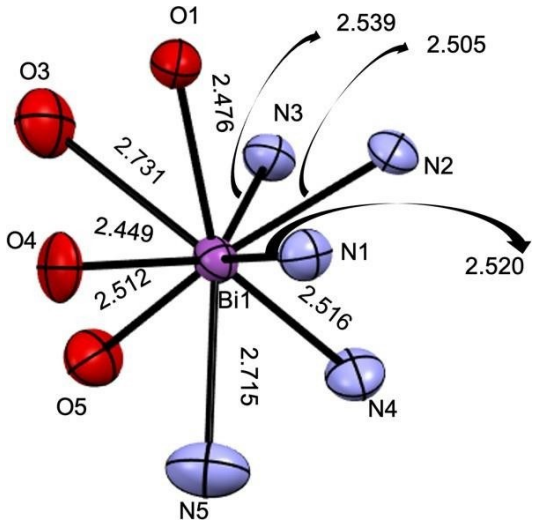

Figure 3.15. Coordination sphere of Bi in Bi(Terpy)[Au(CN)$_2$]$_2$(NO$_3$)(DMSO)$_2$ (4). Colour Scheme: Carbon, gray; Nitrogen, blue; Oxygen, red; Bismuth, purple.

Table 3.4. Selected bond lengths and angles in 4.

Type	Bond lengths (Å)	Type	Bond angles (°)
Bi1 – N1	2.520(8)	N2–Bi1– N1	64.97(3)
Bi1 – N2	2.505(8)	N2–Bi1– N3	64.54(3)
Bi1 – N3	2.539(9)	N1–Bi1– N5	73.52(3)
Bi1 – N4	2.516(10)	N5–Bi1– O4	73.21(4)
Bi1 – N5	2.715(12)	O4–Bi 1– O5	87.44(3)
Bi1 – O1	2.476(8)	O5–Bi1– O3	70.53(3)
Bi1 – O3	2.731(9)	O3–Bi1– O1	48.92(3)
Bi1 – O4	2.449(7)	N4–Bi1– O5	78.59(3)
Bi1 – O5	2.512(7)	N4–Bi1– N3	71.19(3)
Au1 – Au2	3.119(8)	Au1–Au2– C1	86.55(4)
Au2 – C1	1.984(13)	Au1–Au2– C1	93.45(4)
Au1 – C2	1.980(18)	N5–C6– Au3	174.75(14)
Au1 – C3	1.939(16)	C8–S1-C7	100.38(8)

3.2.5. $[Bi(Terpy)(\mu\text{-}OH)(DMSO)_2]_2[Au(CN)_2]_4$ (5)

The addition of one equivalent of terpyridine to one equivalent of bismuth(III) triflate (instead of the nitrate, in **4** above), followed by addition of a DMSO solution of three equivalents of $KAu(CN)_2$ yielded a yellow solution from which crystals of $[Bi(Terpy)(\mu\text{-}OH)(DMSO)_2]_2[Au(CN)_2]_4$ (**5**) were produced after a week. Single crystal X-ray diffraction reveals that the polymeric structure of **5** contains a hydroxide-bridged dimer of the [Bi(terpy)] unit (Figure 3.17). Each bismuth centre is 8-coordinate, consisting of a single terpy ligand, two bridging OH units, two O-bound DMSO units and one N-cyano bound $Au(CN)_2$ anion; an additional $[Au(CN)_2]^-$ counterion is unligated. The Bi-N(terpy) bond lengths are 2.477(3), 2.472(3) and 2.570(4) Å, and the Bi-O bond lengths are 2.725(4), 2.477(3), 2.392(3) and 2.563(4) Å. Hence, the local coordination geometry around the bismuth(III) centre is asymmetric (Figure 3.18), consistent with the presence of a stereochemically active lone pair. (Table 3.5).

Adjacent $[Bi(terpy)(\mu\text{-}OH)]_2$ dimers are linked via two parallel $[Au(CN)_2]^-$ units (Au(2)) with a Bi-N bond length of 3.007 Å to one Bi centre in the dimer; the other N-cyano end of the dicyanoaurate hydrogen-bonds to the bridging H-O unit of the adjacent $[Bi(terpy)(\mu\text{-}OH)]_2$ (Figure 3.17). Thus, overall, the structure can be described as a 1-D columnar chain of $[Bi(terpy)(\mu\text{-}OH)]_2$ units propagated by parallel $[Au(CN)_2]^-$ bridges (Figure 4.6). In addition, each bridging $[Au(CN)_2]$ unit forms an Au1-Au2 aurophilic

interaction of 3.009 Å with the unligated dicyanoaurate; the Au2-Au2 distance is a longer 3.928 Å (Figure 3.17).

The IR spectrum of **5** shows a ν(CN) peak at 2148 cm^{-1}; although two separate peaks would be expected (for the Bi-bound N-cyano and the hydrogen-bonded moiety) only one was observed. The bound DMSO ligand's S=O stretch is found at 1010 cm^{-1}. Finally, the solid state emission spectroscopy results show an excitation peak at 370 nm, with an emission maximum at 530 nm; the measured PLQY was approximately 4% (Figure 3.19.).

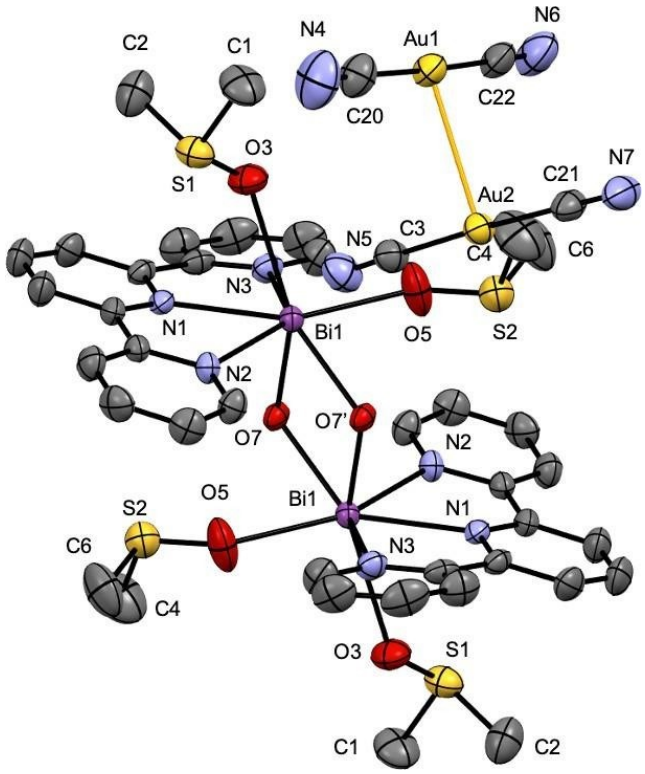

Figure 3.16. Crystal structure of $[Bi(Terpy)(\mu\text{-}OH)(DMSO)_2]_2[Au(CN)_2]_4$ (5). Colour Scheme: Carbon, gray; Nitrogen, blue; Oxygen, red; Gold, yellow; Bismuth, purple.

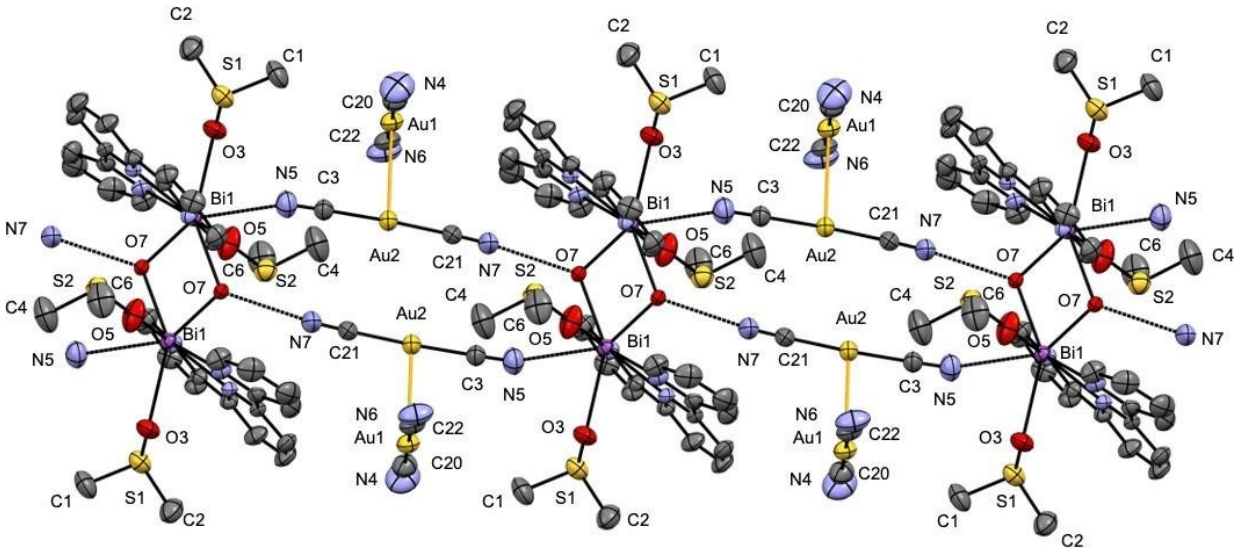

Figure 3.17. 1-D chain structure of $[Bi(Terpy)(\mu\text{-}OH)(DMSO)_2]_2[Au(CN)_2]_4$ (5). Colour Scheme: Carbon, gray; Nitrogen, blue; Oxygen, red; Gold, yellow; Bismuth, purple.

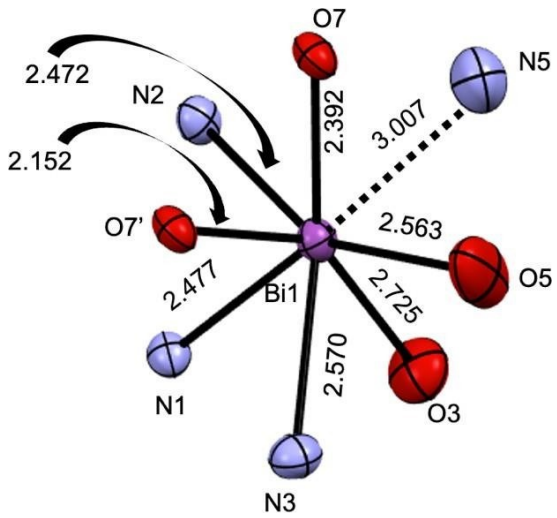

Figure 3.18. Coordination sphere of Bi in $[Bi(Terpy)(\mu\text{-}OH)(DMSO)_2]_2[Au(CN)_2]_4$ (5)

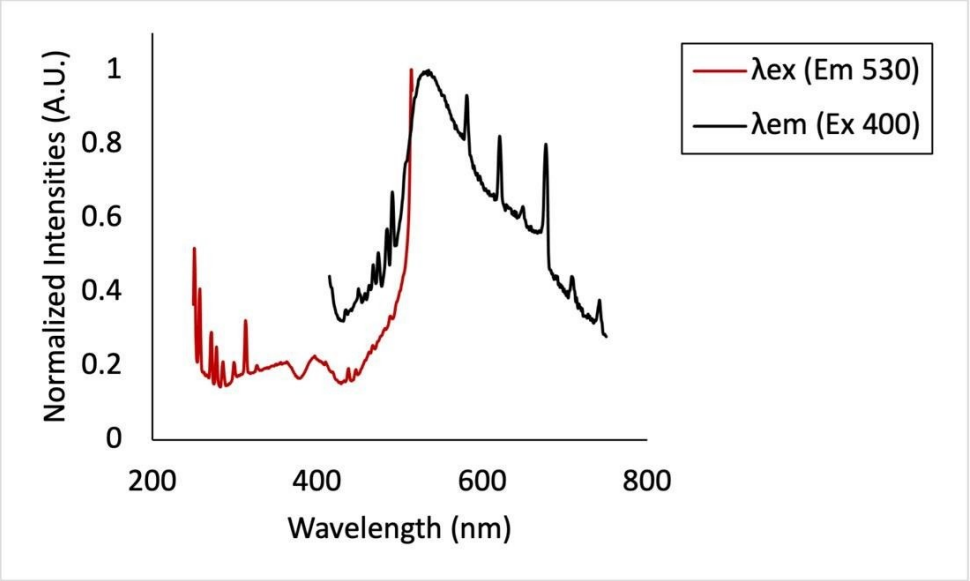

Figure 3.19. Solid state emission spectrum of [Bi(Terpy)(μ-OH)(DMSO)$_2$]$_2$[Au(CN)$_2$]$_4$ (5)

Table 3.5. Selected bond lengths and angles in 5.

Type	Bond lengths (Å)	Type	Bond angles (°)
Bi1 – N1	2.477(3)	N1–Bi1– N2	65.86(12)
Bi1 – N2	2.472(3)	N3–Bi1– N1	65.51(12)
Bi1 – N3	2.570(4)	N3–Bi1– O5	74.62(14)
Bi1 – N5	3.007	O5–Bi1– O7	78.19(14)
Bi1 – O7	2.152(3)	O7–Bi1– N2	80.26(11)
Bi1 – O7’	2.392(3)	N1–Bi1– O3	68.16(12)
Bi1 – O5	2.583(4)	O3–Bi1– O5	96.65(17)
Bi1 – O3	2.725(4)	O7-Bi1-O7’	67.67(11)
Bi1 – O5	2.563(4)	C1–S1– C2	98.15(4)
Au1-Au2	3.009(4)	C4–S2– C6	98.69(4)
Au2-Au2	3.928	C21–Au2– C3	177.40(2)
Au1 – C22	1.963(6)	C20–Au1–	177.11(3)
Au1 – C20	1.982(7)	C22	
Au2 – C21	1.984(5)		
Au2 – C3	1.985(5)		

3.2.6. Bi(Chloro-Terpy)(NO$_3$)$_2$[Au(CN)$_2$] (6)

The addition of two equivalents of 4'-chloro-terpyridine in methanol to one equivalent of bismuth nitrate in water acidified with HNO_3, followed by addition of a

methanol solution of three equivalents of $KAu(CN)_2$ yielded a yellow solution from which crystals of $Bi(Chloro\text{-}Terpy)(NO_3)_2[Au(CN)_2]$ (**6**) were produced in 8 days.

The structure of $Bi(Chloro\text{-}Terpy)(NO_3)_2[Au(CN)_2]$ (**6**) is dimeric, whereby each Bi(III) centre is bridged by a pair of $[Au(CN)_2]^-$ units. Each bismuth centre is 9-coordinate, consisting of a single terpy ligand, two bidentate O-bound nitrate units and the aforementioned two N-cyano bound $[Au(CN)_2]^-$ moieties. Unusually, when compared to the other structures herein, **6** is a simple dimer, with no significant intermolecular interactions, although the cyanoaurate bridges have intramolecular aurophilic interactions of 3.370(5) Å between them (Figure 3.20).

The Bi-N(terpy) bond lengths are 2.675(6) Å, 2.477(4) Å and 2.540(5) Å respectively. The Bi-O bond lengths are 2.601(5)Å, 2.460(5) Å, 2.438(4) Å, and 2.613(5) Å. Hence, the local coordination geometry around the bismuth(III) centre is asymmetric (Figure 3.21), but markedly less than in other systems herein (see below), thus there is a stereochemical lone pair, but perhaps less active than in other systems with more basic ligands. (Table 3.6).

The IR spectrum of **6** shows ν(CN) peaks at 2183 and 2147 cm^{-1}, consistent with two crystallographically different CN units, although they would have been expected to be closer in energy to each other (since both are N-bound to Bi(III)). The chelating nitrate anions can be seen at 1478 and 1293 cm^{-1}.[35]

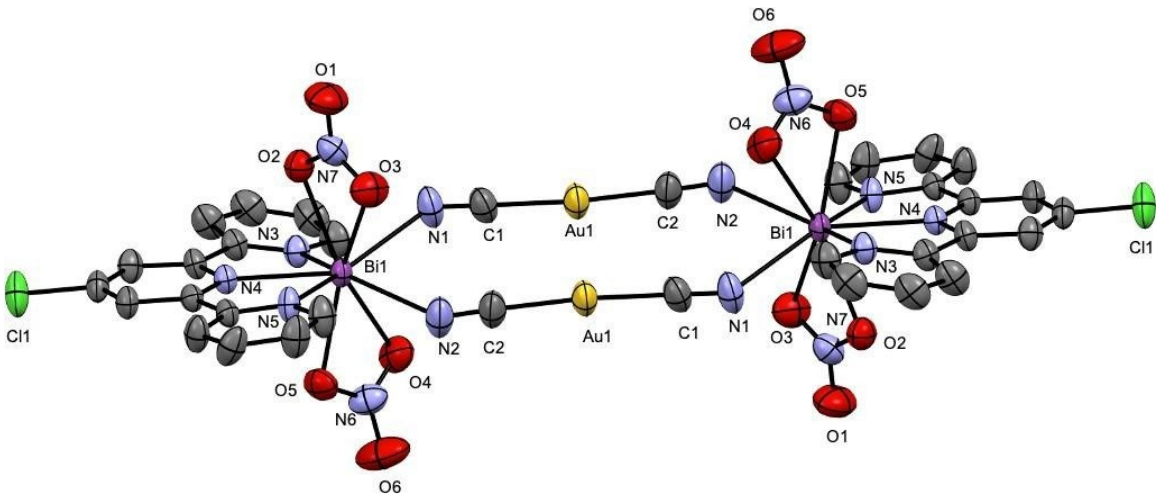

Figure 3.20. Dimer of $Bi(Chloro\text{-}Terpy)(NO_3)_2[Au(CN)_2]$ (6). Colour Scheme: Carbon, gray; Nitrogen, Blue; Oxygen, red; Gold, yellow; Bismuth, purple, Chlorine, green.

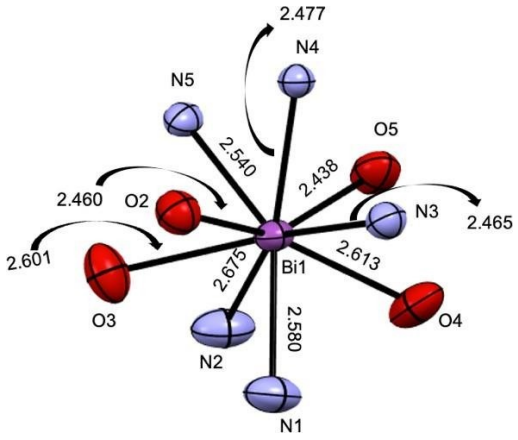

Figure 3.21. Coordination sphere of Bi in Bi(Chloro-Terpy)$(NO_3)_2[Au(CN)_2]$ (6)

Table 3.6. Selected bond lengths and angles in 6.

Type	Bond lengths (Å)	Type	Bond angles (°)
Bi1 – N3	2.465(5)	O5–Bi1– O4	50.65(15)
Bi1 – N4	2.477(4)	O5–Bi1– N3	91.09(17)
Bi1 – N5	2.540(5)	N3–Bi1– N4	66.01(15)
Bi1 – N1	2.580(5)	N4–Bi1– N5	65.14(14)
Bi1 – N2	2.675(6)	N1–Bi1– N3	79.63(18)
Bi1 – O4	2.613(5)	N1–Bi1– N2	79.47(18)
Bi1 – O5	2.438(4)	N2–Bi1– N5	79.27(16)
Bi1 – O2	2.460(5)	O4–Bi1-O5	50.65(15)
Bi1 – O3	2.601(5)	N1-Bi1-O4	77.85(19)
Au1-Au1	3.370(5)	O2–Bi1– O3	50.43(16)
Au1 – C1	1.991(7)	C1–Au1– C2	175.33(3)
Au1 – C2	1.983(7)	N1–Bi1– O3	75.09(2)
C10 – Cl1	1.733(6)		

3.2.7. [Chloro-terpy-H_2]$(NO_3)[Au(CN)_2]$•H_2O (7)

When the same reaction between 4'-chloroterpy and bismuth nitrate (in this case, both in HNO_3-acidified water) was added to three equivalents of $[^nBu4N][Au(CN)_2]$•1/2 H_2O in methanol, a yellow solution formed, which yielded crystals of [Chloro-terpy-H_2]$(NO_3)[Au(CN)_2]$•H_2O (**7**) over 10 days; no Bi(III) was incorporated in this case. The acidification of the ligand solution generated di-protonated 4'-Chloro-Terpy in solution, which crystallized with a nitrate and $[Au(CN)_2]^-$ anion. The structure of [Chloro-terpy-H_2]$(NO_3)[Au(CN)_2]$•H_2O (**7**) (Figure 3.22; Table 3.7) shows two protonated rings of terpy

(with the H-atoms located and found in the structure), which hydrogen- bond to a nitrate anion in a "receptor"-type fashion; the $[Au(CN)_2]^-$ anion remains free, with no aurophilic interactions (closest Au-Au contact is 3.829 Å). The IR spectrum shows ν(CN) peaks at 2235 cm^{-1} (this is AuCN, formed from the interaction with the acid), for the free $[Au(CN)_2]^-$ unit in **7**. The nitrate peaks are at 1479 and 1596 cm^{-1}.

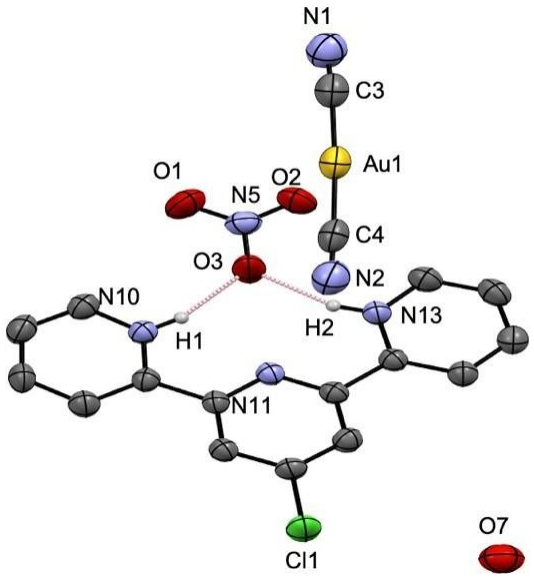

Figure 3.22. Solid-state structure of $[Chloro\text{-}terpy\text{-}H_2](NO_3)[Au(CN)_2]\bullet H_2O$ (7). Colour Scheme: Carbon, gray; Nitrogen, blue; Oxygen, red; Gold, yellow; Chlorine, green.

Table 3.7. Selected bond lengths and angles in 7.

Type	Bond lengths (Å)	Type	Bond angles (°)
Au1 – C3 Au1 – C4 O1 – N5 O3 – N5 O2 – N5 C12 – Cl1 Au1 – Au1	1.997(6) 1.990(5) 1.225(5) 1.264(5) 1.226(4) 1.729(3) 3.828	O1–N5– O3 O1–N5– N2 O2–N5–O3 C3–Au1– C4	119.3(4) 122.98 118.03(4) 176.62(19)

3.3. Phenanthroline-containing bismuth cyanoaurate coordination polymers

3.3.1. $[Bi(Phen)_2(\mu\text{-}OH)]_2[Au(CN)_2]_4 \bullet 2MeOH$ (8)

Compared to tridentate terpyridine, analogous reactions with 1,10-phenanthroline, which is bidentate and less basic than terpyridine, were surveyed to examine the resulting structural impact. Thus, the addition of one equivalent of bismuth triflate to two equivalents of 1,10-phenanthroline in methanol, followed by the addition of 3 equivalents of $KAu(CN)_2$ in methanol, yielded shiny yellow crystals of $[Bi(Phen)_2(\mu\text{-}OH)]_2[Au(CN)_2]_4 \bullet 2MeOH$ (**8**) after 3 days.

Single crystal X-ray diffraction shows that the polymeric structure of $[Bi(Phen)_2(\mu\text{-}OH)]_2[Au(CN)_2]_4 \bullet 2MeOH$ (**8**) where the Bi(III) centre is coordinated to two phenanthroline ligands, two bridging hydroxides and two N-cyano bound $[Au(CN)_2]^-$ units (Figure 3.23); note that four coordination sites are now blocked by two bidentate phenanthroline ligands, rather than a single tridentate terpyridine (see complexes **1** and **3** in particular). Each bismuth centre is thus 8- coordinate; an additional $[Au(CN)_2]^-$ counterion and interstitial methanol are unligated. The Bi- N(Phen) bond lengths are 2.646(13), 2.687(12), 2.576(14) and 2.551(14) Å respectively, i.e., they are similar, while the bridging Bi-O(hydroxide) lengths are slightly more asymmetric, at 2.190(10) and 2.322 (11)Å. The $[Bi(phen)_2(\mu\text{-}OH)]_2$ units are linked via two parallel $[Au(CN)_2]^-$ units (Au(1)), having Bi-N bond lengths of 2.725(14) Å. Hence, the local coordination geometry around the bismuth(III) centre is still asymmetric (Figure 3.24.), consistent with the presence of a stereochemically active lone pair, but the asymmetry appears to be less than in similar terpyridine- containing structures **1** and **3** (see Section 3.5 for discussion). Thus, overall, the structure can be described as a 1-D columnar chain of $[Bi(Phen)_2(\mu\text{-}OH)]_2$ units propagated by $[Au(CN)_2]^-$ bridges (Figure 3.25.). These cyanoaurate bridges, along with the unligated $[Au(CN)_2]^-$ units, form a pseudo-linear tetramer of Au(I) centres between the $[Bi(Phen)_2(\mu\text{-}OH)]_2$ units (Figure 3.26.), with aurophilic interactions of 3.325 (12) Å for Au1-Au2 and a very long 3.622 Å for Au1-Au1'; this latter distance is just beyond the aurophilic cutoff and so this tetranuclear unit could also be considered to be a pair of dimeric gold-gold interactions. (Table 3.8).

The IR spectrum of **8** shows a ν(CN) peak at 2143 cm^{-1}, assigned to the free Au-CN moiety. This compound was not visibly emissive when irradiated with 375 nm light.

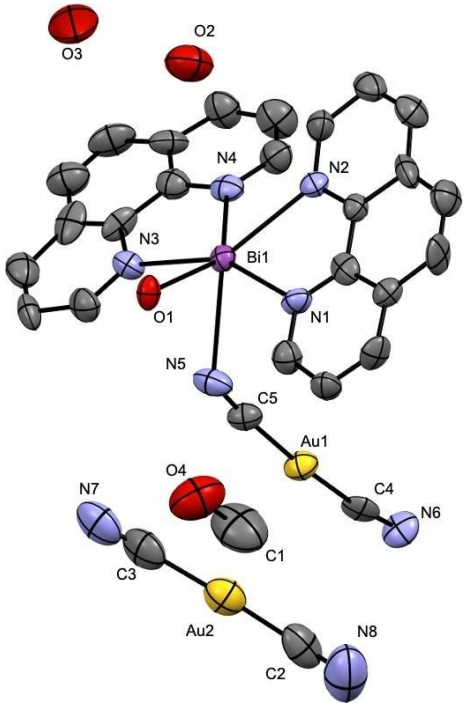

Figure 3.23. Asymmetric unit of the solid-state structure of $[Bi(Phen)_2(\mu\text{-}OH)]_2[Au(CN)_2]_4 \bullet 2MeOH$ (8). Colour Scheme: Carbon, gray; Nitrogen, blue; Oxygen, red; Gold, yellow; Bismuth purple.

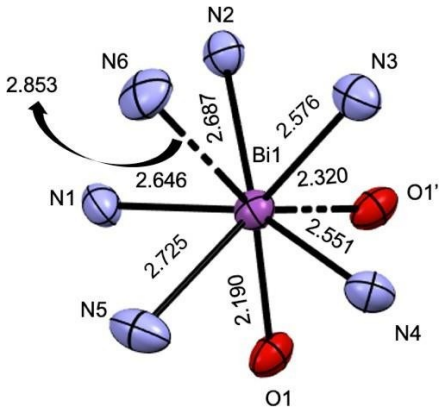

Figure 3.24. Coordination sphere of $[Bi(Phen)_2(\mu\text{-}OH)]_2[Au(CN)_2]_4 \bullet 2MeOH$ (8). Colour Scheme: Nitrogen, blue; Oxygen, red; Bismuth purple.

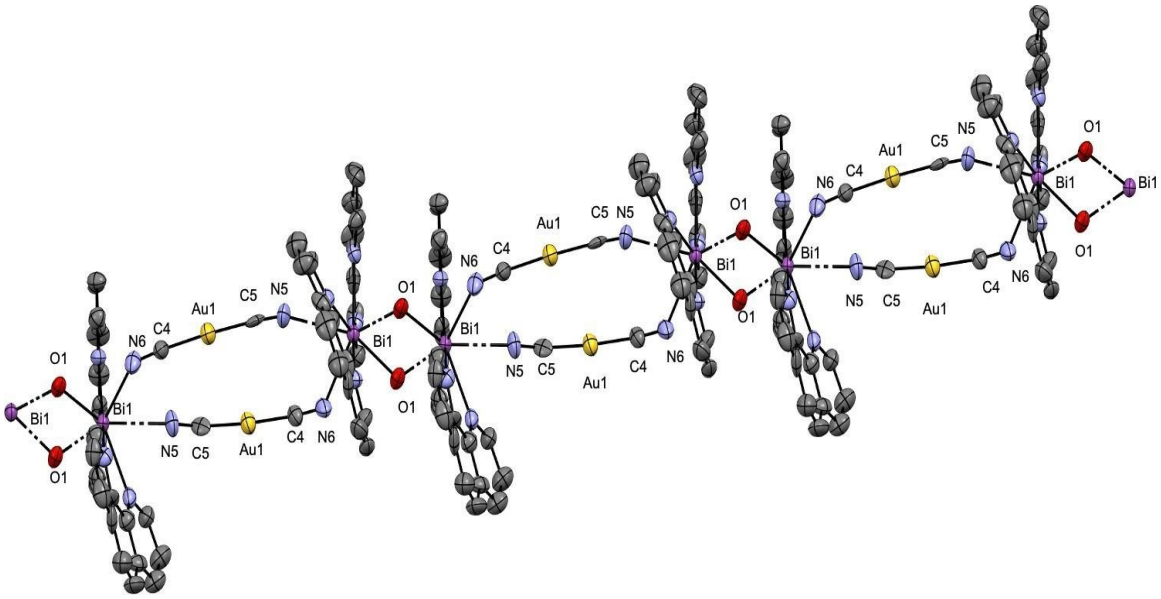

Figure 3.25. **1-D chain structure of $[Bi(Phen)_2(\mu\text{-}OH)]_2[Au(CN)_2]_4 \bullet 2MeOH$ (8). Colour Scheme: Carbon, gray; Nitrogen, blue; Oxygen, red; Gold, yellow; Bismuth, purple. Solvent molecules are omitted for clarity.**

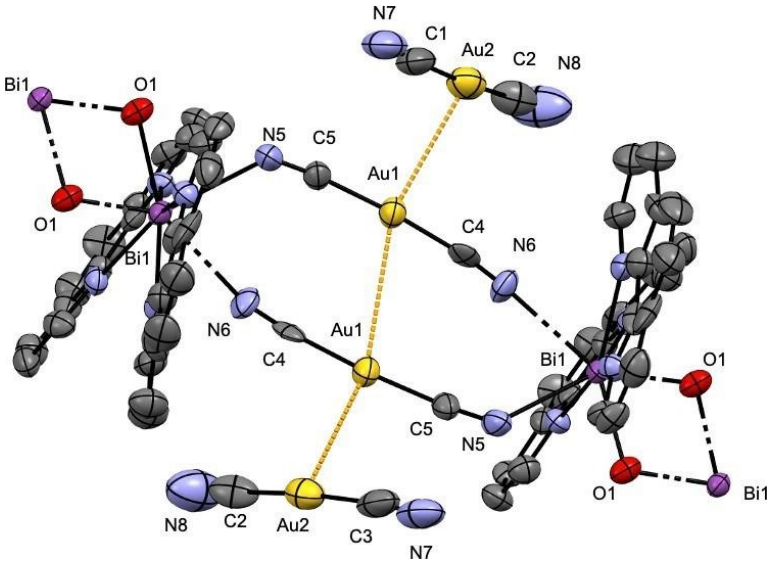

Figure 3.26. **Gold-Gold interaction in $[Bi(Phen)_2(\mu\text{-}OH)]_2[Au(CN)_2]_4 \bullet 2MeOH$ (8). Colour Scheme: Carbon, gray; Nitrogen, blue; Oxygen, red; Gold, yellow; Bismuth, purple. Solvent molecules are omitted for clarity.**

Table 3.8. Selected bond lengths and angles in 8.

Type	Bond lengths (Å)	Type	Bond angles (°)
Bi1 – N1	2.646(13)	N2–Bi1– N1	61.74(4)
Bi1 – N2	2.687(12)	N2–Bi1– N3	83.83(4)
Bi1 – N3	2.576(14)	N1–Bi1– N5	80.74(5)
Bi1 – N4	2.551(14)	N4–Bi1– N5	78.72(5)
Bi1 – N5	2.725(14)	N5–Bi1– N6	73.46
Bi1 – O1'	2.322 (11)	N2–Bi1– N6	78.31
Bi1 – O1	2.190 (10)	N3–Bi1– N4	64.96(4)
Au1 – Au2	3.325(12)	N3–Bi1– N6	66.50
Au1 – Au1'	3.622	O1–Bi 1– O1'	68.25(5)
Au2 – Au2	11.19	O1–Bi1– N2	76.05(4)
Au1 – C5	1.939(17)	O1–Bi1– N1	80.10(4)
Au1 – C4	1.934(19)	O1'–Bi1– O1	66.29(5)
Au2 – C3	2.026(3)	N3–N1– O1	85.46
Au2 – C2	1.966(3)	O1–Bi1– N5	75.90(4)

3.3.2. $[Bi(Phen)_2(\mu{-}OH)(H_2O)]_2[Au(CN)_2]_2(CF_3SO_3)_2$ (9)

The addition of two equivalents of bismuth triflate in water (vs. methanol in the case of complex **8**) to a methanol solution of one equivalent of phen, followed by the addition of three equivalents of $KAu(CN)_2$ in methanol, yielded yellow crystals of $Bi(Phen)_2(\mu{-}OH)(H_2O)]_2[Au(CN)_2]_2(CF_3SO_3)_2$ (**9**) after 3 days. Single crystal X-ray diffraction shows a dimeric structure of $[Bi(Phen)_2(\mu{-}OH)(H_2O)]_2[Au(CN)_2]_2$, where bismuth centre is 8- coordinate, consisting of two phen ligands, two bridging hydroxide units, an aqua ligand and an N-bound $[Au(CN)_2]^-$ moiety. (Figure 3.27), The Bi-N(Phen) bond lengths are 2.610(4), 2.578(4), 2.659(4) and 2.581(4) Å, while the Bi-N(cyano) distance is a longer 2.782(5) Å. The bridging Bi- OH bond lengths are much shorter, at 2.255(3) and 2.259(3) Å, while the Bi-OH2 aqua distance is much longer 2.620(4) Å, as would be expected for neutral vs. anionic oxygen-donors. Hence, the local coordination geometry around the bismuth(III) centre is asymmetric (Figure 3.28), consistent with the presence of a stereochemically active lone pair. Each dimer is connected by a long Au-Au interaction between dimers of 3.572(x) Å (Figure 3.28), and the dangling N-cyano unit also hydrogen bonds to the Bismuth-bound aqua ligand of the next dimer (N1-O2 distance = 2.795 Å), reinforcing the 1-D chain structure. Thus, overall, the structure can be

described as a 1-D columnar chain of $[Bi(Phen)(\mu\text{-}OH)_2]_2$ units propagated by $[Au(CN)_2]^-$ bridges (Figure 3.28). (Table 3.9).

The IR spectrum of shows ν(CN) peaks at 2154 and 2162 cm^{-1}, consistent with two inequivalent CN groups, as is observed in the structure; one is weakly bound to Bi(III), while the other hydrogen-bonds to a Bi-OH2 unit. For that reason, both peaks are shifted from the typical 2141-2145 cm^{-1} observed for unbound $[Au(CN)_2]^-$ units. The (unligated) triflate ion's typical signature peak is also observed, at 1283 cm^{-1}. (Figure 3.29). This compound was not visibly emissive when irradiated with 375 nm light.

Note that the synthetic difference between isolating **8** and **9** is primarily that of a change of solvent, where **8** is isolated from a methanol solution while **9** is an aqueous/methanol mixture, where the water provides a blocking ligand to the Bi(III) centre in **9**, which is taken by a bridging N-cyano group in **8**; as a result, the structure of **8** is considerably more complex. This shows that small changes in synthetic procedure and conditions can lead to substantially different products, where the energy (and crystallization preference) differences between the isolated products are likely quite low.

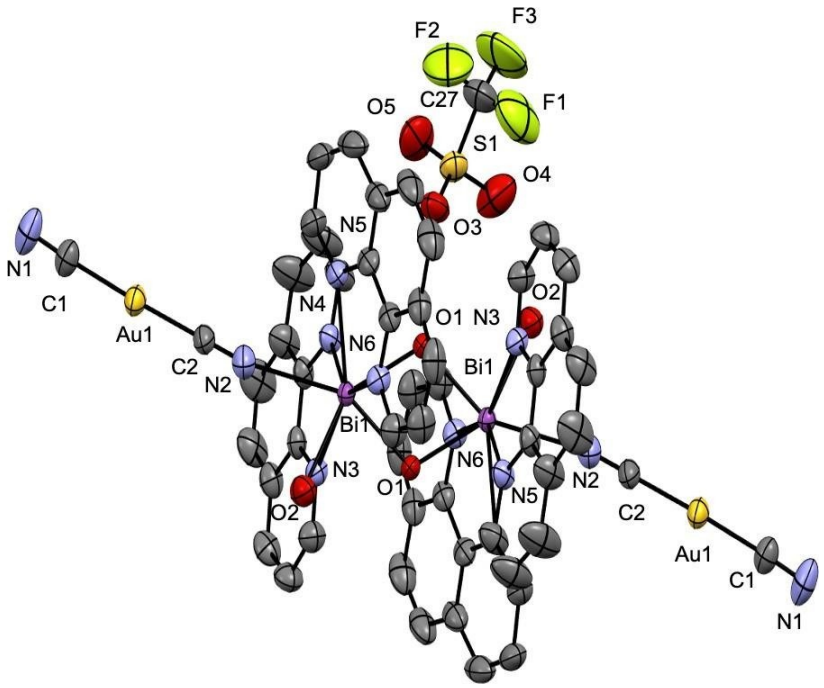

Figure 3.27. Solid-state structure of $Bi(Phen)_2(\mu\text{-}OH)(H_2O)]_2[Au(CN)_2]_2(CF_3SO_3)_2$ (9). Colour Scheme: Carbon, gray; Nitrogen, blue; Oxygen, red; Gold, yellow; Sulfur, yellow; Fluorine, green; Bismuth, purple.

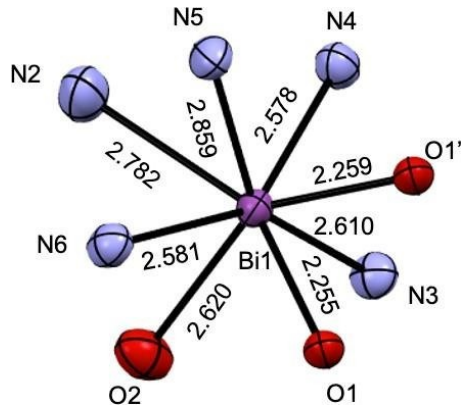

Figure 3.28. Coordination sphere of bismuth in $Bi(Phen)_2(\mu-OH)(H_2O)]_2[Au(CN)_2]_2(CF_3SO_3)_2$ (9).

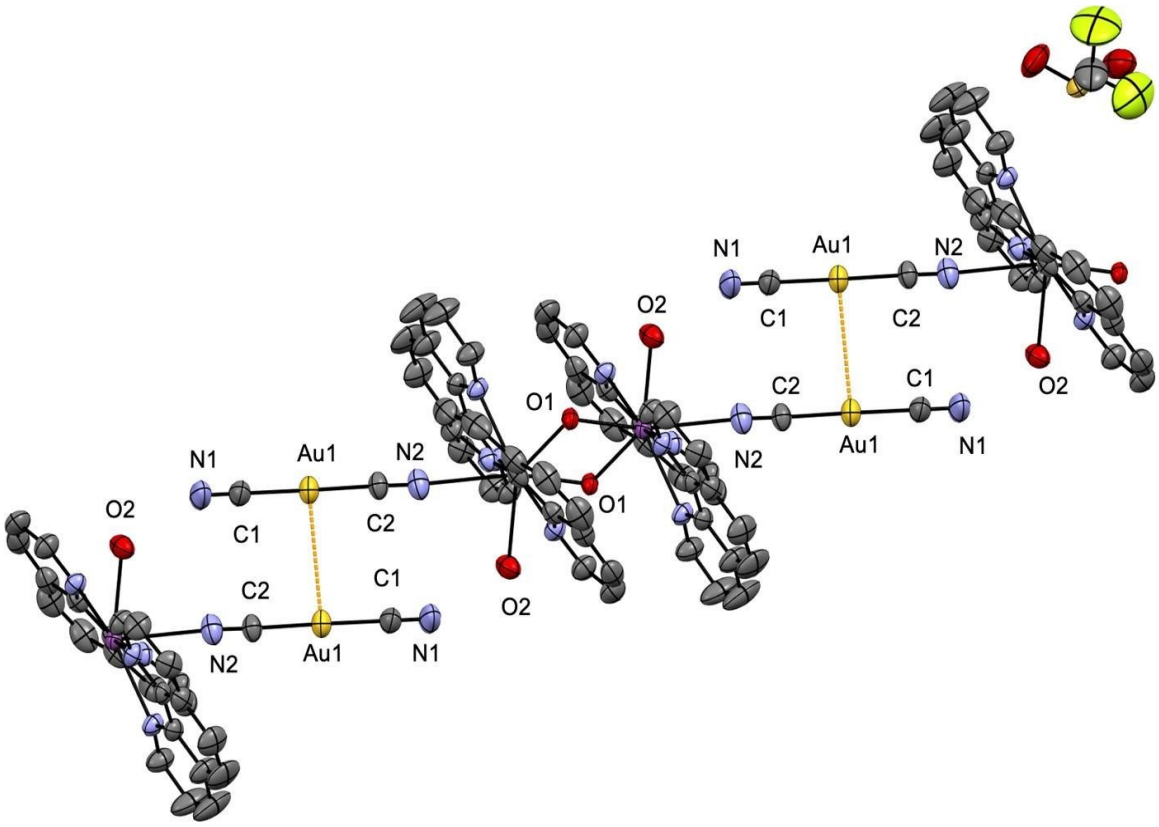

Figure 3.29. Aurophilic interaction in $Bi(Phen)_2(\mu-OH)(H_2O)]_2[Au(CN)_2]_2(CF_3SO_3)_2$ (9). Colour Scheme: Carbon, gray; Nitrogen, blue; Oxygen, red; Gold, yellow; Sulfur, yellow; Fluorine, green; Bismuth, purple.

Table 3.9. Selected bond lengths and angles in 9.

Type	Bond lengths (Å)	Type	Bond angles (°)
Bi1 – N4	2.578(4)	N3–Bi1– N4	63.33(13)
Bi1 – N3	2.610(4)	N5–Bi1– N4	87.74(14)
Bi1 – N2	2.782(5)	N6–Bi1– N2	113.13(15)
Bi1 – N6	2.581(4)	N2–Bi1– N3	83.28(15)
Bi1 – N5	2.659(4)	N6–Bi1– N5	62.92(13)
Bi1 – O1'	2.255(3)	N2–Bi1– N4	69.24(16)
Bi1 – O1	2.259(3)	N5–Bi1– N2	75.57(15)
Bi1 – O2	2.620(4)	N4–Bi1– N6	87.74(13)
Au1 – Au1	3.572	O1–Bi 1– O1'	67.34(13)
Au1 – C1	1.982(6)	O1–Bi 1– O2	142.56(13)
Au1 – C2	1.977(6)	O1–Bi1– N3	79.69(13)
		O1–Bi1– N6	80.11(13)
		N5–Bi1– O1	76.27(12)
		N4–Bi1– O1	78.91(13)
		N3–Bi1– O1	79.69(12)
		N3–Bi1– O1	113.23(13)
		N3–Bi1– O2	77.95(14)
		N2–Bi1– O2	78.89(15)
		N6–Bi1– O2	75.65(14)

Examining all the Bi/Au$(CN)_2$-based materials described above, most of the structures were one-dimensional chains (with a wide range of different structures within that general dimensionality), with a few zero-dimensional dimers or clusters (compounds **2** and **6**). No 2- or 3- D structures were obtained, which is not surprising given that terpy and phen were utilized as dimensionality-restricting capping ligands. To increase dimensionality of these materials, likely it would be necessary to reduce the denticity of the capping ligands, or remove them entirely (efforts were made in this regard but the resulting products could not be crystallized, likely due to the higher dimensionality and resulting rapid precipitation). Indeed, it is interesting to see how similar some of the structures are when using phen vs. terpy, for example, 1-7 and 10 are related 1-D columnar chains, while 8 and 9 are similarly-structured 1-D chains as well.

3.4. Bismuth(III) coordination complexes of terpy- and phen-based ligands

During efforts to synthesize and crystallize the bismuth/$Au(CN)_2$-based coordination polymers described above, an interesting collection of simple bismuth(III) coordination complexes with chelating heterocyclic amine ligands but without $[Au(CN)_2]^-$ counterions were isolated as crystalline side-products and their crystal structures determined. These products were not prepared in a rational synthesis and thus their yields and characterization data are very limited (beyond the crystal structures); however, they do provide insight into simple coordination chemistry of bismuth(III) and give guidance for the future targeting of these potentially valuable starting materials and coordination complexes. The synthetic conditions and crystal structure descriptions of these coordination complexes, which utilize terpyridine-based and phenanthroline ligands with Bi(III) centres, are outlined below.

3.4.1. Bi(Terpy)$(H_2O)_2$(μ-OH)$(Triflate)_2$ (10)

The addition of one equivalent of an aqueous solution of bismuth triflate to two equivalents of a methanol solution of terpyridine yielded a yellow solution from which crystals of Bi(Terpy)$(H_2O)_2$(μ-OH)$(Triflate)_2$ (**10**) were produced after several hours. Bi(Terpy)$(H_2O)_2$(μ-OH)$(Triflate)_2$ is a hydroxide-bridged dimer of [Bi(terpy)$(H_2O)_2$(triflate)] units (Figure 3.30); an additional triflate anion is unbound. Each bismuth centre is eight-coordinate, consisting of a single terpy ligand, two bridging OH units, an O-bound triflate and two water molecules. The Bi-N(terpy) bond lengths are 2.437(3), 2.478(3) and 2.590(3) Å, while the bridging hydroxides form a short/long pattern of 2.152(3) and 2.408(3) Å; the terminal aqua ligands are much longer, at 2.654(3) and 2.896 Å, while the triflate Bi-O bond is a long 2.874 Å (Table 3.10). Hence, the local coordination geometry around the bismuth(III) centre is asymmetric (Figure 3.31), consistent with the presence of a stereochemically active lone pair.

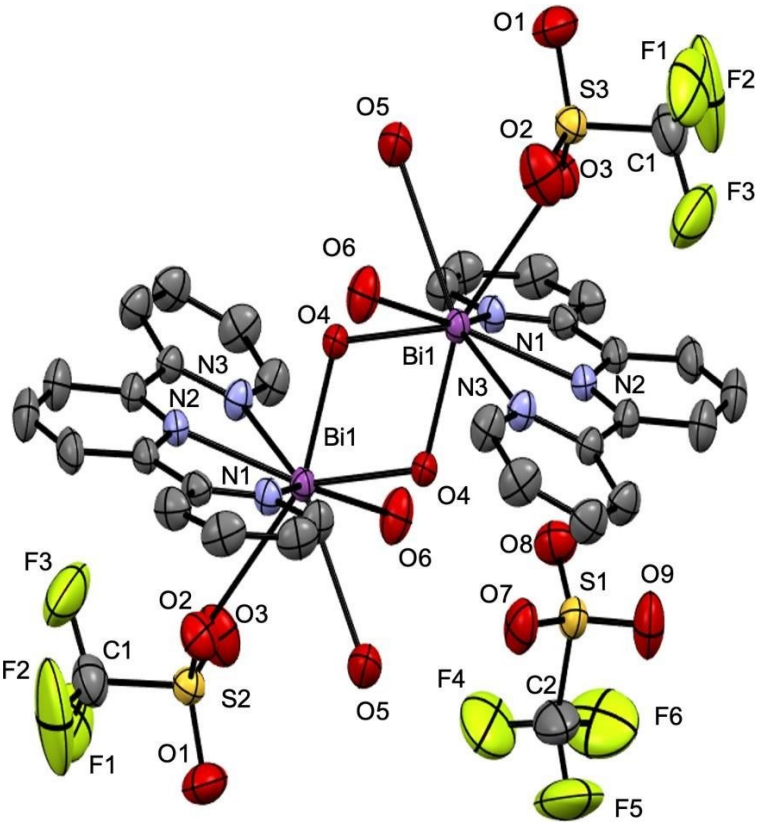

Figure 3.30. Structure of Bi(Terpy)(H_2O)$_2$(μ-OH)(Triflate)$_2$ (10). Colour Scheme: Carbon, gray; Nitrogen, blue; Oxygen, red; Sulfur, yellow; Fluorine, green; Bismuth, purple.

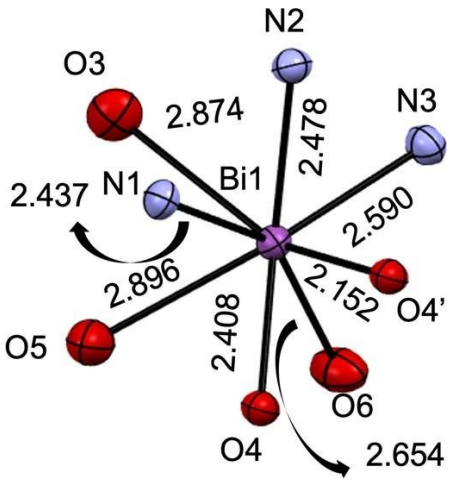

Figure 3.31 Coordination sphere of Bi(III) in Bi(Terpy)(H_2O)$_2$(μ-OH)(Triflate)$_2$ (10)

Table 3.10. Selected bond lengths and angles for 10.

Type	Bond lengths (Å)	Type	Bond angles (°)
Bi1 – O3	2.874	O5–Bi1– O3	63.61
Bi1 – O5	2.896	O5–Bi1– O6	77.15
Bi1 – O4	2.408(3)	O4–Bi1– O4’	65.90(11)
Bi – O6	2.654(3)	O6–Bi1– O4	73.78(12)
Bi1 – O4’	2.152(3)	O3–Bi1– N3	98.54
Bi1 – N1	2.437(3)	N3–Bi1– N2	64.89(11)
Bi1 – N2	2.478(3)	O4–Bi1– N2	85.27(10)
Bi1 – N3	2.590(3)	O1–Bi1– N2	64.89
		O6–Bi1– N3	78.26(11)
		O5–Bi1–O4	68.54
		O3–Bi1–N1	70.40
		O3–Bi1–N2	67.62
		N1–Bi1–N2	66.49(11)
		N1–Bi1–O4	82.30(10)

3.4.2. Bi(4'-Amino-Terpy)$(NO_3)_3$ (11)

The addition of one equivalent of acidic water solution of bismuth nitrate was added to two equivalents of a methanol solution of 4'-amino-terpyridine, followed by addition of three equivalents of $KAu(CN)_2$ in methanol solution; from this yellow solution, crystals of Au-free Bi(4'- Amino-Terpy)$(NO_3)_3$ were produced after two days.

Single crystal X-ray diffraction revels that the structure of Bi(4'- Amino-Terpy)$(NO_3)_3$ (Figure 3.32). contains a nitrate-bridged dimer of the [Bi(4'-amino-terpy)$(NO_3)_2$] unit, where each bismuth centre is ten-coordinate, consisting of a single terpy ligand, two η^2-chelating NO3 units, and two bridging nitrate units, which each bind η^2 to one Bi and η^1 to the other (generating three Bi-O bonds to each Bi centre collectively).[36] The Bi-N(amino-terpy) bond lengths are a very similar 2.462(19), 2.463(19) and 2.467(18) Å. The Bi-O bond lengths for the chelating, non-bridging nitrates are quite asymmetric, with each nitrate showing a short and long Bi-O distance (2.438(19) Å and 2.794 Å; 2.399(2) Å and 2.772 Å for the pair), while each bridging nitrate (which are symmetrically equivalent) has a Bi-O distance of 2.825 Å for the non-bridging N-O bond and a long 2.916 Å for the N-O unit that bridges the two Bi-centres (Figure 3.33), consistent with the presence of a stereochemically active lone pair. Each dimer interactions via hydrogen bonding between the back-side amino-group and non-bridging nitrate-O atoms

of the adjacent dimer (N-H---O distances of 3.085 and 3.185 Å). The FTIR spectrum shows a range of nitrate N-O stretches between 1292 and 1598 cm^{-1}.(Table 3.11).

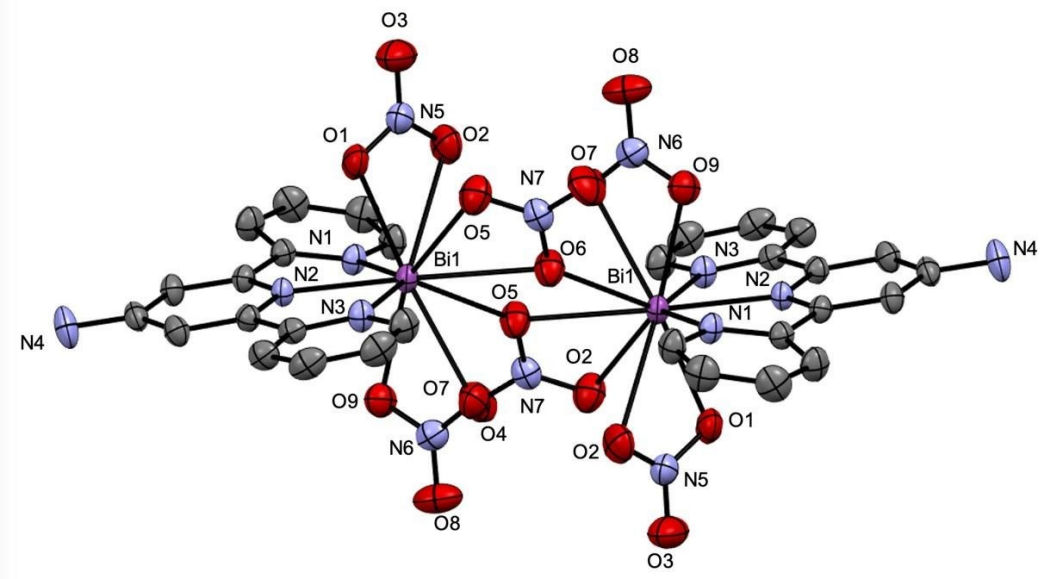

Figure 3.32 Structure of Bi(4'-Amino-Terpy)$(NO_3)_3$ (11). Colour Scheme: Carbon, gray; Nitrogen, blue; Oxygen, red; Bismuth, purple.

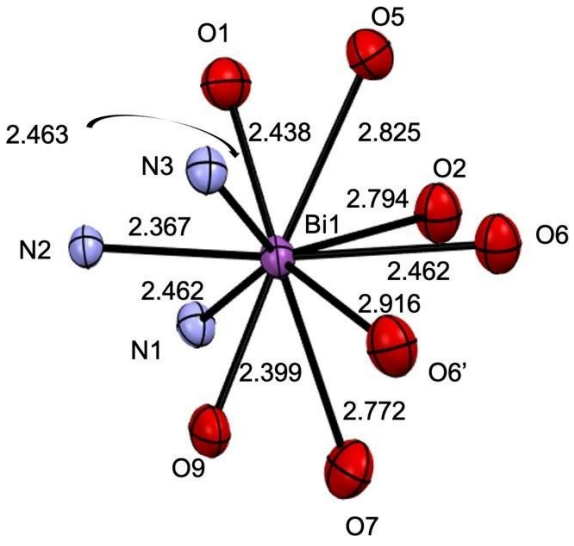

Figure 3.33. Coordination sphere of Bi(4'-Amino-Terpy)$(NO_3)_3$ (11)

Table 3.11. Selected bond lengths and angles for 11.

Type	Bond lengths (Å)	Type	Bond angles (°)
Bi1 – O1	2.438(19)	O7–Bi1– O6	61.74
Bi1 – O2	2.794	O5–Bi1– O6	43.90
Bi1 – O6	2.462	O5–Bi1– O2	65.79
Bi – O9	2.399(2)	O1–Bi1–O2	47.82
Bi1 – O7	2.772	O1–Bi1– N1	80.45(7)
Bi1 – N1	2.462(19)	N2–Bi1–N1	67.65(6)
Bi1 – N2	2.367(18)	N2–Bi1– O9	72.01(7)
Bi1 – N3	2.463(19)	O9–Bi1– O7	48.63(2)
Bi1 – O6'	2.916		
Bi1 – O5	2.825		

3.4.3. Bi(4'-para-bromoPhenyl-Terpy)$(NO_3)_3$ (12)

The addition of one equivalent of an acidic aqueous solution of bismuth nitrate to <2 equivalents of a methanol solution of 4'-para-bromophenyl-terpyridine, followed by addition of three equivalents of $KAu(CN)_2$ in methanol yielded a yellow solution from which Au-free crystals of Bi(4'-para-bromophenyl-Terpy)$(NO_3)_3$ were isolated after four days.

The structure of Bi(4'-para-bromophenyl-Terpy)$(NO_3)_3$ (Figure 3.34.) features a nine-coordinate bismuth centre, with a single 4´-para-bromophenyl-Terpy ligand and two η^2-chelating and one η^1- nitrate units. The Bi-N(Terpy) bond lengths (Table 3.12) are a very similar 2.443(14), 2.428(12) and 2.457(13) Å. Two of the chelating nitrate groups have a short/long Bi-O bonding pattern (2.389/2.661 Å and 2.486/2.684 Å) while the third group is η^1-bound, with one long distance of 2.759 Å; a bound methanol has a long Bi-O distance of 2.645 Å. Overall, this indicates the presence of a stereochemically active lone-pair (Figure 3.35).

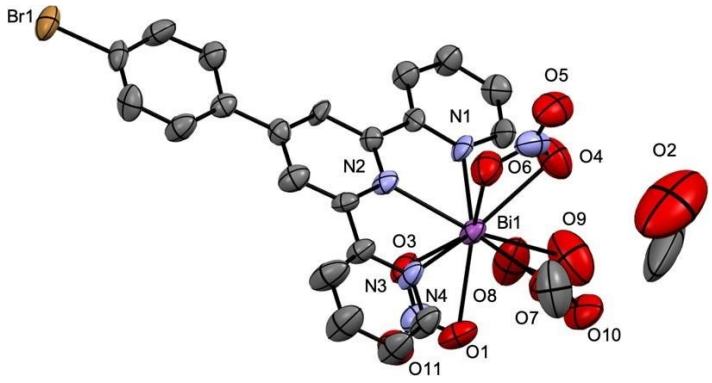

Figure 3.34. Bi(Bromo-Phenyl-Terpy)(NO_3)$_3$ (12). Colour Scheme: Carbon, gray; Nitrogen, blue; Oxygen, red; Bismuth, purple; Bromine, pale yellow.

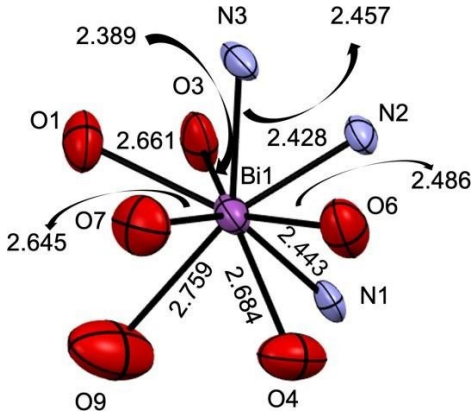

Figure 3.35. Coordination sphere of Bi(Bromo-Phenyl-Terpy)(NO_3)$_3$ (12)

Table 3.12. Selected bond lengths and angles for 12.

Type	Bond lengths (Å)	Type	Bond angles (°)
Bi1 – O1	2.661(13)	O9–Bi1– O4	68.19
Bi1 – O3	2.389(13)	O4–Bi1– O7	73.04(6)
Bi1 – O7	2.645(14)	O7–Bi1– O6	74.91(5)
Bi – O9	2.759	O6–Bi1–N3	73.39(5)
Bi1 – O4	2.684(16)	N3–Bi1– N2	66.12(4)
Bi1 – N3	2.457(13)	N2–Bi1–O3	70.53(4)
Bi1 – N2	2.428(12)	O3–Bi1– O1	49.97(4)
Bi1 – N1	2.443(14)	O1–Bi1– O7	81.49(5)
		O4–Bi1– N1	69.42(5)
		O6–Bi1– N2	73.36(4)
		O3–Bi1– N1	82.67(5)
		O9–Bi1– O1	75.03

3.4.4. {Bi(Phen)$(NO_3)_2$(μ-OH)}$_2$ (13)

To an excess of $Bi(NO_3)_3$•$5H_2O$ in acidified aqueous solution was added an aqueous solution of 1,10-phenanthroline, followed by addition of a methanolic solution of three equivalents of $KAu(CN)_2$; this yielded a yellow solution, from which crystals of the gold-free {Bi(Phen)$(NO_3)_2$(μ-OH)}$_2$ (**13**) were produced after three days.

The structure of {Bi(Phen)$(NO_3)_2$(μ-OH)}$_2$ has been previously reported[37] and contains a hydroxide-bridged dimer of the Bi(Phen)$(NO_3)_2$ unit,(Figure 3.37) where each bismuth centre is eight-coordinate, consisting of a single phen ligand, two bridging OH units and two η^2-nitrate moieties. The Bi-N(Phen) bond lengths are 2.531(4) and 2.416(4) Å and the nitrate Bi-O bond lengths are 2.651(5), 2.780, 2.657(5) and 2.846 Å (Figure 3.37), while the bridging hydroxides are a shorter 2.220(4) Å. (Table 3.13) this is more symmetric than the terpy-based hydroxide bridges in **10**. Overall, this Bi(III) centre is slightly less asymmetric (i.e., its stereochemical lone pair is less active) than in the terpy-containing analogues. Weak hydrogen bonding between the bridging OH and an unbound nitrato-O unit on an adjacent dimer of 2.773 Å also is present. The FTIR spectrum shows nitrate at 1315 cm^{-1}.

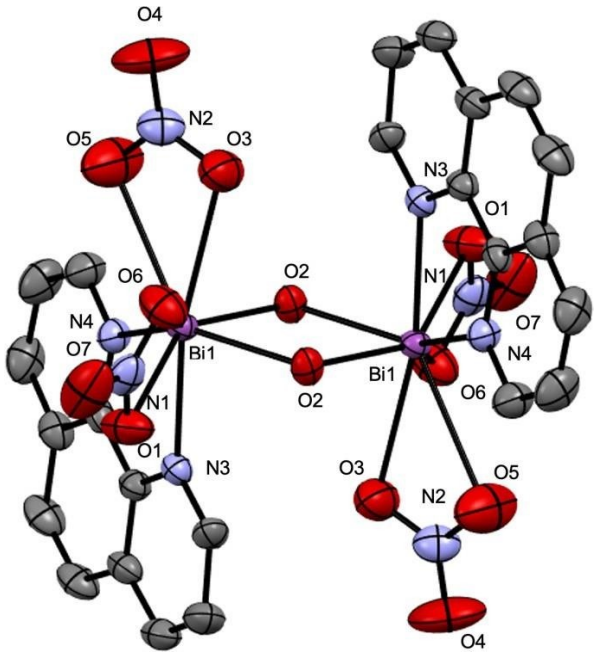

Figure 3.36. Structure of {Bi(Phen)$(NO_3)_2$(μ-OH)}$_2$ (13). Colour Scheme: Carbon, gray; Nitrogen, blue; Oxygen, red; Bismuth, purple.

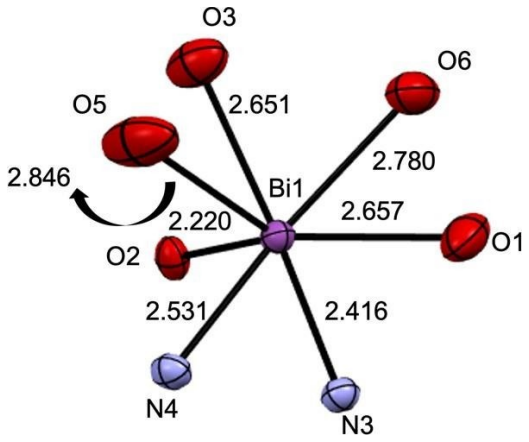

Figure 3.37. Coordination Sphere of {Bi(Phen)$(NO_3)_2$(μ-OH)}$_2$ (13). Two Bi-O2 bonds are present, but only one is shown.

Table 3.13. Selected bond lengths and angles for 13.

Type	Bond lengths(Å)	Type	Bond angles(°)
Bi1–O1	2.657(5)	O5–Bi1–O3	44.75
Bi1–O5	2.846	O3–Bi1–O6	66.12
Bi1–O6	2.780	O1–Bi1–O6	46.02
Bi–O3	2.651(5)	O1–Bi1–N3	72.04(15)
Bi1–O2	2.220(4)	O2–Bi1–N3	87.38(15)
Bi1–N4	2.531(4)	O2–Bi1–O3	82.07(15)
Bi1–N3	2.416(4)	O5–Bi1–N4	75.99

3.4.5. [H-Phen][Bi(Phen)$(NO_3)_4$] (14)

The addition of one equivalent of an acidic aqueous solution of bismuth nitrate was mixed with two equivalents of an aqueous acidic solution of Phen, to which 3 equivalents of $KAu(CN)_2$ in methanol were added, yielding a clear solution from which crystals of Au-free [H-Phen][Bi(Phen)$(NO_3)_4$] were produced after two days. Single crystal X-ray diffraction revealed the structure of [H-Phen][Bi(Phen)$(NO_3)_4$] (**14**) (Figure 3.38), containing a ten-coordinate bismuth(III) centre, consisting of a single phen ligand and four η^2-nitrate units. The Bi-N(Phen) bond lengths are 2.437(3) and 2.510(3) Å. There are two different types of chelating nitrate ligands: two are symmetrically bound (with similar Bi-O bond lengths ranging from 2.458(10)-2.645 (3) Å and two are more asymmetrically bound, with Bi-O bond length pairs of 2.494/2.931 Å and 2.474/2.726 Å, indicating the presence of some stereochemical lone-pair activity (Figure 3.39), consistent with the presence of a

stereochemically active lone pair. There is a hydrogen bond between the protonated [Phen-H] cation[38] and an unbound nitrato-O unit on the bismuthate anion (N(8)-O (9) distance = 2.909 Å).(Table 3.13).

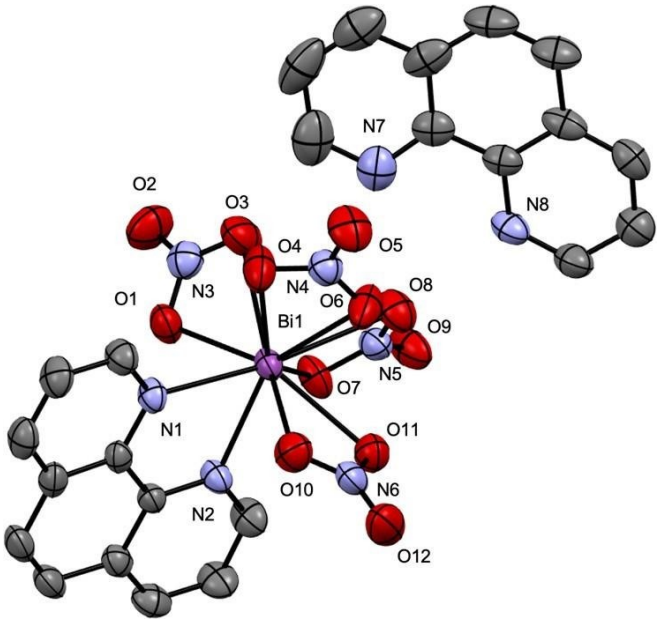

Figure 3.38. Structure of [H-Phen][Bi(Phen)(NO_3)$_4$] (14). Colour Scheme: Carbon, gray; Nitrogen, Blue; Oxygen, red; Bismuth, purple.

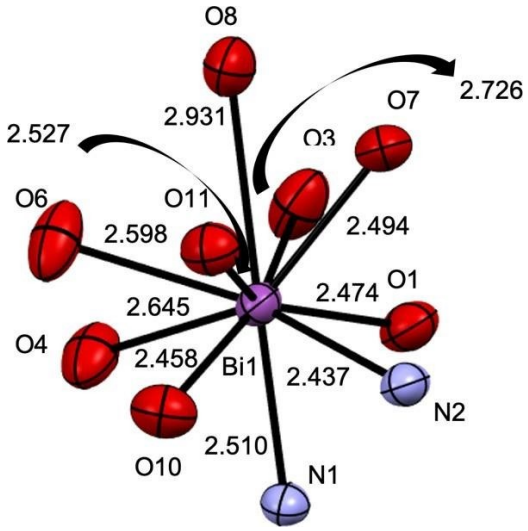

Figure 3.39. Coordination sphere of [[H-Phen][Bi(Phen)(NO_3)$_4$] (14)

Table 3.14. Selected bond lengths and angles for 14.

Type	Bond lengths(Å)	Type	Bond angles(°)
Bi1–O1	2.474(3)	O6–Bi1–O10	73.21(10)
Bi1–O7	2.494(3)	O4–Bi1–O10	85.34(10)
Bi1–O3	2.726(3)	O4–Bi1–N1	76.00(9)
Bi–O8	2.931	N1–Bi1–N2	67.41(9)
Bi1–O11	2.527(3)	O1–Bi1–N2	76.60(9)
Bi1–O6	2.598(3)	O1–Bi1–O3	48.58(8)
Bi1–O4	2.645(3)	O3–Bi1–O7	74.13(10)
Bi1–N2	2.437(3)	O8–Bi1–O7	45.85
Bi1–N1	2.510(3)	O8–Bi1–O11	69.09
Bi–O10	2.458(3)	O6–Bi1–O11	72.78(8)
		O10–Bi1–N2	75.39
		O3–Bi1–O4	74.61(10)
		N2–Bi1–O7	75.30
		O6–Bi1–O8	65.84

3.4.6. [H-Phen][Bi(Phen)Cl_3NO_3] (15)

The addition of one equivalent of stock acidic solution of bismuth chloride was mixed with three equivalent of Phen and two equivalent of $^{n}Bu_4N[Au(CN)_2 \bullet 0.5H_2O$ yielded a clear solution followed by crystals of [H-Phen][Bi(Phen)Cl_3NO_3] (**15**) were produced after three days. The structure contains a protonated [H-Phen] cation and a [Bi(Phen)Cl_3NO_3] anion, which π-π stack with each other.[39] The bismuthate anion contains an η^2-bound nitrate and a seven-coordinate bismuth(III) centre (**15**) (Figure 3.40). The Bi-N(Phen) bond lengths are 2.501(7) and 2.562(7) Å. The nitrato Bi-O bond lengths are 2.693(8) and 2.647(8) Å, while the Bi-Cl bonds lie within the tight range of 2.654(3)-2.7949'3) Å (Figure 3.41), (Table 3.14). suggesting a less stereochemically active lone pair in this system compared to the terpy- and chloride-free complexes. Weak hydrogen bonding between the cation and a bound Cl-unit in the anion also exists (N(4)-Cl(3) distance = 3.205 Å).

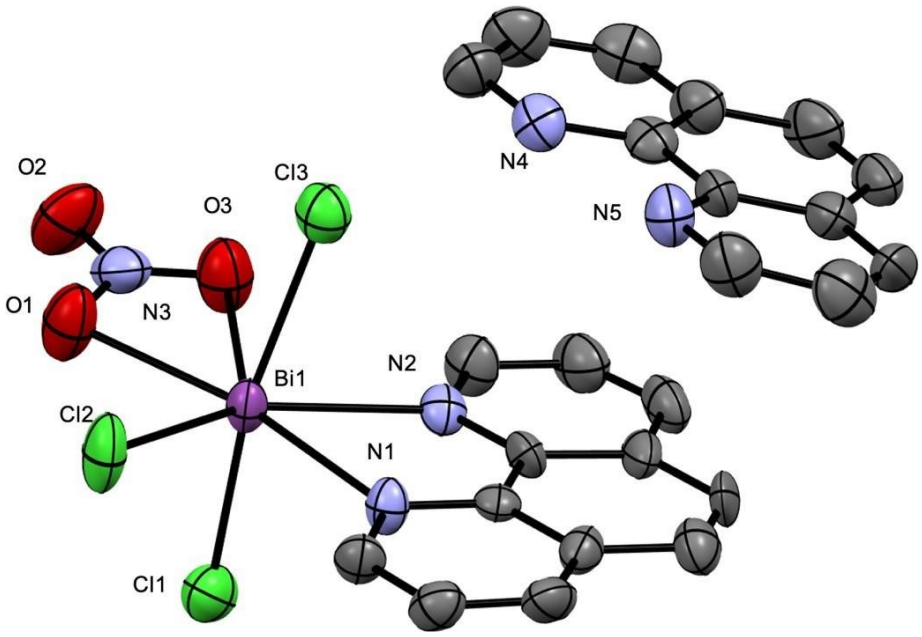

Figure 3.40. Structure of [H-Phen][Bi(Phen)Cl_3NO_3] (15). Colour Scheme: Carbon, gray; Nitrogen, Blue; Oxygen, red; Chlorine, green; Bismuth, purple.

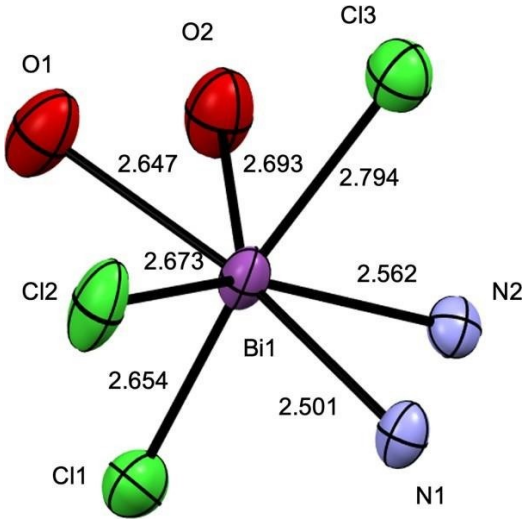

Figure 3.41. Coordination sphere of [H-Phen][Bi(Phen)Cl_3NO_3] (15)

Table 3.15. Selected bond lengths and angles for 15.

Type	Bond lengths (Å)	Type	Bond angles (°)
Bi1 – O1	2.647(8)	O2–Bi1– N2	76.79(2)
Bi1 – O2	2.693(8)	N2–Bi1– Cl3	84.57(17)
Bi1 – Cl1	2.654(3)	Cl3–Bi1– N1	85.16(2)
Bi –Cl2	2.673(3)	N1–Bi1–Cl2	84.51(18)
Bi1 – Cl3	2.794(3)	Cl1–Bi1– Cl2	95.38(12)
Bi1 – N1	2.501(7)	O1–Bi1–Cl1	86.96(2)
Bi1 – N2	2.562(7)	O1–Bi1– O2	47.69(2)
		Cl1–Bi1– N1	85.99(2)
		Cl2–Bi1– Cl3	67.69(11)
		O2–Bi1– Cl3	85.89(2)

3.4.7. {Bi(Phen)(H_2O)$_2$(μ-OH)(Triflate)$_2$}$_2$•H_2O (16)

The addition two equivalents of bismuth triflate with two equivalents of Phen in methanol generated a transparent solution, to which was three equivalents of $KAu(CN)_2$ (85 mg, 0.295 mmol), yielding a clear solution. After three days, crystals of gold-free {Bi(Phen)(H_2O)$_2$(μ-OH)(Triflate)$_2$}$_2$•H_2O (**16**) were produced. The structure of **16** contains a hydroxide-bridged dimer of the [Bi(Phen)(H_2O)$_2$(Triflate)$_2$] unit (Figure 3.42), where each bismuth centre is eight- coordinate, consisting of a single phen ligand, two bridging OH units, two bound aqua ligands and two weakly O-bound triflate units. The Bi-N(Phen) bond lengths are 2.493(14) and 2.602(5) Å, while the Bi-O bond lengths vary widely depending on the type of O-donor, ranging from short 2.154(6) and 2.329(3) Å for the (asymmetrically bridging) hydroxides, 2.634(4) Å and 2.616 (3) Å for the terminal aqua ligands, and 2.762 Å and 2.907 Å for the O-bound triflate ions (Figure 3.43). (Table 3.15).

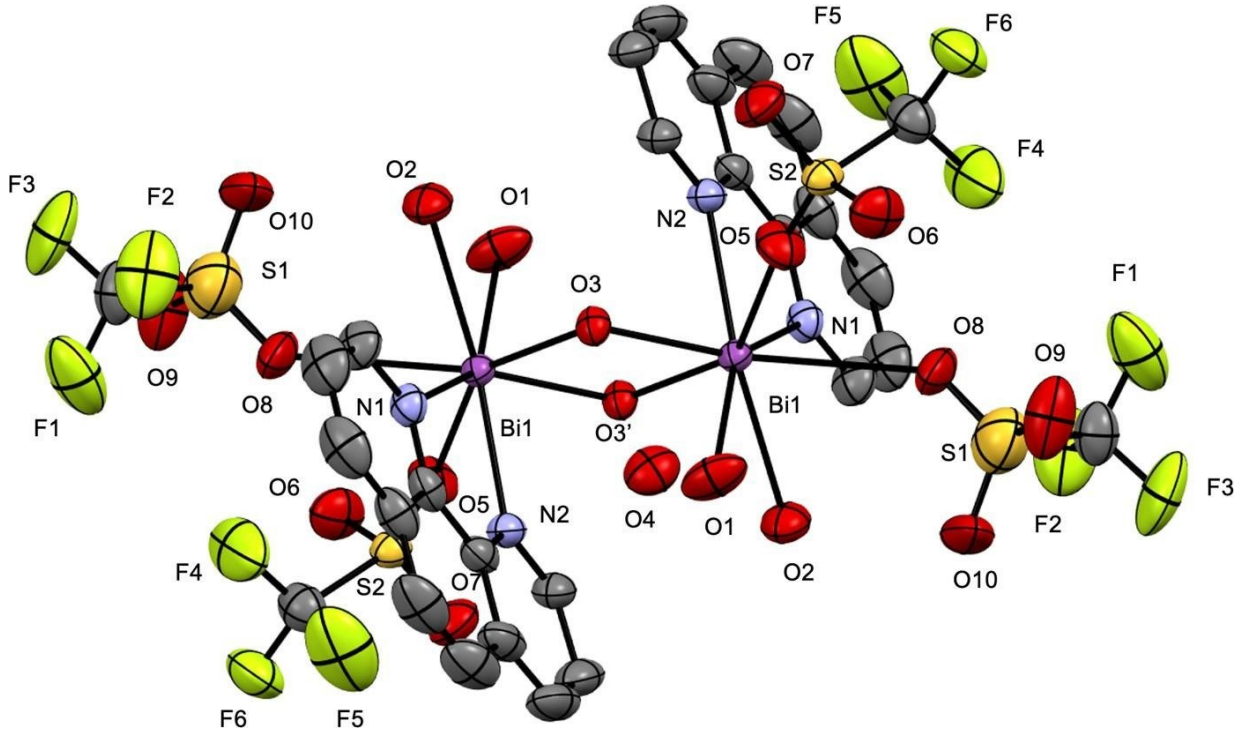

Figure 3.42. Structure of {Bi(Phen)(H_2O)$_2$(μ-OH)(Triflate)$_2$}$_2$•H_2O (16), Colour Scheme: Carbon, gray; Nitrogen, Blue; Oxygen, Red; Fluorine, green; Sulfur, yellow; Bismuth, purple.

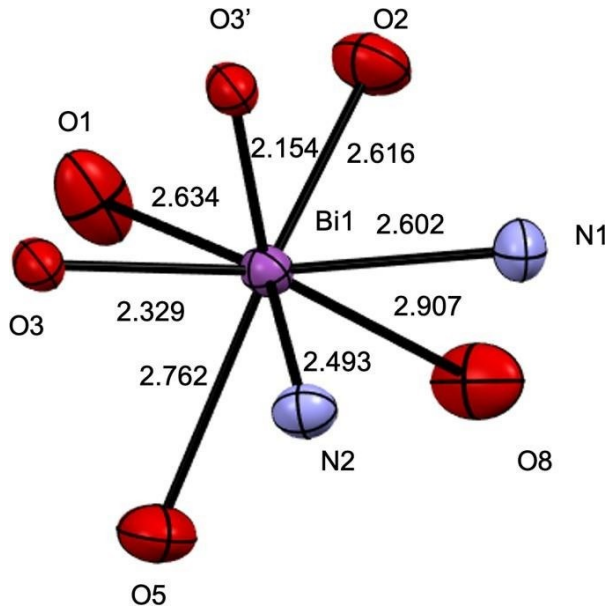

Figure 3.43. Coordination sphere of Structure of {Bi(Phen)(H_2O)$_2$(μ-OH)(Triflate)$_2$}$_2$•H_2O

Table 3.16. Selected bond lengths and angles for 16.

Type	Bond lengths (Å)	Type	Bond angles (°)
Bi1 – O1	2.634(4)	O3–Bi1– N2	80.20(5)
Bi1 – O3'	2.154(6)	N2–Bi1– O5	76.60
Bi1 – O2	2.616(3)	O5–Bi1– O8	77.84
Bi –O8	2.907(4)	O1–Bi1–O8	92.74
Bi1 – N2	2.493(14)	O1–Bi1– O2	68.42(19)
Bi1 – O5	2.762	O3–Bi1–O3'	67.45(4)
Bi1 – O3	2.329(3)	N1–Bi1– N2	65.12(7)
Bi1 – N1	2.602(5)	O5–Bi1– O1	80.36
Bi1 – N2	2.493(14)	N1–Bi1– O2	79.41(4)
		O1–Bi1– O3	72.41(10)

3.4.8. [H-Phen][Bi(Phen)(NO_3)$_4$] polymorph (17)

One equivalent of bismuth nitrate was mixed with two equivalents of Phen; to the resulting clear solution was added three equivalents of $KAu(CN)_2$. After three days, crystals of [H-Phen][Bi(Phen)(NO_3)$_4$] (**17**) were produced and the crystal structure obtained. Note that **17** has the same chemical formula and overall connectivity as **14** but has a different unit cell (triclinic in **17** vs. monoclinic in **14**); it is thus a polymorph of **14**.[40] (Figure 3.44),(Table 3.16). The bond lengths and angles are very similar, but not identical to, compound **14**.[37]

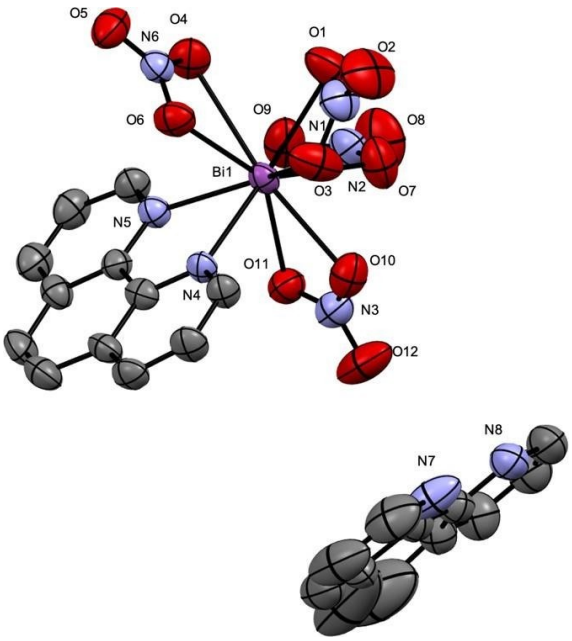

Figure 3.44. Structure of [H-Phen][Bi(Phen)(NO_3)$_4$] (17). Colour Scheme: Carbon gray; Nitrogen Blue; Oxygen, Red; Bismuth purple.

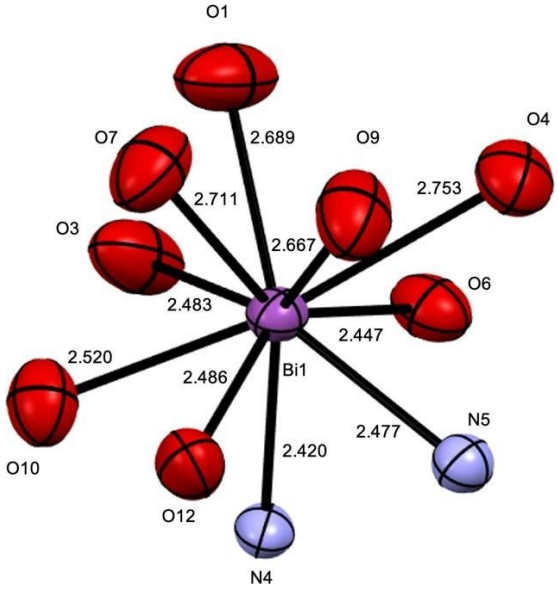

Figure 3.45. Coordination sphere of [H-Phen][Bi(Phen)(NO_3)$_4$] polymorph 17.

Table 3.17. Selected bond lengths and angles for 17.

Type	Bond lengths (Å)	Type	Bond angles (°)
Bi1 – O1	2.689(6)	O6–Bi1– N5	76.80(17)
Bi1 – O9	2.667(6)	O6–Bi1– N4	73.10(15)
Bi1 – O4	2.753(6)	O3–Bi1– N4	79.82(18)
Bi –O6	2.447(5)	O10–Bi1–O3	70.42(2)
Bi1 – N5	2.477(5)	O10–Bi1– O12	50.79(17)
Bi1 – N4	2.420(4)	O7–Bi1–O12	69.78(19)
Bi1 – O12	2.486(5)	O7–Bi1– O9	48.42(18)
Bi1 – O3	2.483(5)	O9–Bi1– N5	75.99(17)
Bi1 – O7	2.711(6)	O1–Bi1– O4	70.37(2)
		O1–Bi1– O7	75.32(2)
		O4–Bi1– N5	72.54(17)

3.5. Structural comparison of Bi(III) complexes and coordination polymers in this thesis

The body of structural information from the wide series of Bi(III)-containing coordination polymers with $[Au(CN)_2]^-$ using both terpy and phen, as well as the simpler coordination complexes, all described above, can be analyzed in terms of relative lone-pair stereochemical activity, the impact of using different anions (specifically triflate vs. nitrate) and synthesis in different solvents. Table 3.18 below examines the structural differences between terpy- vs. phen- based complexes, specifically their resulting coordination number, whether a hydroxo-bridged dimer was isolated or not, and critically, the spread between the shortest and longest M-L bond length (“spread” and “delta” in the table) as well as the difference between the longest and second - longest M-L length; this latter value is useful to ensure that a single long M-L distance in the overall spread does not unduly skew the conclusions regarding stereochemical activity. Aurophilic distances are included where applicable, and the anion used in the bismuth starting material was also noted.

Table 3.18. Structural comparisons of the coordination polymers and complexes in this thesis.

Compound [ligand, Bi salt]	Coordination number [solvent(s)]	OH-Bridged dimer	Bond length range [Au-Au distances]	Δd_{max} (M-L)	Two longest Bi-L bonds [$\Delta d_{longest}$]
1 [terpy, triflate)	7 [methanol]	Yes	2.183 - 2.798 Å [3.261 - 3.439 Å]	0.615 Å	N-cyano (2.798 Å) N-cyano (2.665 Å) [0.133 Å]
2 [terpy, nitrate]	9 [methanol, H_2O]	No	2.378 - 2.733 Å [3.544 Å]	0.355 Å	O-NO_2 (2.733 Å) N-cyano (2.664 Å) [0.069 Å]
3 [terpy, nitrate]	7 [methanol, acidified H_2O]	yes	2.151 - 2.900 Å [3.201 - 3.354 Å]	0.749 Å	N-cyano (2.900 Å) hydro (2.718Å) [0.182 Å]
4 [terpy, nitrate]	9 [DMSO]	No	2.449 - 2.731 Å [3.544 Å]	0.282 Å	N-cyano (2.731 Å) O-S (2.715 Å) [0.016 Å]
5 [terpy, triflate]	8 [DMSO]	Yes	2.152 - 3.007 Å [3.009 Å]	0.885 Å	N-cyano (3.007Å) O-S (2.725 Å) [0.282 Å]
6 [terpy, nitrate]	9 [methanol, acidified H_2O]	No	2.438 - 2.675 Å [3.370 Å]	0.237 Å	N-cyano (2.675 Å) to nitrate (2.613 Å) [0.062]
7 [terpy]	[methanol, acidified H_2O]	N/A	N/A	N/A	N/A
10 [terpy, triflate]	8 [methanol]	yes	2.152 - 2.896 Å [N/A]	0.717 Å	hydro (2.896 Å) N(terpy) (2.874 Å) [0.022 Å]
11 [terpy, nitrate]	10 [methanol, acidified H_2O]	No	2.367 - 2.916 Å [N/A]	0.549 Å	nitrate (2.916 Å) nitrate (2.825 Å) [0.091 Å]
12 [terpy, nitrate]	9 [methanol, acidified H_2O]	No	2.389 - 2.759 Å [N/A]	0.37 Å	nitrate (2.759 Å) Nitrate (2.684 Å) [0.075 Å]

Table 3.18 (continued)

8 [phen, triflate]	8 [methanol]	yes	2.190 - 2.853 Å [3.325 - 11.19 Å]	0.663 Å	N-cyano (2.853Å) N-cyano (2.725 Å) [0.128 Å]
9 [phen, triflate]	8 [H_2O, methanol]	yes	2.255 - 2.859 Å [3.572 Å]	0.604 Å	N(phen) (2.859 Å) N-cyano (2.782 Å) [0.077 Å]
13 [phen, nitrate]	8 [methanol, acidified H_2O]	yes	2.220 - 2.846 Å [N/A]	0.626 Å	nitrate (2.846 Å) nitrate (2.780 Å) [0.066 Å]
14 [phen, nitrate]	10 [methanol, acidified H_2O]	No	2.437 - 2.931 Å [N/A]	0.494 Å	nitrate (2.931 Å) nitrate (2.726 Å) [0.205 Å]
15 [phen, chloride]	7 [acidified methanol]	No	2.501 - 2.794 Å [N/A]	0.293 Å	Cl (2.794 Å) nitrate (2.693 Å) [0.101 Å]
16 [phen, triflate]	8 [methanol]	Yes	2.154 – 2.907 Å [N/A]	0.753 Å	O-S (2.907 Å) OH (2.762 Å) [0.145 Å]
17 [phen, nitrate]	10 [methanol, acidified H_2O]	No	2.420 - 2.753 Å [N/A]	0.553 Å	nitrate (2.753 Å) Nitrate (2.711 Å) [0.042 Å]

The structures can clearly be separated into those that incorporate μ-hydroxo dimers, and those that do not. In terms of synthesis, the use of un-acidified solutions of Bismuth triflate yields exclusively hydroxo-bridged dimers in all cases, but these structures do not necessarily include the triflate anion itself. The situation is less clear for Bismuth nitrate, where even weakly acidified solutions could give either hydroxo-bridged dimers or hydroxo-free systems.

In terms of other structural impacts of using triflate or nitrate-based bismuth salts, in the case of nitrate (especially when acidified with HNO_3), the resulting structures usually incorporated at least one nitrate, and often several nitrates, which also readily chelate; when there is no cyanoaurate anion competing with the nitrates, then nitrates are always bound (i.e., in the simple coordination compounds in section 3.4). As a result, in general, the coordination numbers for the nitrate-containing complexes are higher on average than those that started with bismuth triflate (whether triflate is included in the structure or not); specifically, the nitrate-containing species are 9- or 10-coordinate (except for compound

13), while the nitrate-free species are all 7- or 8- coordinate. This is also reflected in the different stereochemical activity; for high-coordinate bismuth centres with multiple nitrates, the stereochemical activity is generally lower than the activity observed for lower-coordinate complexes, as reflected in the larger overall spreads. On average, the spread for the 7- and 8- coordinate species is 0.656 while for the 9- and 10- coordinate complexes it is much smaller, at 0.406.

Since triflates are weak donor ligands, they generally do not bind to the Bi(III) centre in the presence of other anions are available, e.g., the $[Au(CN]^-$ unit in compound **9**. Where no other anion is available, the triflates do bind (albeit very weakly), along with the formation of hydroxo- bridged dimers (compounds **10** and **16**). Comparing compounds **13** and **16**, which are hydroxo- bridged dimers that also contain either triflate or nitrate and are both 8-coordinate, the stereochemical activity is slightly higher for the triflate-bound species than the nitrato-analogue (as indicated by the bond length spread).

When trying to deconvolute the stereochemical impact on the lone pair of using terpy vs. phen, it is necessary to compare sets of complexes where the other factors are changing as little as possible - in particular, the coordination number should be the same. By comparing only complexes that are 8-coordinate and are also hydroxo-bridged dimers, it is possible to try to isolate the impact of the two different capping ligands, although since there are many different factors, it is still difficult to make clear conclusions. Using this more limited set of complexes, in general the terpy- containing complexes (**5** and **10**) have higher stereochemically active lone-pairs than the similar phen-containing ones (compounds **8**, **9**, and **13**; compound **16** is an outlier). This is broadly consistent with the fact that more basic ligands are known to induce higher stereochemical activity in Pb(II) systems,[30] and terpy is more basic than phen. Also consistent with this is the unique compound **15**, which has chloride ligands and, although it is low-coordinate (7), its lone pair is not especially stereochemically active (spread = 0.293). Thus, the nature of the ligands as well as the coordination number are both important factors in observing and inducing stereochemical lone pair activity.

The choice of solvent appears to play little role in whether □-hydroxo dimers are formed or not; the presence of water, either as a solvent or as part of a solvent mixture, gives the Bi(III) centre the opportunity to bind aqua ligands, but in fact, only a few compounds do so (specifically, **2**, **3**, **7** and **16**). In most cases, methanol (which also

contains some water) was used as a solvent but was never found bound to the Bi(III) centre. In contrast, the use of DMSO solvent ensures that some DMSO will be O-bound to the Bi(III) centre (compounds **4** and **5**), i.e., it takes up a coordination site and blocks potential increases in dimensionality when coupled with the $[Au(CN)_2]^-$ linker. Even with the use of DMSO and nitrates, 1-D chain structures could be obtained in some cases, illustrating that even the use of these coordination-site blocking groups does not necessarily restrict coordination polymer growth, at least in one dimension. That said, it is more likely that using triflate as a starting material will generate multidimensional systems and future efforts towards this goal should focus on the triflate starting material rather than the chelating nitrate donors.

Structural-emission property correlation. Overall, the majority of Au-containing Bi(III) coordination polymers herein were non-emissive or very weakly emissive, which is surprising given that they all contain aurophilic interactions (Table 3.17); thus, there must be a quenching mechanism in these systems that is greatly reducing their emissive properties, unfortunately. Three systems had measurable emission properties – compounds **1**, **3** and **5** – but it is difficult to correlate the Au-Au distance to their emission maxima because the form of the aurophilic network is quite different in each case. Specifically, compound **1** has a tetranuclear cluster of Au(I) ions; compound **2** has a very non-linear 1-D chain of Au(I) units, while compound **3** has a single tight $[Au(CN)_2]^-$ based dimer. Interestingly, the lowest emission energy of 560 nm lies with compound **1**, which has the *longest* average Au-Au distance, but it is plausible that the cluster-nature of this emissive system is at least as important as the value of the distances. Excluding compound **1**, the shorter aurophilic distance in **5** is consistent with the lower-energy emission of 530 nm compared to compound **3** (510 nm), however given the large structural differences this comparison should be noted with caution.

3.6. Global Conclusions and Future Work

The goal of this thesis research was to try to make new coordination polymers with Bi(III) instead of Pb(II), using terpy, phen, and bipy as capping ligands and dicyanoaurate. In particular, whether Bi(III) analogues of the previously reported Pb(II)cyanoaurates could be prepared was of interest. The research was successful in preparing the first new coordination polymer materials containing bismuth(III) and $[Au(CN)_2]^-$, specifically reporting five containing terpy and three with phen (the bipy-containing species could not

be crystallized) and all were structurally characterized. The $[Bi(Terpy)(\mu\text{-}OH)]_2[Au(CN)_2]_4$ Complex (**1**) is structurally very similar to the Pb(II) analogue, showing that Bi(III) can be a viable structural replacement of Pb(II). However, similar properties may or may not manifest. For example, although most of these new materials contained aurophilic interactions, they were weakly emissive or non-emissive, unlike their Pb(II) counterparts. Most importantly, these are the first Bismuth(III) coordination polymers not only with $[Au(CN)_2]^-$ linkers but, to our knowledge, they represent the first structurally characterized examples of any bismuth cyanometallate coordination polymer in general.

The stereochemical activity of the lone pair on bismuth(III) was analyzed using not only the Au-containing coordination polymers but also a series of simple coordination complexes with terpy and phen. In general, Bi(III) does have a stereochemically active lone pair; specific conclusion about this stereochemical activity include:

- Both the nature of the ligands and the coordination number are essential in observing and inducing stereochemical lone pair activity.
- The stereochemical activity is slightly higher for the triflate-bound species than for the nitrato-analogues.
- Terpy-containing complexes have more stereochemically active lone pairs than similar phen-containing complexes.
- For high-coordinate bismuth centres with multiple nitrates, the stereochemical activity is generally lower than that observed for lower-coordinate complexes.

Future work should build on these efforts, and could include expansion of the types of capping ligands used with bismuth(III) centres. Different cyanometallates such as $[Pt(CN)_4]^{2-}$, $[Ag(CN)_2]^-$ and $[Fe(CN)_6]^{4-}$ should also be targeted, although it is important to be aware of the high acidity of the bismuth(III) centre and thus future synthetic efforts should focus on the use of bismuth triflate as the starting material - ideally, in non-aqueous media - since using bismuth triflate as a starting material should generate multidimensional systems. Efforts should also be made towards structurally characterizing the ligand-free Bi/$Au(CN)_2^-$ based system, which will likely require powder X-ray diffraction techniques to understand its structure.

In addition, the simple coordination complexes in section 3.4 provide a fascinating window into fundamental bismuth(III) coordination chemistry; as noted above, these complexes were isolated as side-products from reactions that were targeting coordination polymer products. It would be worthwhile to design rational syntheses for these complexes and pair their already- completed X-ray structural data herein with a bulk synthetic procedure and accompanying characterization, which will also allow these complexes to be utilized in further reactions.

Thus, to summarize the main global conclusions:

1. Pb(II) can be replaced with Bi(III) and they can exhibit stereochemical lone pair activity

2. 1-D coordination polymer chains were created through Au-Au interactions and other motifs

3. The range of stereochemical activity varied from high (low coordination number) to low (high coordination number)

4. These are the first Bi(III) cyanometallate coordination polymers

5. The Bi(III) + $[Au(CN)_2]^-$ materials are weakly to non-emissive

In general, it is clear that bismuth(III)-containing coordination polymers are worthy of continued substantial investigation in the future, both with respect to a fundamental understanding of the lone-pair effects on structure and property, as well as the potential use of these bismuth(III) cyanometallate coordination polymers in a range of applications that harness the stereochemical lone-pair activity in the same fashion as lead(II).

3.7. Experimental Section

3.7.1. General procedures and physical measurements

All manipulations were performed in air at room temperature. $[^nBu4N][Au(CN)_2]\bullet 1/2\ H_2O$ was synthesized from a literature procedure.[41] All other reagents were obtained from commercial sources and used as received. Infrared spectra were recorded on a Thermo Nicolet Nexus 670 FT-IR spectrometer equipped with a Pike MIRacle attenuated total

reflection (ATR) sampling accessory. Thermogravimetric analysis was performed by Dr. Wen Zhou using a Shimadzu TGA- 50 instrument in air at a rate of 2 °C per min. Emission spectra were collected on an Edinburgh FS5 Spectrofluorometer using a xenon arc lamp. Experimental specifications were 1 nm excitation and emission slit widths, 0.5 – 0.9 second dwell times, and 1 – 3 averaged scans per spectra. Microanalyses (C, H, N) were performed by Dr. Wen Zhou at Simon Fraser University on a Carlo Erba EA 1110 elemental analyzer.

Single crystal X-ray Diffraction. Crystals were affixed to MiTeGen MicroMounts using paratone oil. All crystallographic data were collected on a Bruker SMART ApexII Duo CCD diffractometer with TRIUMPH graphite-monochromated Mo Kα (λ = 0.71073 Å) sealed tube or a Cu Kα (λ = 1.54184 Å) Incoatec microsource. An Oxford Cryosystems Cryostream was used to cool and maintain a temperature of 98 K during data collection. Absorption corrections were done using the multi-scan method using the SADABS software, as appropriate. All structures were solved using intrinsic phasing[42] in APEX II and subsequent refinements were performed using a combination of Olex2[43] and ShelxLe.[44] All non-hydrogen atoms were refined anisotropically, and all hydrogen atoms were added geometrically using a riding model. Diagrams were prepared using Mercury[45] with thermal ellipsoids drawn at 50 % probability. Additional crystallographic data can be found in the accompanying cif-files.

3.7.2. Synthesis of $[Bi(Terpy)(\mu\text{-}OH)]_2[Au(CN)_2]_4$ (1)

To a 10 mL aqueous solution of $Bi(triflate)_3$ (65 mg, 0.099 mmol) was added a 10 mL methanol solution of terpy (23 mg, 0.099 mmol). To the resulting pale-yellow solution was added a 20 mL methanol solution of $KAu(CN)_2$ (85 mg, 0.295 mmol). Crystals of $[Bi(Terpy)(\mu\text{-}OH)]_2[Au(CN)_2]_4$ (**1**) began to form after a day and were filtered. Yield: 0.095 g (99%). Anal. Calcd. for $C_{19}H_{12}N_7Au_2BiO$: C, 23.84%; H, 1.26%; N, 10.24%. Found: C, 24.10%; H, 0.92%; N, 10.36%. IR (cm^{-1}): 730 (m),772 (s), 831 (w), 1012 (w), 1160 (m), 1171 (m), 1198 (m), 1238 (w), 1310 (m), 1434 (m), 1449 (m), 1480 (m), 1573 (m), 1579 (m), 1593 (m), 2144 (s, νCN), 2161 (s, νCN), 3042 (w), 3081 (w),3112 (w).

3.7.3. Synthesis of $Bi(Terpy)(NO_3)_2[Au(CN)_2](H_2O)$ (2)

To a solution of terpy (46 mg, 0.198 mmol) in methanol was added a methanol solution of $KAu(CN)_2$ (85 mg, 0.295 mmol). A bismuth nitrate solution (5 mL) was prepared using $Bi(NO_3)_3•5H_2O$ (93 mg, 0.19 mmol) in acidic water (1:100 mL conc. nitric acid : water), which was added to the methanol solution containing terpy and $KAu(CN)_2$. Crystals of $Bi(Terpy)(NO_3)_2[Au(CN)_2](H_2O)$ (**2**) began to form after a week and were filtered. Yield: 0.065 g (43%). Anal. Calcd. for $C_{17}H_{13}N_7AuBiO_7$: C, 24.50%; H, 1.57%; N, 11.77%. Found: C, 24.10%; H, 1.67%; N, 11.36%. IR (cm^{-1}): 720 (m), 768 (s), 788 (w), 1010 (s), 1051 (m), 1290 (s), 1350 (s), 1410 (s), 1510 (m), 2150 (s, νCN), 3008 (w).

3.7.4. Synthesis of $[Bi(terpy)(H_2O)(OH)]_2[Au(CN)_2]_4$ (3)

Bismuth nitrate ($Bi(NO_3)_3•5H_2O$; 48 mg, 0.1 mmol) was dissolved in 10 mL of water to which 0.1 mL of concentrated nitric acid had been added. Terpy (47 mg, 0.2 mmol) in 20 mL methanol was mixed with a 30 mL methanol solution of $KAu(CN)_2$ (85 mg, 0.295 mmol) and this mixture was added to the bismuth nitrate solution. Crystals of $[Bi(terpy)(H_2O)(OH)]_2[Au(CN)_2]_4$ (**3**) began to form after 5 days and were filtered. Yield 0.085 g (86%). IR (cm^{-1}): 779 (s), 786 (m), 824 (w), 993 (m), 1024 (m), 1168 (w), 1296 (s), 1377 (m), 1431 (s), 1587 (w), 1614 (w), 2186 (w, νCN), 3103 (w).

3.7.5. Synthesis of $Bi(Terpy)[Au(CN)_2]_2(NO_3)(DMSO)_2$ (4)

Bismuth nitrate ($Bi(NO_3)_3•5H_2O$; 24 mg, 0.05 mmol) was dissolved in 0.5 mL of DMSO. Terpy (11 mg, 0.05 mmol) was dissolved in a separate 1 mL of DMSO, and the solutions were mixed. To the resulting transparent solution was added a 1.5 mL DMSO solution containing $KAu(CN)_2$ (44 mg, 0.15 mmol). Crystals of $Bi(Terpy)[Au(CN)_2]_2(NO_3)(DMSO)_2$ (**4**) began to form after 10 months and were filtered. Yield 0.15 g (17%). Not enough crystals were isolated to obtain elemental analysis or infrared spectral data.

3.7.6. Synthesis of $Bi(Terpy)(OH)(DMSO)_2[Au(CN)_2]_2$ (5)

Bi(triflate)3 (65 mg, 0.099 mmol) was added to a 1 mL DMSO solution of terpy (23 mg, 0.099 mmol). To the resulting pale-yellow solution was added a 3 mL DMSO solution

of $KAu(CN)_2$ (85 mg, 0.295 mmol). Crystals of $Bi(Terpy)(OH)(DMSO)_2[Au(CN)_2]_2$ (**5**) began to form after a week and were filtered. Yield 0.19 g (16%). IR (cm^{-1}): 772 (s), 998 (w), 1010 (s), 1070 (w), 1160 (s), 1170 (w), 1289 (m), 1389 (s), 1457 (m), 1470 (w), 1483 (m), 1596 (m), 2140 (s, νCN), 3018 (w).

3.7.7. Synthesis of $Bi(Chloro\text{-}Terpy)(NO_3)_2[Au(CN)_2]$ (6)

Bismuth nitrate ($Bi(NO_3)_3$•5H2O; 48 mg, 0.1 mmol) was added to an acidic aqueous solution (10 mL water: 0.1 mL concentrated HNO_3). 4'-Chloro-terpy (54 mg, 0.2 mmol) in 20 mL methanol was mixed with a 10 mL methanol solution of $KAu(CN)_2$ (85 mg, 0.295 mmol) and was added to the bismuth nitrate-containing solution. Crystals of $Bi(Chloro\text{-}Terpy)(NO_3)_2[Au(CN)_2]$ (**6**) began to form after 8 days and were filtered. Yield 0.055 g (64%). IR (cm^{-1}): 726 (w), 790 (w), 830 (w), 1013 (m), 1293 (w), 1478 (w), 2147 (m, νCN), 2168 (m, νCN), 2183 (m, νCN).

3.7.8. Synthesis of $[Chloro\text{-}terpy\text{-}H_2](NO_3)[Au(CN)_2]•H_2O$ (7)

Bismuth nitrate ($Bi(NO_3)_3$•$5H_2O$; 48 mg, 0.1 mmol) in an acidic solution (10 mL water: 0.1 mL HNO_3) was prepared. 4'-chloroTerpy (47 mg, 0.2 mmol) in 5 mL of the same acidic solution was added to a 20 mL methanol solution of $[^nBu4N][Au(CN)_2]$•1/2 H_2O (150 mg, 0.3 mmol) and the two solutions were mixed. Crystals of $[Chloro\text{-}terpy\text{-}H_2](NO_3)[Au(CN)_2]•H_2O$ **(7)** began to form after 10 days and were filtered. Yield 0.035 g (63.3%). IR (cm^{-1}): 729 (s), 795 (m), 828 (m), 893 (s), 1011 (s), 1256 (s), 1271 (w), 1420 (s), 1479 (s), 1596 (m), 2139 (s, νCN), 3078 (w).

3.7.9. Synthesis of $[Bi(Phen)_2(\mu\text{-}OH)]_2[Au(CN)_2]_4$ • 2MeOH (8)

$Bi(triflate)_3$ (65 mg, 0.099 mmol) was dissolved in 10 mL of methanol. Separately, phen•H2O (40 mg, 0.2 mmol) was dissolved in 10 mL of methanol and the two solutions were mixed. To the resulting pale yellow solution was added a 20 mL methanol solution of $KAu(CN)_2$ (85 mg, 0.295 mmol). Crystals of $[Bi(Phen)_2(\mu\text{-}OH)]_2[Au(CN)_2]_4$ • 2MeOH (**8**) began to form after three days and were filtered. Yield 0.075 g (42.7%). IR (cm^{-1}): 718(s), 723(s), 768(w), 843 (s), 862 (m), 1011 (s), 1099 (m), 1220 (w), 1341 (m), 1425 (s), 1514 (s), 1590 (w), 1622 (w), 2143 (s, νCN), 3054 (w).

3.7.10. Synthesis of $[Bi(Phen)_2(\mu{-}OH)(H_2O)]_2[Au(CN)_2]_2(CF_3SO_3)_2$ (9)

Bi(triflate)$_3$ (65 mg, 0.1 mmol) was added to 10 mL of water. A 10 mL methanol solution of phen•H2O (20 mg, 0.1 mmol) was prepared and added to the Bi-containing aqueous solution. To the resulting transparent solution was added a 20 mL methanol solution of $KAu(CN)_2$ (85 mg, 0.295 mmol). Crystals of $[Bi(Phen)_2(\mu{-}OH)(H_2O)]_2[Au(CN)_2]_2(CF_3SO_3)_2$ (**9**) began to form after 3 days and were filtered. Yield 0.025 g (16.7%). IR (cm^{-1}): 719 (s), 732 (w), 815 (w), 852 (m), 1031 (w), 1100(w), 1222 (w), 1283 (m), 1392(m), 1427 (m), 1519 (w), 2154 (s, ν(CN)), 2162 (m, ν(CN)).

3.7.11. Synthesis of $Bi(Terpy)(H_2O)_2$(m-OH)$(Triflate)_2$ (10)

Bi(triflate)3 (65 mg, 0.1 mmol) was added to 10 mL of water. A 20 mL methanol solution of terpy (46 mg, 0.198 mmol) was added to this solution. Crystals of $Bi(Terpy)(H_2O)_2$(m- OH)$(Triflate)_2$ (**10**) began to form after few hours and were filtered. Yield 0.035 g (44.1%). IR (FTIR, cm^{-1}): 721 (w), 780 (s), 1006 (s), 1029 (s), 1157 (s), 1274 (s), 1449 (w), 1460 (w), 1600 (w), 2900 (w), 3102 (w).

3.7.12. Synthesis of Bi(4'-Amino-Terpy)$(NO_3)_3$ (11)

$Bi(NO_3)_3$•$5H_2O$ (65 mg, 0.135 mmol) was dissolved in a 10 mL of an acidic solution of water and 15M nitric acid (10 mL water : 0.1 mL HNO_3) and mixed with a methanol solution of 4'- amino-terpy (50 mg, 0.2 mmol). To the resulting yellow solution was added a 20 mL methanol solution of $KAu(CN)_2$ (85 mg, 0.295 mmol). Crystals of Bi(Amino-Terpy)$(NO_3)_3$ (**11**) began to form after 2 days and were filtered. Yield 0.039 g (61%). IR (cm^{-1}): 703 (w), 746 (w), 791 (s), 807 (w), 859 (w), 989 (w), 1010 (s), 1098 (w), 1160 (w), 1282 (s), 1297 (s), 1370 (m), 1598 (s), 1632 (m), 3342 (m).

3.7.13. Synthesis of Bi(4'-para-bromophenyl-Terpy)$(NO_3)_3$ (12)

$Bi(NO_3)_3$•$5H_2O$ (65 mg, 0.135 mmol) was dissolved in a 10 mL of acidic solution of water and 15M nitric acid (10 mL water : 0.1 mL HNO_3) and mixed with a methanol solution of 4'-para- bromophenyl-terpy (62 mg, 0.16 mmol). To the resulting clear solution was added a 20 mL methanol solution of $KAu(CN)_2$ (85 mg, 0.295 mmol). Crystals of Bi(4'-

para-bromophenyl- Terpy)$(NO_3)_3$ (**12**) began to form after 4 days and were filtered. Yield 0.066 g (84.3%). IR (cm^{-1}): 728 (m), 786 (m), 833 (m), 1004 (m), 1170(w), 1290 (s), 1426 (s), 1432 (m), 1438 (s), 1455 (m), 1472 (m), 1599(s).

3.7.14. Synthesis of {Bi(Phen)$(NO_3)_2$(μ-OH)}$_2$ (13)

$Bi(NO_3)_3$•$5H_2O$ (195 mg, 0.4 mmol; was dissolved in 30 mL of an acidic aqueous solution (10 mL water : 0.1 mL concentrated HNO_3) and mixed with 20 mL of an aqueous solution of phen•H_2O (40 mg, 0.2 mmol). To the resulting yellow solution was added a 20 mL methanol solution of $KAu(CN)_2$ (85 mg, 0.295 mmol). Crystals of {Bi(Phen)$(NO_3)_2$(μ-OH)}$_2$ (**13**) began to form after 3 days and were filtered. Yield 0.025 g (44.2%). IR 716 (w), 804 (w), 853 (w), 1040 (w), 1315 (s), 2989 (s). This complex and its structure has been previously reported.[37]

3.7.15. Synthesis of [H-Phen][Bi(Phen)$(NO_3)_4$] (14)

$Bi(NO_3)_3$•$5H_2O$ (65 mg, 0.135 mmol) was dissolved in a 10 mL acidic solution of water and 15M nitric acid (10 mL water : 0.1 mL HNO_3) and mixed with phen•H2O (40 mg, 0.2 mmol) which was pre-dissolved in the same aqueous acid mixture. To the resulting clear solution was added a 20 mL methanol solution of $KAu(CN)_2$ (85 mg, 0.295 mmol). Crystals of [H-Phen][Bi(Phen)$(NO_3)_4$] (**14**) began to form after 2 days and were filtered. Yield 0.025 g (29.2%). IR (cm^{-1}): 719 (w), 780 (w), 848 (w), 1296 (w), 1376 (m),1427 (w).

3.7.16. Synthesis of [H-Phen][Bi(Phen)Cl_3NO_3] (15)

A volume of 10 mL of Bismuth chloride stock solution (5 mL Bismuth chloride stock solution was prepared. Phen (120 mg, 0.3mmol) in 30 mL methanol was mixed). To the resulting clear solution was added a 20 mL methanol solution of $KAu(CN)_2$ (85 mg, 0.295 mmol). Crystals of Au-free [H- Phen][Bi(Phen)Cl_3NO_3] (**15**) began to form after 3 days, and were filtered. Yield 0.075 g (85.6%).IR (FTIR, cm^{-1}): 771 (s), 1012 (s), 1062 (m), 1160 (s), 1234 (s), 1267 (s), 1296 (m), 1311 (w), 1439 (w), 1596 (w).

3.7.17. Synthesis of {Bi(Phen)(H_2O)$_2$(μ-OH)(Triflate)$_2$}$_2$•H_2O (16)

Bi(triflate)$_3$ (130 mg, 0.2 mmol) in 20 mL methanol was added to a 30 mL methanol solution of Phen•H_2O (46 mg, 0.23 mmol). To the resulting transparent solution was added a 30 mL methanol solution of $KAu(CN)_2$ (85 mg, 0.295 mmol). Crystals of Au-free Structure of {Bi(Phen)(H_2O)$_2$(μ-OH)(Triflate)$_2$}$_2$•H_2O (**16**) began to form after three days and were filtered. Yield 0.045 g (58.5%). IR (FTIR, cm^{-1}): 723 (m), 729 (w), 844 (m), 848 (w), 1031 (m), 1102 (w), 1169 (m), 1244 (s), 1280 (s), 1366 (w), 1426 (w), 1520 (w), 2849 (w), 2929 (w).

3.7.18. Synthesis of [H-Phen][Bi(Phen)(NO_3)$_4$]-Polymorph of (14-17)

$Bi(NO_3)_3$•$5H_2O$ (65 mg, 0.135 mmol) was dissolved in a 10 mL of acidic solution of water and 15M nitric acid (10 mL water :0.1 mL HNO_3) and mixed with 20 mL methanol solution of Phen (39.83 mg, 0.2 mmol). To the resulting clear solution was added a 30 mL methanol solution of $KAu(CN)_2$ (85 mg, 0.295 mmol). Crystals of [H-Phen][Bi(Phen)(NO_3)$_4$] began to form after a day and were filtered. Yield 0.055 g (64.4%). IR (FTIR, cm^{-1}): 701 (w), 765 (w), 848 (m), 1067 (m),1213 (w), 1462 (w), 2922 (m), 2931 (w), 2989 (w).

References

1. S.R. Batten, S.M. Neville and D.R. Turner. “Coordination Polymers: Design, Analysis and Application”, RSC Publishing, Cambridge, 2009.

2. Öhrström, L.; Larsson, K. “Molecule-Based Materials: The Structural Network Approach” Elsevier, Amsterdam, 2005.

3. S. R. Batten, N. R. Champness, X.-M. Chen, J. Garcia-Martinez, S. Kitagawa, L. Öhrström, M. O’Keeffe, M. Paik Suh, and J. Reedijk, “Terminology of metal-organic frameworks and coordination polymers (IUPAC Recommendations 2013),” *Pure Appl. Chem.*, **2013**, *85*, 1715-1724. http://dx.doi.org/10.1351/PAC-REC-12-11-20

4. Furukawa, H.; Cordova, K. E.; O’Keeffe, M.; Yaghi, O. M. The Chemistry and Applications of Metal-Organic Frameworks. *Science* **2013**, *341*, 1230444. https://doi.org/10.1126/science.1230444.

5. (a) Li, H.; Wang, K.; Sun, Y.; Lollar, C. T.; Li, J.; Zhou, H.-C. Recent Advances in Gas Storage and Separation Using Metal–Organic Frameworks. *Materials Today* **2018**, *21*, 108–121. https://doi.org/10.1016/j.mattod.2017.07.006 (b) Jia, T.; Gu, Y.; Li, F. Progress and Potential of Metal-Organic Frameworks (MOFs) for Gas Storage and Separation: A Review. *J. Environ. Chem. Eng.* **2022**, *10*, 108300. https://doi.org/10.1016/j.jece.2022.108300.

6. Bavykina, A.; Kolobov, N.; Khan, I. S.; Bau, J. A.; Ramirez, A.; Gascon, J. Metal–Organic Frameworks in Heterogeneous Catalysis: Recent Progress, New Trends, and Future Perspectives. *Chem. Rev.* **2020**,*120*, 8468–8535. https://doi.org/10.1021/acs.chemrev.9b00685.

7. (a) Yi, F.-Y.; Chen, D.; Wu, M.-K.; Han, L.; Jiang, H.-L. Chemical Sensors Based on Metal– Organic Frameworks. *ChemPlusChem* **2016**, *81*, 675–690. https://doi.org/10.1002/cplu.201600137. (b) Sohrabi, H.; Ghasemzadeh, S.; Ghoreishi, Z.; Majidi, M. R.; Yoon, Y.; Dizge, N.; Khataee, A. Metal-Organic Frameworks (MOF)-Based Sensors for Detection of Toxic Gases: A Review of Current Status and Future Prospects. *Mater. Chem. Phys.* **2023**, *299*, 127512. https://doi.org/10.1016/j.matchemphys.2023.127512

8. (a) Leong, W. L.; Vittal, J. J. One-Dimensional Coordination Polymers: Complexity and Diversity in Structures, Properties, and Applications. *Chem. Rev.* **2011**, *111*, 688–764. https://doi.org/10.1021/cr100160e . (b) Moulton, B.; Zaworotko, M. J. From Molecules to Crystal Engineering: Supramolecular Isomerism and Polymorphism in Network Solids. *Chem. Rev.* **2001**, *101*, 1629–1658. https://doi.org/10.1021/cr9900432

9. J.W. Steed, J.L. Atwood, "Supramolecular Chemistry", John Wiley & Sons, 2009.

10. Spingler, B.; Schnidrig, S.; Todorova, T.; Wild, F. Some Thoughts about the Single Crystal Growth of Small Molecules. *CrystEngComm* **2012**, *14*, 751–757. https://doi.org/10.1039/C1CE05624G

11. Stock, N.; Biswas, S. Synthesis of Metal-Organic Frameworks (MOFs): Routes to Various MOF Topologies, Morphologies, and Composites. *Chem. Rev.* **2012**, *112*, 933–969. https://doi.org/10.1021/cr200304e

12. Herrera, R. P.; Gimeno, M. C. Main Avenues in Gold Coordination Chemistry. *Chem. Rev.* **2021**, *121*, 8311–8363. https://doi.org/10.1021/acs.chemrev.0c00930

13. Moreno-Alcántar, G.; Picchetti, P.; Casini, A. Gold Complexes in Anticancer Therapy: From New Design Principles to Particle-Based Delivery Systems. *Angew. Chem. Int. Ed.* **2023**, *62*, e202218000. https://doi.org/10.1002/anie.202218000

14. cf. the articles collected in *Chem. Rev.* **2021**, *121*, issue 14. "Gold Chemistry", Guest Ed., Hashmi, S.

15. (a) Schmidbaur, H.; Schier, A. Aurophilic Interactions as a Subject of Current Research: An Up-Date. *Chem. Soc. Rev.* **2012**, *41*, 370–412. https://doi.org/10.1039/C1CS15182G. (b) Pyykkö, P. Strong Closed-Shell Interactions in Inorganic Chemistry. *Chem. Rev.* **1997**, *97*, 597–636. https://doi.org/10.1021/cr940396v

16. (a) Schmidbaur, H.; Schier, A. A Briefing on Aurophilicity. *Chem. Soc. Rev.* **2008**, *37*, 1931–1951. https://doi.org/10.1039/B708845K . (b) Bardají, M.; Laguna, A. Gold Chemistry: The Aurophilic Attraction. *J. Chem. Educ.* **1999**, *76*, 201. https://doi.org/10.1021/ed076p201

17. Katz, M. J.; Sakai, K.; Leznoff, D. B. The Use of Aurophilic and Other Metal–Metal Interactions as Crystal Engineering Design Elements to Increase Structural Dimensionality. *Chem. Soc. Rev.* **2008**, *37*, 1884–1895. https://doi.org/10.1039/B709061G

18. (a) Stender, M.; Olmstead, M. M.; Balch, A. L.; Rios, D.; Attar, S. Cation and Hydrogen Bonding Effects on the Self-Association and Luminescence of the Dicyanoaurate Ion, [Au(CN)2]−. *Dalton Trans.* **2003**, 4282–4287. https://doi.org/10.1039/B310085E (b) He, X.; Yam, V. W.-W. Luminescent Gold(I) Complexes for Chemosensing. *Coord. Chem. Rev.* **2011**, *255*, 2111–2123. https://doi.org/10.1016/j.ccr.2011.02.003 (c) Seifert, T. P.; Naina, V. R.; Feuerstein, T. J.; Knöfel, N. D.; Roesky, P. W. Molecular Gold Strings: Aurophilicity, Luminescence and Structure–Property Correlations. *Nanoscale* **2020**, *12*, 20065–20088. https://doi.org/10.1039/D0NR04748A

19. Roberts, R. J.; Bélanger-Desmarais, N.; Reber, C.; Leznoff, D. B. The Luminescence Properties of Linear vs. Kinked Aurophilic 1-D Chains of Bis(Dithiocarbamato)Gold(I) Dimers. *Chem. Commun.* **2014**, *50*, 3148–3150. https://doi.org/10.1039/C3CC47944G

20. Katz, M. J.; Michaelis, V. K.; Aguiar, P. M.; Yson, R.; Lu, H.; Kaluarachchi, H.; Batchelor, R. J.; Schreckenbach, G.; Kroeker, S.; Patterson, H. H.; Leznoff, D. B. Structural and Spectroscopic Impact of Tuning the Stereochemical Activity of the Lone Pair in Lead(II) Cyanoaurate Coordination Polymers via Ancillary Ligands. *Inorg. Chem.* **2008**, *47*, 6353– 6363. https://doi.org/10.1021/ic800425f

21. Roberts, R. J.; Li, X.; Lacey, T. F.; Pan, Z.; Patterson, H. H.; Leznoff, D. B. Heterobimetallic Lanthanide–Gold Coordination Polymers: Structure and Emissive Properties of Isomorphous $[^{n}Bu_4N]_2[Ln(NO_3)_4Au(CN)_2]$ 1-D Chains. *Dalton Trans.* **2012**, *41* (23), 6992–6997. https://doi.org/10.1039/C2DT30156C.

22. Gil-Rubio, J.; Vicente, J. The Coordination and Supramolecular Chemistry of Gold Metalloligands. *Chem. Eur. J.* **2018**, *24* (1), 32–46. https://doi.org/10.1002/chem.201703574.

23. Mirzadeh, N.; Privér, S. H.; Blake, A. J.; Schmidbaur, H.; Bhargava, S. K. Innovative Molecular Design Strategies in Materials Science Following the Aurophilicity Concept. *Chem. Rev.* **2020**, *120* (15), 7551–7591. https://doi.org/10.1021/acs.chemrev.9b00816

24. Dunbar, K. R.; Heintz, R. A. Chemistry of Transition Metal Cyanide Compounds: Modern Perspectives. In *Progress in Inorganic Chemistry*; John Wiley & Sons, Ltd, 1996; pp 283–391. https://doi.org/10.1002/9780470166468.ch4

25. (a) J. Lefebvre and D. B. Leznoff, “Structural diversity, physical properties and applications of cyanometallate coordination polymers,” in Metal and Metalloid containing Polymers (A. S. Abd-El-Aziz, C. E. Carraher, Jr., C. U. Pittman, Jr., and M. Zeldin, eds.), vol. 5, p. 155, New York: Wiley, 2005. (b) Iwamoto, T. In *ComprehensiVe Supramolecular Chemistry*; Lehn, J. M., Atwood, J. L., Davies, J. E. D., MacNicol, D. D., Vo¨gtle, F., Alberti, G., Bein, T., Eds.; Pergamon Press: Oxford, U.K., 1996.

26. Alexandrov, E. V.; Virovets, A. V.; Blatov, V. A.; Peresypkina, E. V. Topological Motifs in Cyanometallates: From Building Units to Three-Periodic Frameworks. *Chem. Rev.* **2015**, *115* (22), 12286–12319. https://doi.org/10.1021/acs.chemrev.5b00320

27. (a) Katz, M. J.; Ramnial, T.; Yu, H.-Z.; Leznoff, D. B. Polymorphism of $Zn[Au(CN)_2]_2$ and Its Luminescent Sensory Response to NH3 Vapor. *J. Am. Chem. Soc.* **2008**, *130* (32), 10662–10673. https://doi.org/10.1021/ja801773p (b) Hoskins, B. F.; Robson, R.; Scarlett, N. V. Y. Six Interpenetrating Quartz-Like Nets in the Structure of $ZnAu_2(CN)_4$. *Angew. Chem. Int. Ed.* **1995**, *34* (11), 1203–1204. https://doi.org/10.1002/anie.199512031

28. D.W. Bennett, "Understanding single-crystal X-ray crystallography", Wiley-VCH, 2010; L.-L. Ooi, Principles of X-ray Crystallography, Oxford University Press, 2010.

29. J.R. Lakowicz, "Principles of fluorescence spectroscopy", 3rd ed., Springer, 2006.

30. Shimoni-Livny, L.; Glusker, J. P.; Bock, C. W. Lone Pair Functionality in Divalent Lead Compounds. *Inorg. Chem.* **1998**, *37*, 1853–1867. https://doi.org/10.1021/ic970909r.

31. Greer, B. J.; Michaelis, V. K.; Katz, M. J.; Leznoff, D. B.; Schreckenbach, G.; Kroeker, S. Characterising Lone-Pair Activity of Lead(II) by ^{207}Pb Solid-State NMR Spectroscopy: Coordination Polymers of $[N(CN)_2]^-$ and $[Au(CN)_2]^-$ with Terpyridine Ancillary Ligands. *Chem. Eur. J.* **2011**, *17* (13), 3609–3618. https://doi.org/10.1002/chem.201002913

32. (a) Davidovich, R. L. Stereochemistry of Pb(II) Complexes with Aminopolycarboxylic Ligands. The Role of a Lone Electron Pair. *Russ. J. Coord. Chem*. **2005**, *31*, 455–466. https://doi.org/10.1007/s11173-005-0120-4. (b) Davidovich, R. L.; Stavila, V.; Marinin, D. V.; Voit, E. I.; Whitmire, K. H. Stereochemistry of Lead(II) Complexes with Oxygen Donor Ligands. *Coord. Chem. Rev.* **2009**, *253*, 1316– 1352. https://doi.org/10.1016/j.ccr.2008.09.003 (c) Reger, D. L.; Wright, T. D.; Little, C. A.; Lamba, J. J. S.; Smith, M. D. Control of the Stereochemical Impact of the Lone Pair in Lead(II) Tris(Pyrazolyl)Methane Complexes. Improved Preparation of Na{B[3,5-$(CF_3)_2C_6H_3]_4$}. *Inorg. Chem*. **2001**, *40*, 3810–3814. https://doi.org/10.1021/ic0100121

33. Barszcz, B.; Masternak, J.; Kowalik, M. Structural Insights into Coordination Polymers Based on $6s^2$ Pb(II) and Bi(III) Centres Connected *via* Heteroaromatic Carboxylate Linkers and Their Potential Applications. *Coord. Chem. Rev.* **2021**, *443*, 213935. https://doi.org/10.1016/j.ccr.2021.213935

34. Katz, M. J.; Aguiar, P. M.; Batchelor, R. J.; Bokov, A. A.; Ye, Z.-G.; Kroeker, S.; Leznoff, D. B. Structure and Multinuclear Solid-State NMR of a Highly Birefringent Lead−Gold Cyanide Coordination Polymer. *J. Am. Chem. Soc.* **2006**, *128*, 3669–3676. https://doi.org/10.1021/ja0566634

35. K. Nakamoto, "Infrared and Raman Spectra of Inorganic and Coordination Compounds", John Wiley & Sons, 2009.

36. (a) Junk, P. C.; Louis, L. M. Dimeric Structure of $[(\eta^2\text{-}NO_3)_2(tpy)Bi(\mu\text{-}OH)_2Bi(tpy)(\eta^2\text{-}NO_3)_2]$.*Z. Anorg. Allg. Chem.* **2000**, *626*, 556–559. https://doi.org/10.1002/(SICI)1521-3749(200002)626:2<556::AID-ZAAC556>3.0.CO;2-V (b) Adcock, A. K.; Marwitz, A. C.; Sanz, L. A.; Ayscue, R. L.; Bertke, J. A.; Knope, K. E. Synthesis, Structural Characterization, and Luminescence Properties of Heteroleptic Bismuth-Organic Compounds. *CrystEngComm* **2021**, *23*, 8183–8197. https://doi.org/10.1039/D1CE01242H

37. Barbour, L. J.; Belfield, S. J.; Junk, P. C.; Smith, M. K. Bidentate Nitrogen Base Adducts of Bismuth(III) Nitrate. *Aust. J. Chem.* **1998**, *51*, 337–342. https://doi.org/10.1071/c97170

38. Li, F.; Zhai, J.; Wang, D.-Q.; Yin, H.-D. 1,10-Phenanthrolinium Tetraiodo(1,10-Phenanthroline-κ^2N,N′)Bismuthate(III) 1,10-Phenanthroline. *Act Cryst. E* **2006**, *62*, m1170–m1172. https://doi.org/10.1107/S1600536806014991

39. (a) Morsali, A.; Mahjoub, A. R. Synthesis and Crystal Structure of a Mixed-Ligand Bismuth(III) Complex, $[Bi_2(Phen)_2Br_5(NO_3)]_n$ (Phen=1,10-Phenanthroline). *J. Coord. Chem.* **2006**, *59*, 1427–1431. https://doi.org/10.1080/00958970600764381

40. Bernstein, J. *Polymorphism in Molecular Crystals*; Oxford University Press: Oxford, 2002.

41. Lefebvre, J.; Chartrand, D.; Leznoff, D. B. Synthesis, Structure and Magnetic Properties of 2-D and 3-D [Cation]{$M[Au(CN)_2]_3$} (M = Ni, Co) Coordination Polymers. *Polyhedron* **2007**, *26*, 2189–2199. https://doi.org/10.1016/j.poly.2006.10.045

42. Sheldrick, G. M. SHELXT – Integrated Space-Group and Crystal-Structure Determination. *Acta Cryst. A* **2015**, *71*, 3–8. https://doi.org/10.1107/S2053273314026370

43. Bourhis, L. J.; Dolomanov, O. V.; Gildea, R. J.; Howard, J. a. K.; Puschmann, H. OLEX2: A Complete Structure Solution, Refinement and Analysis Program. *J. Appl. Cryst.* **2009**, *42*, 339–341. https://doi.org/10.1107/S0021889808042726

44. Hübschle, C. B.; Sheldrick, G. M.; Dittrich, B. ShelXle: A Qt Graphical User Interface for SHELXL. *J. Appl. Cryst.* **2011**, *44*, 1281–1284. https://doi.org/10.1107/S0021889811043202

45. Macrae, C. F.; Bruno, I. J.; Chisholm, J. A.; Edgington, P. R.; McCabe, P.; Pidcock, E.; Rodriguez-Monge, L.; Taylor, R.; Streek, J. van de; Wood, P. A. Mercury CSD 2.0 — New Features for the Visualization and Investigation of Crystal Structures. *J. Appl. Cryst.* **2008**, *41*, 466–470. https://doi.org/10.1107/S0021889807067908